

INFORMATION TO USERS

The most advanced technology has been used to photograph and reproduce this manuscript from the microfilm master. UMI films the text directly from the original or copy submitted. Thus, some thesis and dissertation copies are in typewriter face, while others may be from any type of computer printer.

The quality of this reproduction is dependent upon the quality of the copy submitted. Broken or indistinct print, colored or poor quality illustrations and photographs, print bleedthrough, substandard margins, and improper alignment can adversely affect reproduction.

In the unlikely event that the author did not send UMI a complete manuscript and there are missing pages, these will be noted. Also, if unauthorized copyright material had to be removed, a note will indicate the deletion.

Oversize materials (e.g., maps, drawings, charts) are reproduced by sectioning the original, beginning at the upper left-hand corner and continuing from left to right in equal sections with small overlaps. Each original is also photographed in one exposure and is included in reduced form at the back of the book.

Photographs included in the original manuscript have been reproduced xerographically in this copy. Higher quality 6" x 9" black and white photographic prints are available for any photographs or illustrations appearing in this copy for an additional charge. Contact UMI directly to order.



University Microfilms International
A Bell & Howell Information Company
300 North Zeeb Road, Ann Arbor, MI 48106-1346 USA
313 761-4700 800 521-0600

Order Number 9115793

Quasistatic manipulation with compliance and friction

Kao, Imin, Ph.D.

Stanford University, 1991

Copyright ©1990 by Kao, Imin. All rights reserved.

U·M·I
300 N. Zeeb Rd.
Ann Arbor, MI 48106

NOTE TO USERS

**THE ORIGINAL DOCUMENT RECEIVED BY U.M.I. CONTAINED PAGES
WITH BLACK MARKS. PAGES WERE FILMED AS RECEIVED.**

THIS REPRODUCTION IS THE BEST AVAILABLE COPY.

QUASISTATIC MANIPULATION WITH COMPLIANCE AND FRICTION

**A DISSERTATION
SUBMITTED TO THE DEPARTMENT OF MECHANICAL ENGINEERING
AND THE COMMITTEE ON GRADUATE STUDIES
OF STANFORD UNIVERSITY
IN PARTIAL FULFILLMENT OF THE REQUIREMENTS
FOR THE DEGREE OF
DOCTOR OF PHILOSOPHY**

**By
Imin Kao
December 1990**

© Copyright 1990 by Imin Kao
All Rights Reserved

I certify that I have read this dissertation and that in my opinion it is fully adequate, in scope and in quality, as a dissertation for the degree of Doctor of Philosophy.



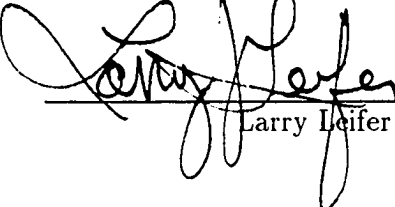
Mark R. Cutkosky
(Principal Adviser)

I certify that I have read this dissertation and that in my opinion it is fully adequate, in scope and in quality, as a dissertation for the degree of Doctor of Philosophy.



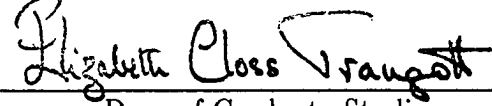
Bernard Roth

I certify that I have read this dissertation and that in my opinion it is fully adequate, in scope and in quality, as a dissertation for the degree of Doctor of Philosophy.



Larry Leifer

Approved for the University Committee on Graduate Studies:



Elizabeth Closs Trampush
Dean of Graduate Studies

Abstract

Grasp compliance and the friction properties of robotic fingers are first explored individually and then combined to provide a method for planning and predicting the sliding motions of the fingers with respect to a grasped object.

The compliance of a grasp is expressed as a function of grasp geometry, contact conditions between the fingers and the grasped object, and kinematic properties of the fingers. The resulting compliance and stiffness matrices are useful for characterizing the grasp of a robotic hand on a tool or workpiece when small motions and low velocities are involved. The results depend on structural compliance and small changes in the grasp geometry. The problem of specifying servo gains at the joints of a robotic hand so as to achieve, as nearly as possible, a desired overall grasp compliance is also examined.

Friction models of point-contact and soft fingers are also studied. The relationship between forces and moments applied by a soft finger are described with a three dimensional limit surface. Based on the grasp compliance and contact friction, two measures are proposed to predict the onset of sliding for multifingered hands grasping an object.

Finally, the grasp compliance and friction limit surfaces are combined in a method for modeling manipulation with sliding fingers. The method is useful for describing how a grasp will behave in the presence of external forces and for planning how to control the fingers so that the object will follow a desired trajectory. The approach

is first developed in terms of a single sliding, compliant fingertip and is illustrated with several examples. Experimental results are also presented. The analysis is then extended to grasps with multiple sliding and non-sliding fingers. A minimization scheme is presented that decomposes the combined finger motions into orthogonal rigid-body and non-rigid-body components, to simplify the analysis.

Acknowledgements

First and the foremost, I would like to thank Professor Cutkosky for his guidance throughout this work. His intuition and physical insight to the problems have been a great learning experience to me. His encouragement and understanding throughout this research work have made my education process an exciting experience.

I would also like to express my gratefulness to Professor Bernard Roth, who has made many suggestions in the final draft of this dissertation, and Professor Larry Leifer for his careful reading of this dissertation. Thanks are also due to Professor Stephen Boyd for fruitful discussions.

The road to the Ph.D. would not have been as easy without my friends and colleagues at the Center for Design Research: Prasad Akella, Rob Howe, Soo-Hong Lee, Warren Packard, Nicolas Popp, and many others. Particular thanks are due to Ron Fearing for his help in doing the experiments on the Stanford/JPL hand. Thanks also to Richard Murray for his help in doing experiments at U. C. Berkeley.

I would also like to thank my parents and family, who have partly supported me financially, for their caring and love.

Last but not the least, I deeply appreciate the support of my wife, Elaine, during these years. Her constant encouragements have helped push me through these learning and trying years. There have been hard times and happy hours, and we have shared them together with our three loving children, Wee-Tin, Jonathan, and Emmeline.

After studying grasping/manipulation and implementing controllers for robots, I can not but appreciate and praise Him, the creator of the human beings, a most delicate creation. I have also come to better realize how much we all take for granted.

This work has been supported by the National Science Foundation under grants DMC8552691 and DMC8602847, with additional support from the Stanford Institute for Manufacturing and Automation (SIMA).

Contents

Abstract	iv
Acknowledgements	vi
1 Introduction	1
1.1 Introduction and background	1
1.2 Preview and outline of following chapters	2
1.3 Terminology and notations	4
1.3.1 Nomenclature	5
1.3.2 Notations	9
2 Literature Review	11
2.1 Previous investigations on grasp compliance and stiffness	11
2.2 Contact and friction models	12
2.3 Previous investigations on sliding	13

3 Stiffness and Compliance	15
3.1 Introduction	15
3.2 Stiffness and Compliance	16
3.2.1 The importance of stiffness and compliance	16
3.3 Dual relationships of force and motion	18
3.3.1 Forward force/motion relationships	20
3.3.2 Contact constraints	21
3.3.3 Concatenated force/motion relationships	21
3.4 Forward stiffness computation	22
3.4.1 Stiffness of a grasp – \mathbf{K}_b and \mathbf{K}_J	23
3.4.2 Computing \mathbf{K}_b : the effects of restoring forces	23
3.4.3 Computing \mathbf{K}_J : the effects of changes in geometry	26
3.4.4 Scaling \mathbf{K}_e by the characteristic length of the grasp	30
3.4.5 Examples of the forward procedure	31
3.5 Reverse stiffness computation – controlling the grasp stiffness	37
3.5.1 An approach to reverse stiffness computation	42
3.5.2 Examples of the reverse procedure	43
3.5.3 Reverse procedure for redundant grasps	45
3.6 Changes in stiffness, $\Delta\mathbf{K}$	47
3.7 Manipulation with finite motions	50

3.8 Experiments	51
3.9 Summary	54
4 Friction Models and Prediction of Slipping	56
4.1 Introduction	56
4.2 Friction models	57
4.2.1 Coordinates and transformations	57
4.2.2 Friction model for soft fingers	57
4.3 Grasp compliance and contact forces	61
4.4 Measures to predict the onset of sliding	62
4.4.1 Worst-case-finger measure for point contacts	62
4.4.2 Worst-case-finger measure for soft fingers	66
4.4.3 Progression-toward-friction-limit measure for point contacts .	66
4.4.4 Progression-toward-friction-limit measure for soft fingers . .	70
4.5 Strategies to stabilize a grasp	71
4.6 Critical configurations	76
4.7 Summary	78
5 Quasistatic Manipulation With Sliding	80
5.1 Introduction	80
5.2 Analytic form of sliding trajectory of a single finger	81

5.2.1	Minimum power principle with Coulomb friction	82
5.2.2	Curves and parameterization	84
5.2.3	Limit surface constraints for soft and point contact fingers . .	86
5.2.4	Equations of sliding motion	88
5.2.5	Solving for sliding trajectories	90
5.2.6	Analytic solutions for a point-contact finger sliding on a plane	91
5.3	Examples of single-finger sliding manipulation	94
5.3.1	Planning and predicting trajectories for a point-contact finger	94
5.3.2	A three dimensional grasp with a soft finger	103
5.4	Summary	107
6	Motions of Sliding Manipulation	108
6.1	Introduction	108
6.2	Extensions to multifingered manipulation	109
6.3	RB and NRB motions of sliding manipulation	111
6.3.1	RB and NRB vector spaces	111
6.3.2	Compatibility equations of sliding motion	114
6.3.3	Solution of the NRB motion of grasps by minimization	115
6.4	Examples of multi-fingered sliding manipulation	119
6.4.1	Achieving a prescribed motion	119

6.4.2 Applying forces	123
6.5 Experimental results	131
6.6 Summary	135
7 Conclusions and Future Work	137
Appendices	140
A Forward and reverse procedures	140
A.1 Structural compliance of fingers	140
A.2 Symbolic matrix inverse for point-contacts	141
A.3 Differential Jacobian	142
A.4 Equations and expressions in examples	143
A.4.1 Example 3.1	143
A.4.2 Example 3.2	144
A.4.3 Example 3.3	145
A.4.4 Example 3.4	146
A.5 Positive definiteness of the forward procedure	147
A.6 Obtaining joint stiffness in the reverse procedure	148
A.7 Derivation of changes in stiffness, ΔK	150
A.8 A two-fingered five-bar planar manipulator	151

B Grasp measures for sliding	154
B.1 Results of the spherical grasp example	154
B.2 “Progression-toward-friction-limit” measure - the first order approximation	156
B.2.1 First order approximation	156
B.2.2 Error analysis of the approximation	156
B.3 Results of the 2D grasp examples	157
C Quasistatic sliding manipulation	159
C.1 Analytical solution of the trajectories of the frame and disk for an applied force profile	159
C.2 The cartesian stiffness matrices for example 5.5	160
D Motions of sliding manipulation	161
D.1 Weighting matrix of function “g”	161
D.2 The optimal solution with minimum norm	162
D.3 Proof that $v_y = 0$ in the business card example	163
D.4 Results of unsymmetric grasp example	164
Bibliography	166

List of Tables

3.1	Forward force/motion relationships for finger and object	19
3.2	Typical structural compliances in the Stanford/JPL hand	25
3.3	Minimum number of fingers needed to control \mathbf{K}_e with and without coupling	45
3.4	Parameters of the planar manipulator used in the experiments	52
4.1	Changes recommended to make the 3D grasp example more resistant to slipping according to the “worst-case-finger” measure	72
4.2	Changes recommended to make the 2D grasp example more resistant to slipping according to the “progression-toward-friction-limit” measures	73
4.3	Slipping measures for a 3D soft finger example	75
4.4	Changes recommended to make the grasp more resistant to slipping .	75
A.1	Link length of the five-bar planar manipulator	152

List of Figures

1.1	Three steps of the quasistatic manipulation	3
3.1	Coordinate systems for a single finger touching a grasped object	19
3.2	Coordinate systems for a finger rolling on a grasped object	29
3.3	Inserting a rivet with two soft-tipped fingers	33
3.4	A possibly unstable grasp with point-contact fingers	34
3.5	Coordinates and center of compliance for a planar grasp	39
3.6	A 2-link planar manipulator	49
3.7	A typical plot of stiffness experiment when an external force is applied	53
4.1	A fingertip sliding on an object surface	58
4.2	Friction limit surface in force/moment space for soft fingers	59
4.3	Comparison of friction models and experimental results	61
4.4	Contact coordinates and forces for a point-contact finger with Coulomb friction	63

4.5	Example of “worst-case-finger” slip measure for three fingers holding a sphere	64
4.6	Friction cone and progression-toward-friction-limit measure for point contact fingers	67
4.7	A 2D grasp example for progression-toward-friction-limit measures	69
4.8	Example of two four-joint soft-contact fingers grasping a rectangular block	74
4.9	Polar plot ($f_c/ f_n $ radial, θ_c angular) of onset of slipping with respect to the external force showing predicted and experimental critical angles at which both fingers slip simultaneously	77
5.1	Coordinate systems and vectors for a finger/object contact sliding on the surface of a grasped object	85
5.2	Trajectory and motion vectors for a compliant finger sliding on the surface of an object	86
5.3	Relationships between limit surface and the unit normal, \mathbf{p}	87
5.4	Coordinate system and trajectory for a point-contact fingertip sliding on a surface	92
5.5	Schematic of idealized fingertip for sliding experiments	95
5.6	The required locus of $\mathbf{r}_e(\tau)$ to obtain a circular trajectory of $\mathbf{r}(\tau)$	96
5.7	Theoretical and numerical solutions for $\mathbf{r}(\tau)$ if $\mathbf{r}_e(\tau)$ is a circle	98
5.8	Experimental results for $\mathbf{r}(\tau)$ obtained by moving the frame, $\mathbf{r}_e(\tau)$, in a circle	98

5.9 (a) Diagram of motion of frame, \mathbf{r}_e , and disk, \mathbf{r} (b) Tangential force trajectory $f_t(\tau)$	99
5.10 Comparison of analytic solution and experimental results for the disk trajectory	101
5.11 Given a force trajectory, find the trajectories of $\mathbf{r}(\tau)$ and $\mathbf{r}_e(\tau)$	102
5.12 Coordinate setup for a soft-contact finger sliding along an arc on a spherical surface	104
5.13 Results for a soft finger sliding on a spherical surface	106
6.1 Geometric visualization of the solution spaces	113
6.2 The “twirling” motion: manipulating a wedge-shaped object between a sliding and stationary finger	120
6.3 Trajectory of the angles α_1 and α_2 of the “twirling” motion	122
6.4 Two fingers sliding on a sheet of paper	124
6.5 Perspective and plan view of two soft fingers manipulating a business card with linear and rotational sliding	126
6.6 Two soft fingers manipulating a business card with respect to COR .	128
6.7 Locus of fiducials tracked by the vision camera for cases I and II . . .	133
6.8 Comparison of the unit normals for the two cases in sliding manipulation	135
A.1 A finger composed of m serial links	141
A.2 Correlation between elements of \mathcal{K}_θ and coupled joint control	146
A.3 Sketch of a five-bar direct-drive finger	152

D.1 Geometric visualization of the row space and null space	162
---	-----

Chapter 1

Introduction

1.1 Introduction and background

In many low-speed manipulation tasks with dexterous robotic hands, the equations of motion are dominated by contact friction and compliance terms. Under these circumstances, the manipulation process can be treated as “quasistatic”. In this dissertation, a quasistatic analysis in which models of the grasp compliance are combined with models of contact friction, is developed for dexterous manipulation with sliding and non-sliding fingers. The results are useful for predicting the behavior of a grasp when subjected to external forces and for gross-motion planning of compliant, sliding manipulations.

A systematic approach to compute the compliance of each finger and the grasp is first presented. The compliance results can be useful in remote center of compliance (RCC) applications and for stiffness/impedance control. When external forces are applied, the compliant motion of the fingers and object, and the changes in grasp forces, can be determined. This is shown in step I of Figure 1.1. In step II of Figure 1.1, the contacts are modeled as either point or soft contacts which are characterized by a 2D circular or 3D ellipsoidal limit surface, respectively. Once the grasp forces

and limit surfaces are known, the sliding motion can be determined. With known sliding motion, one can solve a first-order differential equation to obtain the motion of the fingertips or object, as outlined in step III of Figure 1.1.

1.2 Preview and outline of following chapters

In Chapter 2, previous investigations of grasp compliance and stiffness, friction models and their application in manipulation, and sliding analysis are reviewed.

In Chapter 3, an approach for computing the stiffness and compliance of a grasp is developed. Two procedures are developed: the forward procedure and reverse procedure. In the forward procedure, the effective stiffness matrix of a grasp, \mathbf{K}_e , is expressed as the sum of: (1) \mathbf{K}_b , which depends upon the structural compliance, the kinematic and elastic properties of fingers and contacts, and the servoing compliance; and, (2) \mathbf{K}_J , which is a function of the grasp configuration and its rate of change. The positive-definiteness of the stiffness matrix, \mathbf{K}_e , determines the instantaneous grasp stability. In the reverse procedure, the servoing compliance is computed to achieve a desired grasp stiffness, accounting for the kinematic and mechanical properties of the fingers and contacts. Experimental results to verify the stiffness procedure conducted on a planar manipulator are also presented.

In Chapter 4, the Coulomb friction model is first reviewed and a model for soft fingers is investigated. The relationship between forces and moments applied by a soft finger is described by a three dimensional limit surface. Based upon the grasp compliance analysis in Chapter 3 and the friction models, two measures are proposed to predict the onset of sliding for multifingered hands grasping an object. The “worst-case-finger” measure finds the finger which will be the first to slide for an external force applied in a particular direction. This establishes an upper bound on the magnitude of the applied force. The “progression-toward-friction-limit” measure considers whether a change in the magnitude and direction of an external force will make each finger more or less vulnerable to slipping, that is, whether the contact forces at each finger

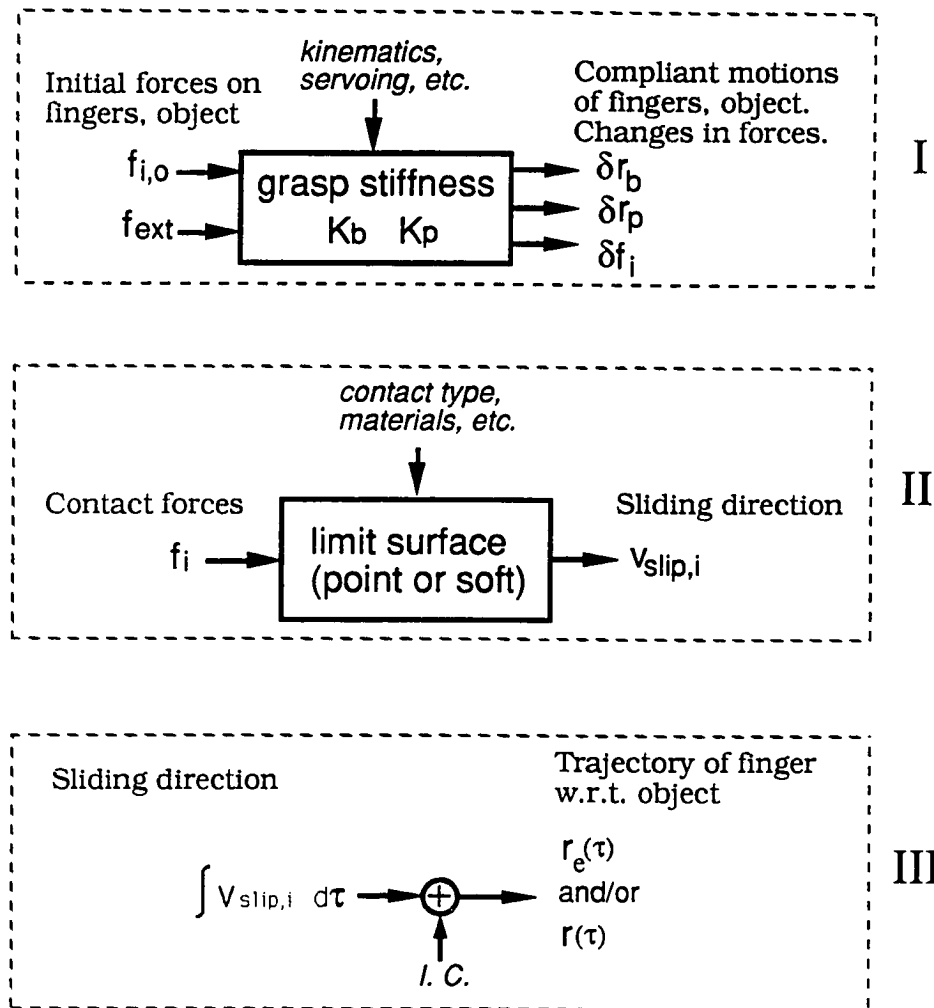


Figure 1.1: Three steps in quasistatic manipulation. Step I: The grasp is modeled with stiffness. Step II: The contacts are modeled as point or soft contacts, characterized by their different limit surfaces. The instantaneous sliding direction is determined from the grasp forces and limit surfaces. Step III: With a known sliding direction, we can integrate to get fingertip trajectories and the sliding motion of the object.

will move toward or away from their respective friction limits.

In Chapter 5, the results of the compliance and friction limit surfaces are combined to explore a new approach for modeling dexterous manipulation with sliding objects. The method is useful for describing how a grasp will behave in the presence of external forces (e.g., when and how the fingertips will slide) and for planning how to control the fingers so that the grasped object will follow a desired trajectory. The sliding motion is described by a first-order time-varying differential equation with a transient and a steady-state solution. The underlying theory is first discussed and illustrated with several single-finger examples. Experimental results are also presented.

In Chapter 6, the sliding analysis is extended to grasps with multiple sliding and non-sliding fingers. The object motions are solved for by formulating equations of force equilibrium, constitutive equations (stiffness and friction relationships), and equations of geometric compatibility (motion constraints). To simplify the analysis, the instantaneous motions of sliding fingers can be thought of as a vector space consisting of two components: rigid-body (RB) motions and non-rigid-body (NRB) motions. The actual sliding motion is obtained by finding the orthogonal RB and NRB motions through minimization of an objective function. The multi-finger analysis is illustrated with several examples. Experimental results are also presented.

1.3 Terminology and notations

The terminology used in this dissertation is listed and briefly described in this section.

quasistatic: A category of motion in which the compliance and friction forces dominate and dynamic effects can be neglected. This is usually true in low-speed manipulation [Jameson 1985, Peshkin 1986].

undeflected position: The location and orientation of a fingertip where there is no resultant force and moment applied to the fingertip by the environment. The

finger will remain stationary when it is brought to this position without any externally applied bias forces.

nominal position: The location and orientation of a fingertip after an external bias force is applied. The instantaneous linear stiffness matrix can be formulated based upon this position such that the proportional force/motion relationship, $\delta\mathbf{f} = \mathbf{K} \delta\mathbf{x}$, holds. This need not be the “undeflected position”.

stiffness matrix: This is a matrix that characterizes a linear relationship between the force/moment applied and the displacements incurred at the finger or grasped object, i.e., $\mathbf{K} \triangleq \partial\mathbf{f}/\partial\mathbf{x}$.

compliance matrix: The inverse of a stiffness matrix, i.e., $\mathbf{C} \triangleq \partial\mathbf{x}/\partial\mathbf{f}$

1.3.1 Nomenclature

The terms used in this dissertation are as follows:

coordinate frames:

- $B(xyz)$: Body coordinate frame
- $F(abc)$: Coordinate frame at the contact point on the fingertip
- $P(lmn)$: Coordinate frame at the contact point on the object
- $O(XYZ)$: Stationary world coordinate frame

position and orientation vectors:

- \mathbf{r} : 3×1 vector giving the point of contact with respect to the object; expressed in $P(lmn)$ coordinates: $\mathbf{r} = [r_l, r_m, r_n]^T$.
- \mathbf{r}_e : 3×1 vector describing the point of contact, at an undeflected position, with respect to the object
- $\delta\mathbf{r}$: Defined as $(\mathbf{r} - \mathbf{r}_e)$
- $\theta_1, \theta_2, \dots$: Joint angles of fingers
- $\delta\theta$: Changes of joint angles of fingers

- $\delta\mathbf{x}_f$: 6×1 vector describing a small change in the location and orientation of the fingertip, $\delta\mathbf{x}_f = \mathbf{J}_\theta \delta\theta$
- $\delta\mathbf{x}_p$: 6×1 vector describing a small change in the location and orientation of a contact with respect to the object, $\delta\mathbf{x}_p = [\delta\mathbf{r}^T, \delta\boldsymbol{\rho}^T]^T$, where $\delta\boldsymbol{\rho} = [\delta\theta_l, \delta\theta_m, \delta\theta_n]^T$ represents infinitesimal rotations about the l, m and n axes
- $\delta\mathbf{x}_{tr}$: Motion transmitted through the contact, $\mathbf{H}\delta\mathbf{x}_p = \mathbf{H}\delta\mathbf{x}_f = \delta\mathbf{x}_{tr}$
- $\delta\mathbf{x}_b$: A 6×1 vector expressing a small change in the location and orientation of the grasped object with respect to the $O(XYZ)$ frame
- $\hat{\mathbf{r}}$: Unit tangent vector along the trajectory $\mathbf{r}(\tau)$; $\hat{\mathbf{r}} = [dr_l/d\tau, dr_m/d\tau]^T \frac{d\tau}{ds}$

force/moment vectors:

- \mathbf{f}_p : 6×1 vector of forces and moments applied at a contact by a finger (\mathbf{f}_{pi} for i 'th finger)
- \mathbf{f}_0 : Initial value of \mathbf{f}_p
- \mathbf{f}_{bi} : 6×1 vector of forces and moments from i 'th finger; expressed in the $B(xyz)$ coordinates
- \mathbf{f}_b : 6×1 vector of forces and moments resulting from all fingers
- \mathbf{f}_f : Grasp force at point F at the fingertip, $\mathbf{f}_f = \mathbf{f}_p$
- \mathbf{f}_{tr} : Force transmitted through the contact, $\mathbf{f}_p = \mathbf{f}_f = \mathbf{H}^T \mathbf{f}_{tr}$
- \mathbf{f}_{slip} : Tangential force and moment at a contact sustained by friction
In 2D: $\mathbf{f}_{slip} = [f_l, f_m, m_n]^T$; in 3D: $\mathbf{f}_{slip} = [f_l, f_m, 0, 0, 0, m_n]^T$
- \mathbf{f}_t : Tangential component of \mathbf{f}_{slip} : $[f_l, f_m]^T$
- f_t : Magnitude of tangential force, $\sqrt{f_t^2 + f_m^2}$
- f_n : Normal force at contact
- $f_{t,max}$: Maximum possible tangential force at a contact
(achievable when there is no moment)
- $m_{n,max}$: Maximum possible moment at a contact (achievable when there is no force)

stiffness and compliance matrices:

- \mathbf{K}_θ : The joint stiffness matrix, $\mathbf{K}_\theta = \mathbf{C}_\theta^{-1}$
- \mathbf{K}_f : The stiffness matrix in the fingertip coordinates, $\mathbf{K}_f = \mathbf{C}_f^{-1}$ if it is invertible

\mathbf{K}_{pi} : 6×6 stiffness matrix for finger i , relating forces and compliant motions at the contact

\mathbf{K}_b : 6×6 stiffness matrix due to servo and structural compliance

\mathbf{K}_s : Stiffness matrix due to changes in geometry

\mathbf{K}_e : Effective stiffness matrix, $\mathbf{K}_e = \mathbf{K}_b + \mathbf{K}_s$

\mathcal{K}_θ : Concatenated servo stiffness

\mathcal{K}_p : $6n \times 6n$ concatenated contact stiffness matrix for nf fingers

\mathcal{C}_θ : Concatenated servo compliance

\mathcal{C}_s : Concatenated structural compliance at the tip coordinates

\mathcal{C}_f : Concatenated fingertip compliance, $\mathcal{C}_f = \mathcal{J}_\theta \mathcal{C}_\theta \mathcal{J}_\theta^T + \mathcal{C}_s$

Jacobian and cartesian transformation matrices:

\mathbf{J}_θ : Joint Jacobian matrix, $\mathbf{J}_\theta \triangleq \frac{\partial \mathbf{x}_p}{\partial \theta}$

${}^P_B \mathbf{J}$: 6×6 cartesian transformation matrix transforming velocities and infinitesimal motions from $B(xyz)$ to $P(lmn)$, ${}^P_B \mathbf{J} \delta \mathbf{x}_b = \delta \mathbf{x}_p$ [Paul 1981, Craig 1989]

\mathcal{J}_θ : Concatenated joint Jacobian matrix as defined in equation (3.16)

${}^P_B \mathcal{J}$: Concatenated transformation matrix for all fingers $[{}^P_B \mathbf{J}_1^T, {}^P_B \mathbf{J}_2^T, \dots, {}^P_B \mathbf{J}_{nf}^T]^T$

\mathcal{J}_c : Cartesian transformation matrix as seen through the contacts, $\mathcal{H} {}^P_B \mathcal{J}$

other matrices and parameters used in compliance analysis:

\mathbf{B} : Joint Jacobian as seen through the contacts, $\mathbf{H} \mathbf{J}_\theta$

\mathbf{D} : Coordinate transformation matrix relating contact coordinates before and after infinitesimal motion

${}^P_B \Delta \mathbf{J}_i^T$: ${}^P_B \mathbf{J}^T (\mathbf{D}_i^T - \mathbf{I})$ that represents a differential Jacobian

\mathbf{H} : Contact constraint matrix which selects those force and moment components transmitted through the contact

\mathcal{H} : Concatenated contact constraint matrix

\mathcal{W} : Concatenated weighting matrix (Appendix D.1)

\mathcal{W}_c : Weighting matrix subject to the contact constraints, $\mathcal{H}^T \mathcal{W} \mathcal{H}$

Ω : $\Omega = (\mathbf{H} \mathbf{C}_s \mathbf{H}^T - \mathbf{H} \mathbf{C}_s \mathbf{H}^T \mathbf{H} \mathbf{K}_p \mathbf{H}^T \mathbf{H} \mathbf{C}_s \mathbf{H}^T)$

\mathbf{l} : The vector of Lagrange multipliers.

m_i : Number of joints for finger i

n_i : Degrees of freedom at contact i

nf : Number of fingers

velocities in sliding analysis:

\mathbf{v}_i : Absolute velocity of the i 'th fingertip with respect to the $O(XYZ)$ frame

$_{RB}\mathbf{v}_i$: The rigid-body component of a set of \mathbf{v}_i

$_{NRB}\mathbf{v}_i$: The non-rigid-body components of a set of \mathbf{v}_i

\mathbf{v}_b : Absolute velocity of the grasped object with respect to $O(XYZ)$
 $(\mathbf{v}_b = d\mathbf{x}_b/d\tau)$

\mathbf{v}_{slip} : Relative sliding velocity of a fingertip with respect to the object

In 2D: $\mathbf{v}_{slip} = [\frac{dx_1}{d\tau}, \frac{dx_m}{d\tau}, \frac{d\theta_n}{d\tau}]^T$; in 3D: $\mathbf{v}_{slip} = [\frac{dx_1}{d\tau}, \frac{dx_m}{d\tau}, 0, 0, 0, \frac{d\theta_n}{d\tau}]^T$

$_{RB}\mathbf{v}_{slip,i}$: The rigid-body component of \mathbf{v}_{slip}

$_{NRB}\mathbf{v}_{slip,i}$: The non-rigid-body components of \mathbf{v}_{slip}

\mathbf{v}_h : The common rigid-body component of the fingertip motions, $_{RB}\mathbf{v}_i$,
expressed at the $B(xyz)$ frame of the object; $_{RB}\mathbf{v}_i = {}_B\mathbf{J}_i \mathbf{v}_h$.

\mathbf{v}'_b : Relative rigid-body motion of object with respect to fingers,
defined as $\mathbf{v}_b - \mathbf{v}_h$

\mathcal{V} : Concatenated fingertip velocities, $[\mathbf{v}_1, \mathbf{v}_2, \dots]^T$

\mathcal{V}_{slip} : Concatenated sliding velocities, $[\mathbf{v}_{slip,1}, \mathbf{v}_{slip,2}, \dots]^T$

$_{RB}\mathcal{V}$: Concatenated RB motions of the fingertips

$_{NRB}\mathcal{V}$: Concatenated NRB motions of the fingertips

$_{RB}\mathcal{V}_{slip}$: Concatenated RB motions of the relative sliding velocity at contacts

$_{NRB}\mathcal{V}_{slip}$: Concatenated NRB motions of the relative sliding velocity at contacts

Other parameters used in limit surface and sliding analysis:

μ : Coulomb coefficient of friction

g : An objective function defined as: $g \triangleq \frac{1}{2} ({}_{NRB}\mathcal{V}^T \mathcal{W}_c {}_{NRB}\mathcal{V})$

\mathbf{p} : 3×1 unit vector normal to friction limit surface, which is related to the
instantaneous direction of sliding motion

\mathbf{p}_s : 3×1 unit vector normal to the normalized spherical friction limit surface

λ : Ratio of the maximum moment and shear force of a soft finger, $\lambda \triangleq \frac{m_{max}}{\mu f_n}$

ψ : Angle of the normalized unit vector \mathbf{p}_s

τ : Independent parameter for all displacements and quasistatic velocities

s : Length along a parameterized curve, $\mathbf{r}(\tau)$, starting from $\tau = 0$

$\Xi(\tau)$: Coefficient matrix for point-contacts, defined as $[\mu f_n \frac{d\tau}{ds}]_{|\mathbf{r}(\tau)}^{-1} \mathbf{K}_p$

1.3.2 Notations

The notations used in this dissertation are:

\mathbf{J}_θ : The joint Jacobian matrix [Craig 1989] which is defined as

$$\mathbf{J}_\theta \triangleq \frac{\partial \mathbf{x}}{\partial \theta}. \quad (1.1)$$

${}^P_B \mathbf{J}$: The cartesian transformation that relates linear velocities at two separate points, B and P , on the same rigid body, and expresses them and the angular velocity of the body in frames with different orientations. The following relation defines ${}^P_B \mathbf{J}$ in terms of two vectors, $\delta \mathbf{x}_b$ and $\delta \mathbf{x}_p$ in the coordinate frames at B and P respectively.

$$\delta \mathbf{x}_p = {}^P_B \mathbf{J} \delta \mathbf{x}_b \quad (1.2)$$

where ${}^P_B \mathbf{J}$ is a 6×6 matrix and $\delta \mathbf{x}_b = [v_{b_x} \ v_{b_y} \ v_{b_z} \ \omega_{b_x} \ \omega_{b_y} \ \omega_{b_z}]^T$ and $\delta \mathbf{x}_p = [v_{p_x} \ v_{p_y} \ v_{p_z} \ \omega_{p_x} \ \omega_{p_y} \ \omega_{p_z}]^T$ are 6×1 vectors. The relation can be derived from the equations

$$\begin{cases} \begin{bmatrix} v_{p_x} \\ v_{p_y} \\ v_{p_z} \\ \omega_{p_x} \\ \omega_{p_y} \\ \omega_{p_z} \end{bmatrix} = \mathbf{A}^T \begin{bmatrix} v_{b_x} \\ v_{b_y} \\ v_{b_z} \\ \omega_{b_x} \\ \omega_{b_y} \\ \omega_{b_z} \end{bmatrix} + \mathbf{A}^T \begin{bmatrix} \omega_{b_x} \\ \omega_{b_y} \\ \omega_{b_z} \end{bmatrix} \times \mathbf{r} \\ \begin{bmatrix} v_{p_x} \\ v_{p_y} \\ v_{p_z} \\ \omega_{p_x} \\ \omega_{p_y} \\ \omega_{p_z} \end{bmatrix} = \mathbf{A}^T \begin{bmatrix} v_{b_x} \\ v_{b_y} \\ v_{b_z} \\ \omega_{b_x} \\ \omega_{b_y} \\ \omega_{b_z} \end{bmatrix} \end{cases} \quad (1.3)$$

where \mathbf{A}^T is a 3×3 orthogonal matrix relating the orientation of the two coordinate frames, $\mathbf{r} = [r_x \ r_y \ r_z]^T$ is a vector from B to P . Comparing equations

(1.2) and (1.3), we can write

$$\overset{\text{p}}{\mathbf{J}} = \left[\begin{array}{c|c} \mathbf{A}^T & \mathbf{A}^T \mathbf{R}^T \\ \hline \cdots & + \quad \cdots \\ 0 & | \quad \mathbf{A}^T \end{array} \right] \quad (1.4)$$

where \mathbf{R} is a 3×3 anti-symmetric matrix expressed as:

$$\mathbf{R} = \left[\begin{array}{ccc} 0 & -r_z & r_y \\ r_z & 0 & -r_x \\ -r_y & r_x & 0 \end{array} \right]$$

H: The contact constraint matrix which selects the components transmitted through the contacts. This is equivalent to the “basis matrix” used in other work on dexterous manipulation [Kerr 1985, Nakamura 1988, Li Hsu and Sastry 1989].

Chapter 2

Literature Review

2.1 Previous investigations on grasp compliance and stiffness

Grasp compliance and stiffness have been studied by several investigators. It has been shown theoretically and experimentally that at low speeds it is accurate to characterize the behaviour of a grasp with a stiffness matrices [Asada 1979, Salisbury 1985, Cutkosky and Kao 1989, Nguyen 1989, Mishra and Silver 1989, Park and Starr 1990]. The stiffness matrices represent the changes in force and torque that accompany small linear and rotational displacements of the grasped object. In the analysis, the object is assumed to be a rigid body and the fingers operate under position control, cartesian stiffness control [Salisbury 1980] or impedance control [Hogan 1985]. In related work, a stiffness map of the workspace has been established for parallel-chain manipulators [Gosselin 1990], which is useful for predicting acceptable zones for manipulation.

The earliest analysis is that of Asada [1979] in which a two-dimensional model of the object and the fingers leads to a potential function for describing stable grasps. The analysis assumes that fingers are essentially springs that move along a given

locus with a single degree of freedom. Friction is ignored at the contacts between the fingers and the object and stable grasps are those for which the object will slide back to its initial equilibrium position after being displaced. The analysis gives intuitively satisfying results for handling slippery objects and where the main concern is that the object should not be dropped. However, in everyday manipulation tasks people and robots take advantage of friction. Consequently, subsequent grasp analyses have generally included friction at the contact points.

Salisbury [1985] augments the resultant force and torque on the object with internal grasp forces so that an invertible 9×9 stiffness matrix is obtained for a three-fingered hand. The resulting stiffness matrix is useful for grasp control and simplifies programming the hand for certain manipulations. Cutkosky [1985] examines the effective stiffness of a grasped object and shows that it is a function not only of the servo parameters but also of fingertip models and of small changes in the grasp geometry as the object is perturbed by external forces. Nguyen [1989] addresses the stiffness and stability of planar and three-dimensional objects grasped by “virtual springs” corresponding to force components, or wrenches, at the finger/object contact points. Nguyen also proposes a least-squares solution for specifying the stiffnesses of the “virtual springs” to obtain a desired grasp stiffness. However, he does not address the relation of “virtual springs” to joints of an actual hand. In Chapter 3 a related problem is considered: specifying the joint servoing in fingers with known structural properties to achieve a desired grasp compliance. The inclusion of the finger kinematics produces somewhat more complexity, but, due to coupling terms, also provides more opportunities for controlling the stiffness matrix.

2.2 Contact and friction models

Contact properties are very important in analyzing grasp stiffness. Several contact models are presented in [Salisbury 1985] and [Cutkosky 1985]. For a point contact finger, only the normal and tangential force is transmitted through the contact; for a

soft finger, the moment along the normal axis is additionally transmitted.

Jameson [1985] has developed an analysis which treats the combined effects of torsion and tangential loading. He uses an indirect approach which assumes an elastic, spherical fingertip and Coulomb friction for each element of the contact area. The distribution of pressure across the contact is assumed to be Hertzian. By assuming various locations of the instantaneous center of rotation, he obtains a set of shear forces and moments which form a nearly elliptical curve when plotted in the shear-moment plane. The relationship between the linear tangential traction and normal moment is also analyzed in [Goyal, Ruina and Papadopoulos 1989]. Experimental results for soft fingers are presented in [Howe, Kao and Cutkosky 1988].

In other work, the spatial motion of a rigid body with line contacts is treated in detail by Cai and Roth [1988]. Montana [1988] derives contact equations to determine the curvature of an unknown object and explores the rolling of a sphere between two arbitrarily shaped fingers.

2.3 Previous investigations on sliding

A number of previous investigations have considered the vulnerability of a robotic grasp to slipping. Kerr [1986] proposes an objective function that allows the grasp forces to be controlled so as to minimize the chance that fingers might slip, subject to kinematic constraints. Nguyen [1988] develops a geometric method for placing the fingers about a grasped object so that arbitrary forces can be exerted, subject to known frictional limitations. Li and Sastry [1989] propose a task-oriented grasp measure that matches an ellipsoid, based on friction limitations, against expected task-induced forces and moments.

Jameson and Leifer [1986] perform a quasistatic analysis of the grasp, in which friction with hard or soft fingers results in a set of inequality constraints that govern the

resulting motion of a grasped object. Ji [1987] expresses sliding motions of point-contact fingers in terms of surface parameters.

The sliding of fingers over the surface of an object is also related to the sliding of objects pushed on a plane with Coulomb friction. The problem of predicting the motion of such objects has been addressed by Mason [1985], Peshkin [1988] and Goyal [1989]. In related work, Brost [1988] has studied the motion of rigid objects squeezed between the jaws of a parallel-jaw gripper. Brock [1988] uses an analysis of constraints in the grasp to predict and control the sliding of an object grasped by a robot hand for certain manipulations (e.g., allowing an object pinched between the thumb and index finger to pivot under the influence of gravity). Gopalswamy and Fearing [1989] discuss the sliding of soft fingertips on a wedge-shaped object.

Chapter 3

Stiffness and Compliance

3.1 Introduction

In this chapter the compliance of a grasp is expressed as a function of grasp geometry, contact conditions between the fingers and the grasped object, and mechanical properties of the fingers. The effects of structural compliance and small changes in the grasp geometry are included in the computation. The factors that can lead a grasp to become unstable, independently of whether it satisfies force closure, are examined. Next, the reverse problem of how to specify servo gains at the joints of a robotic hand so as to achieve, as nearly as possible, a desired overall grasp compliance is investigated. The coupling between the joints of different fingers is useful in this context. The differential changes in the stiffness matrix, $\delta\mathbf{K}$, are discussed. $\delta\mathbf{K}$, a Hessian matrix tensor, is useful for determining how the grasp stiffness changes with respect to changes in geometry. Finally, the model is generalized to apply to finite motions by introducing the concept of the nominal positions of fingertips, in addition to the undeflected (or equilibrium) positions.

3.2 Stiffness and Compliance

The compliance of a grasp is a measure of how the grasped object will move when certain allowable forces and moments are applied. The inverse of compliance is stiffness, which is a measure of how contact forces and moments will change when a grasped object is displaced. The stiffness of a grasp can be expressed as a linearized expression of the relationships between forces applied to the grasp and the resulting motions:

$$\mathbf{K} = \frac{\partial \mathbf{f}}{\partial \mathbf{x}} \quad (3.1)$$

The resulting matrix can describe force/motion relationships both internal and external to the grasped object [Salisbury 1985], but in this thesis only the stiffness of an essentially rigid object with respect to external forces and moments is considered.

As a partial derivative, the grasp stiffness permits us to look beyond instantaneous properties such as connectivity¹ and force-closure² and to examine the *sensitivity* of the grasp to disturbances. In fact, as Salisbury [1985] points out, \mathbf{K} is a direct measure of quasistatic grasp stability. As long as \mathbf{K} is positive definite, the changes in the forces on the object will have a stabilizing effect.

3.2.1 The importance of stiffness and compliance

The effective compliance or stiffness of an object held in a robotic hand is an important quantity in tasks where forces and small motions are imparted to the object. For example, in assembling components it has been demonstrated that the chances of successful assembly are highest if the compliance matrix associated with the grasped part is diagonal at the point where the part first touches a mating component [Whitney 1980]. Similarly, in robotic grinding and deburring, the compliance matrix associated with the tool can be used to simplify the control problem [Cutkosky and Wright 1895].

¹The connectivity of a grasp is the number of degrees of freedom between the grasped object and the palm of the hand [Salisbury 1985].

²A grasp has force-closure if it can resist forces and moments from any direction, assuming the fingertips maintain contact with the object [Ohwovorile 1980].

The analysis in this chapter is built upon previous investigations by Salisbury [1985], Kerr [1986], Cutkosky [1985], Kobayashi [1985] and Nguyen [1988, 1989], in which the instantaneous kinematics of multifingered hands have been defined in terms of Jacobian matrices, and in which servo gains associated with the fingers contribute to the overall stiffness of the grip. As in [Cutkosky 1985], the cases for which soft, anthropomorphic fingers are in contact with the object are investigated. In such cases, deformation and rolling of the fingertips cannot be ignored.

The first problem addressed in this chapter is to obtain the effective compliance of an object held by a multifingered hand. In contrast to previous efforts, it is assumed that the fingers may be constructed from relatively flexible materials (such as molded thermoplastics) so that their structural compliance must be added to the compliance of the fingertips and to the controllable servo compliance of the joints. As Table 3.2 shows, even when fingers are made of aluminum (such as those of the Stanford/JPL hand), elasticity in the drive cables and in the joints produces significant compliance.

The effective compliance or stiffness of the grasped object depends not only on the compliances of the fingers but also on terms that arise from small changes in the grasp geometry as the object is perturbed by external forces. When grasp forces are large, these geometric terms may make the grasp unstable. In Section 3.4 a method for computing the matrix, K_J , that represents these terms is presented.

The overall grasp stiffness matrix, containing structural, servo and geometric terms, is a useful measure of the grasp. The rank and the eigenvalues of this matrix tell us about the mobility and stability of the grasp³. The relative magnitudes of the elements tell us how sensitive the grasp forces are to small motions in various directions. In addition, as will be discussed in Chapter 4, the grasp stiffness is useful in predicting the onset of sliding motion since it provides information about how rapidly the normal and tangential force components will change at each contact when the object is disturbed.

³Only the quasistatic stability is addressed. The drive-train and actuator dynamics and the effects of rapidly varying, task-induced forces are ignored.

Finding the stiffness of a part grasped in a robotic hand is useful for predicting the grasp behavior and for discriminating among competing grasps when contemplating a task with particular requirements. For controls purposes, however, the reverse problem is of more interest: adjusting the servo gains at the finger joints so as to achieve a desired grasp stiffness. In many cases, it is not possible to achieve exactly the desired stiffness, but in Section 3.5 methods that involve coupling the control of joints on different fingers to achieve a best approximation are explored. For fingers with redundant joints, the reverse procedure can render exact solutions using different optimization schemes. The results of the forward and reverse compliance analysis are illustrated with several examples.

3.3 Dual relationships of force and motion

In this section, the kinematic force/motion relationships for the grasp are established. When several fingers like the finger in Figure 3.1 grasp an object, the resulting configuration forms an in-parallel kinematic chain. Although each finger is a serial kinematic chain, the combination of several fingertips pressing against a single object forms an in-parallel mechanism. Computation of the joint forces or motions needed to produce desired forces or motions of the object involves both direct and inverse kinematic computations [Kerr 1985], and must accommodate static indeterminacy, redundancy and over-constraint. In computing the grasp stiffness, we are subject to the same complications since we need to propagate motions from the object out to the finger joints and then propagate changes in the joint forces back to the object. However, as we shall see in the following section, the inclusion of structural compliances permits a systematic approach for arbitrary combinations of fingers, joints and contact types. This is an important advantage since fingers are continually making and breaking contact with the object, and rolling or sliding from faces to edges, as the object is manipulated.

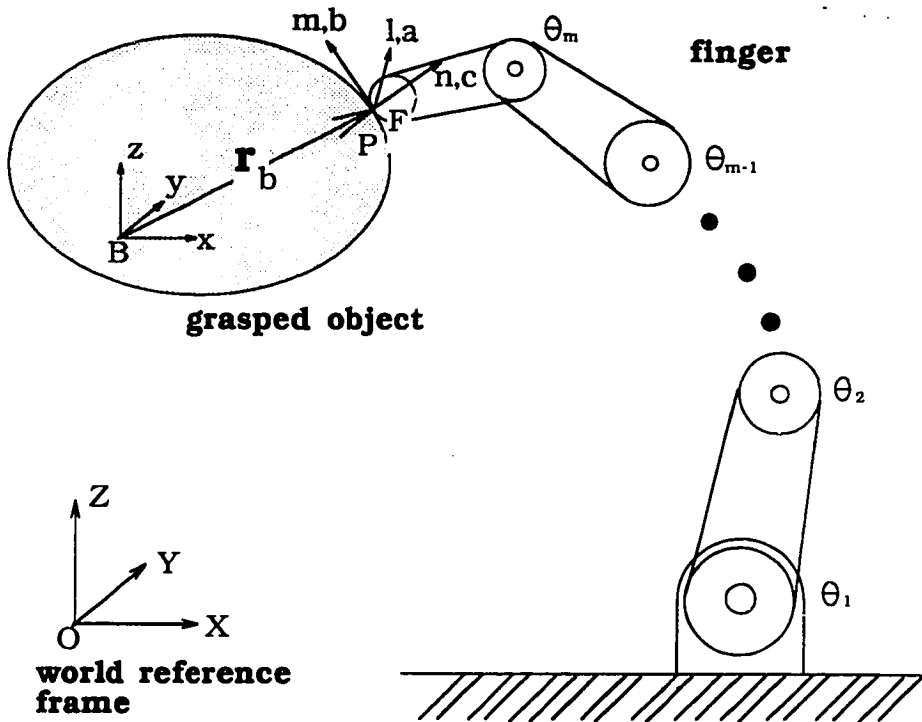


Figure 3.1: Coordinate systems for a single finger touching a grasped object

motion	$\mathbf{J}_\theta \delta\theta = \delta\mathbf{x}_f$ ($6 \times m$) ($m \times 1$)	$\mathbf{H} \delta\mathbf{x}_f = \delta\mathbf{x}_{tr} = \mathbf{H} \delta\mathbf{x}_p$ ($n \times 6$) (6×1) ($n \times 1$)	${}^P_B \mathbf{J} \delta\mathbf{x}_b = \delta\mathbf{x}_p$ (6×6) (6×1) (6×1)
	JOINTS	\iff	CONTACT
force	$\mathbf{J}_\theta^T \mathbf{f}_f = \boldsymbol{\tau}$ ($m \times 6$) (6×1) ($m \times 1$)	$\mathbf{f}_f = \mathbf{H}^T \mathbf{f}_{tr} = \mathbf{f}_p$ (6×1) ($6 \times n$) ($n \times 1$) (6×1)	${}^P_B \mathbf{J}^T \mathbf{f}_p = \mathbf{f}_b$ (6×6) (6×1) (6×1)

Table 3.1: Forward force/motion relationships for finger and object in Figure 3.1

3.3.1 Forward force/motion relationships

Figure 3.1 shows the coordinate systems of a finger with respect to the grasped object. For a given infinitesimal motion $\delta\theta$ in the joint space, the corresponding motion of the fingertip, $\delta\mathbf{x}_f$, can be found by the Jacobian matrix:

$$\mathbf{J}_\theta \delta\theta = \delta\mathbf{x}_f \quad (3.2)$$

where the Jacobian matrix [Craig 1989], \mathbf{J}_θ , relates joint velocities to tip velocities in the $F(abc)$ coordinate system. By employing the principle of virtual work, one can relate the joint torques, τ , and the force applied at the fingertip, \mathbf{f}_f :

$$\tau^T \delta\theta = \mathbf{f}_f^T \delta\mathbf{f}_f = \mathbf{f}_f^T \mathbf{J}_\theta \delta\theta$$

Therefore,

$$\mathbf{J}_\theta^T \mathbf{f}_f = \tau. \quad (3.3)$$

Let us also define a 6×6 cartesian transformation matrix [Craig 1989], ${}^P_B\mathbf{J}_i$, between the $B(xyz)$ coordinate system in the body and the $P(lmn)$ system at the contact point. ${}^P_B\mathbf{J}_i$ relates the motion of the contact point P on the object, $\delta\mathbf{x}_{p_i}$, to the motion of the grasped object, $\delta\mathbf{x}_b$:

$${}^P_B\mathbf{J}_i \delta\mathbf{x}_b = \delta\mathbf{x}_{p_i}. \quad (3.4)$$

From the principle of virtual work, it can also be shown that

$$\mathbf{f}_b = \sum_{i=1}^{n_f} {}^P_B\mathbf{J}_i^T \mathbf{f}_{p_i}. \quad (3.5)$$

where \mathbf{f}_{p_i} is the contact force applied by each fingertip, and \mathbf{f}_b is the resultant force/moment vector expressed in the $B(xyz)$ coordinates of the grasped object. Table 3.1 summarizes the forward force/motion relationships for a single finger touching an object.

3.3.2 Contact constraints

At each contact, the force and velocity constraints are represented by an $n \times 6$ matrix, \mathbf{H} , such that

$$\mathbf{H}\delta\mathbf{x}_p = \mathbf{H}\delta\mathbf{x}_f = \delta\mathbf{x}_{tr}. \quad (3.6)$$

where $\delta\mathbf{x}_{tr}$, is the vector of translation and rotation components that must be identical on each side of the contact. The matrix, \mathbf{H}_i , is a function of the contact type. Thus, for a soft finger as defined by Salisbury [1985]:

$$\mathbf{H} = \begin{bmatrix} 1 & 0 & 0 & 0 & 0 & 0 \\ 0 & 1 & 0 & 0 & 0 & 0 \\ 0 & 0 & 1 & 0 & 0 & 0 \\ 0 & 0 & 0 & 0 & 0 & 1 \end{bmatrix}$$

and for a point contact finger:

$$\mathbf{H} = \begin{bmatrix} 1 & 0 & 0 & 0 & 0 & 0 \\ 0 & 1 & 0 & 0 & 0 & 0 \\ 0 & 0 & 1 & 0 & 0 & 0 \end{bmatrix}$$

The reciprocal force constraints at the contact can be derived from force equilibrium:

$$\mathbf{f}_p = \mathbf{f}_f = \mathbf{H}^T \mathbf{f}_{tr} \quad (3.7)$$

where \mathbf{f}_{tr} is a vector of the force and moment components that are transmitted through the contact. Thus, for a point contact with friction \mathbf{f}_{tr} is a 3×1 vector, and the number of non-zero elements in \mathbf{f}_p or \mathbf{f}_f is three. In the following derivations, the fact that \mathbf{H}^T is the generalized inverse of \mathbf{H} will also be used.

3.3.3 Concatenated force/motion relationships

For a set of nf fingers grasping an object, the matrices ${}^p\mathbf{J}$, \mathbf{H} and \mathbf{J}_θ can be concatenated so that the force/motion relationships for all the fingers of a grasp can

be simultaneously expressed. The new equations have the same form as those in Table 3.1:

$$\mathcal{J}_\theta \delta\theta = \delta\mathbf{x}_f \quad (3.8)$$

$$(\mathcal{J}_\theta)^T \mathbf{f}_f = \tau \quad (3.9)$$

where τ and $\delta\theta$ are concatenated vectors of all the joint torques and infinitesimal joint motions, and \mathbf{f}_f and $\delta\mathbf{x}_f$ are concatenated vectors of forces and infinitesimal motions at the fingertips. The contact equations over all fingertips now become

$$\mathcal{H} \delta\mathbf{x}_p = \mathcal{H} \delta\mathbf{x}_f \quad (3.10)$$

$$\mathbf{f}_p = \mathbf{f}_f = \mathcal{H}^T \mathbf{f}_{tr}. \quad (3.11)$$

Finally, between the contacts and the object $B(xyz)$ coordinate system, we have

$$\begin{array}{ccc} {}^P_B \mathcal{J} & \delta\mathbf{x}_b & = & \delta\mathbf{x}_p \\ (6 \cdot nf \times 6) & (6 \times 1) & & (6 \cdot nf \times 1) \end{array} \quad (3.12)$$

and

$$\begin{array}{ccc} ({}^P_B \mathcal{J})^T & \mathbf{f}_p & = & \mathbf{f}_b \\ (6 \times 6 \cdot nf) & (6 \cdot nf \times 1) & & (6 \times 1) \end{array} \quad (3.13)$$

where ${}^P_B \mathcal{J}$ is a $(6 \cdot nf \times 6)$ matrix transforming infinitesimal motions, $\delta\mathbf{x}_b$, of the object to equivalent motions at all of the contacts.

3.4 Forward stiffness computation

In the following sections a framework for stiffness computation is developed. It includes the effects of:

- servo compliance
- structural compliance
- changes in geometry

- coupling among different joints and fingers
- different contact types
- changes in contact location (e.g. due to rolling)

3.4.1 Stiffness of a grasp – \mathbf{K}_b and \mathbf{K}_J

Equation (3.1) can be expanded by the chain rule, using equations (3.11) and (3.13):

$$\frac{\partial \mathbf{f}_b}{\partial \mathbf{x}_b} = \frac{\partial (\mathbf{^P_B J^T f}_f)}{\partial \mathbf{x}_b} = \underbrace{(\mathbf{^P_B J^T})}_{\mathbf{K}_b} \frac{\partial \mathbf{f}_f}{\partial \mathbf{x}_b} + \underbrace{\frac{\partial (\mathbf{^P_B J^T})}{\partial \mathbf{x}_b} \mathbf{f}_f}_{\mathbf{K}_J}. \quad (3.14)$$

The first part of the right hand side of equation (3.14) expresses the restoring forces at the contacts resulting from the structural and servo stiffnesses of the fingers. The matrix associated with these terms is \mathbf{K}_b , and is derived in Section 3.4.2. The second term, \mathbf{K}_J , represents the effects of small changes in the grasp configuration. These terms become important when the grasp forces, \mathbf{f}_f , are large compared to the restoring forces. \mathbf{K}_J is derived in Section 3.4.3.

3.4.2 Computing \mathbf{K}_b : the effects of restoring forces

In this section the expressions for the compliances of the fingers are derived, beginning with the individual joint and structural compliances. Next, the contact constraints are imposed and the fingertip stiffness matrix is transformed to the body coordinate frame to obtain the contribution of joint and structural compliances to the overall grasp stiffness.

As discussed in previous analyses [Salisbury 1985], the joint stiffnesses, $\mathbf{K}_{\theta_{ij}}$, are due, to first order, to position feedback gains in the fingers. Thus a single finger with m joint servos, would produce an $m \times m$ joint stiffness matrix, \mathbf{K}_θ , which could be inverted to obtain a joint compliance matrix, \mathbf{C}_θ . Often, however, the fingers will

be coupled. For example, the human hand exhibits both active (servo) and passive (structural) coupling among the fingers. If we wiggle our fourth fingers, it is nearly impossible to keep the third and fifth fingers from moving in sympathy. Therefore, a concatenated compliance matrix is established for all joints:

$$\mathcal{C}_\theta = \mathcal{K}_\theta^{-1} = \begin{bmatrix} \mathbf{C}_{\theta_{11}} & \mathbf{C}_{\theta_{12}} & \dots & \mathbf{C}_{\theta_{1,nf}} \\ \mathbf{C}_{\theta_{21}} & \mathbf{C}_{\theta_{22}} & \dots & \mathbf{C}_{\theta_{2,nf}} \\ \vdots & & & \\ \dots & & & \mathbf{C}_{\theta_{nf,nf}} \end{bmatrix}. \quad (3.15)$$

If the $\mathbf{C}_{\theta_{i,i}}$ matrices are not diagonal, we have intra-finger coupling; whereas if $\mathbf{C}_{\theta_{i,j}} \neq 0$ for $i \neq j$, we have inter-finger coupling between fingers i and j .

From equation (3.8), we recall that

$$\underbrace{\begin{bmatrix} \delta x_1 \\ \delta x_2 \\ \vdots \\ \delta x_{nf} \end{bmatrix}}_{\delta \mathbf{x}} = \underbrace{\begin{bmatrix} \mathbf{J}_{\theta_1} & 0 & \dots & 0 \\ 0 & \mathbf{J}_{\theta_2} & \dots & 0 \\ \vdots & & \ddots & \\ 0 & \dots & 0 & \mathbf{J}_{\theta_{nf}} \end{bmatrix}}_{\mathcal{J}_\theta} \underbrace{\begin{bmatrix} \delta \theta_1 \\ \delta \theta_2 \\ \vdots \\ \delta \theta_{nf} \end{bmatrix}}_{\delta \boldsymbol{\theta}} \quad (3.16)$$

We also know that $\delta \boldsymbol{\theta} = \mathcal{C}_\theta \boldsymbol{\tau}$, where $\boldsymbol{\tau}$ is the concatenated vector of all joint torques. Therefore, from equations (3.8) and (3.9), and the principle of virtual work, we can write

$$\delta \mathbf{x}_f = \mathcal{J}_\theta \delta \boldsymbol{\theta} = \mathcal{J}_\theta \mathcal{C}_\theta \boldsymbol{\tau} = \mathcal{J}_\theta \mathcal{C}_\theta \mathcal{J}_\theta^T \mathbf{f}_f \quad (3.17)$$

From equation (3.17), we define

$$\mathcal{C}_j = \mathcal{J}_\theta \mathcal{C}_\theta \mathcal{J}_\theta^T \quad (3.18)$$

where \mathcal{C}_j is the equivalent compliance matrix for the fingertips due to the servo compliance \mathcal{C}_θ . If the fingers are not coupled, \mathcal{C}_j is block-diagonal. More generally, \mathcal{C}_j is a symmetric $(6 \cdot nf \times 6 \cdot nf)$ matrix, (where nf is the number of fingers) but will be singular as long as the fingers have less than 6 degrees of freedom.

To the controllable joint compliances, the uncontrollable structural compliance must be added. In industrial grippers, structural compliance may be negligible but in dexterous hands, the use of actuating cables and soft gripping surfaces leads to significant

<i>component</i>	<i>compliance in m/N</i>
Cable compliance	3.1×10^{-5}
Joint and link compliance	1.0×10^{-5}
Fingertip compliance	1.1×10^{-4}

Table 3.2: Typical structural compliances in the Stanford/JPL hand

compliance. For example, in tests on the Stanford/JPL hand, the typical compliances shown in Table 3.2 were measured. (These values were measured with the fingers extended.) The combined structural compliance, at approximately $10^{-4} N/M$, is roughly 10% of the minimum achievable servo compliance and is therefore significant. In more anthropomorphic hands, with softer links and fingertips, the structural compliance is expected to be correspondingly more important.

The structural compliance matrix varies considerably as a function of finger position, and the problem of computing it is similar to that of computing inertia matrices in robot dynamics. As in dynamics, one possibility is to interpolate among stored values corresponding to different configurations [Raibert 1978]. If the structural compliance is dominated by known flexibilities in the fingertips, links, or cables we can also express the compliance directly in terms of finger orientation. For example, if flexibility in the links is dominant, the structural compliance at each fingertip becomes

$$\mathbf{C}_s = \sum_{j=1}^m \mathbf{J}_{l_j} \mathbf{C}_{l_j} \mathbf{J}_{l_j}^T + \mathbf{C}_{tip} \quad (3.19)$$

where \mathbf{J}_{l_j} is a 6×6 cartesian transformation matrix relating a coordinate system in the j -th link to the $F(abc)$ coordinate system at the fingertip. An example of \mathbf{C}_{tip} is derived in [Cutkosky and Wright 1988] for “very soft” fingertips, and \mathbf{C}_{l_j} can be estimated from elementary beam theory (see Appendix A.1). In general, \mathbf{C}_s is a non-singular 6×6 symmetric matrix, although the terms in \mathbf{C}_s may be small compared to those in \mathbf{C}_j . The individual \mathbf{C}_s matrices can be concatenated directly to form \mathcal{C}_s .

The concatenated fingertip compliance matrix is obtained by summing the joint and

structural compliances for all fingers:

$$\mathcal{C}_f = \mathcal{C}_j + \mathcal{C}_s. \quad (3.20)$$

If \mathcal{C}_f is invertible, which it usually will be if \mathcal{C}_s is not negligible, one can immediately obtain the concatenated fingertip stiffness matrix \mathcal{K}_f . However, as observed earlier, the contact matrices, \mathcal{H} , “filter out” some of the forces and motions at the contacts. Hence not all elements of \mathcal{K}_f will be experienced by the grasped object. Therefore, equations (3.10) and (3.11) are used to define a new stiffness matrix, $(\mathcal{H}\mathcal{C}_f\mathcal{H}^T)^{-1}$ that represents the finger stiffness components seen through the contacts. Then, applying equations (3.10) and (3.11) again, one can expand this stiffness to a (usually singular) matrix for the contact points on the object:

$$\mathcal{K}_p = \mathcal{H}^T (\mathcal{H} \mathcal{C}_f \mathcal{H}^T)^{-1} \mathcal{H}. \quad (3.21)$$

Note that if structural compliance is negligible, the product $(\mathcal{H}\mathcal{C}_f\mathcal{H}^T)^{-1}$ will still be invertible as long as the grasp is fully “manipulable,” i.e., if the fingers can impart arbitrary motions to the object [Salisbury 1985]. As will be discussed in Chapter 4, the expression for \mathcal{K}_p is particularly useful for sliding analyses, as its partitions, $\mathcal{K}_{p_{ij}}$, indicate the stiffnesses that the object “sees” at each contact point.

Finally, in terms of the $B(xyz)$ coordinate system of the object, we apply equations (3.12) and (3.13) to derive

$$\mathbf{f}_b = {}^P_B \mathcal{J}^T \mathbf{f}_p = {}^P_B \mathcal{J}^T \mathcal{K}_p \delta \mathbf{x}_p = ({}^P_B \mathcal{J}^T \mathcal{K}_p {}^P_B \mathcal{J}) \delta \mathbf{x}_b.$$

Therefore, we obtain

$$\mathbf{K}_b = {}^P_B \mathcal{J}^T \mathcal{K}_p {}^P_B \mathcal{J} \quad (3.22)$$

where \mathbf{K}_b is a 6×6 matrix representing the stiffness of the grasped object, due to servo and structural terms.

3.4.3 Computing \mathbf{K}_J : the effects of changes in geometry

When a grasped object is displaced slightly, two things happen which may affect the overall grasp stiffness and stability: the fingers shift slightly with respect to the object

and, if the fingers roll or slide, the contact points move upon the object. To compute the effects of these changes in the grasp geometry we first need to find an expression for the complete motions of the fingertips.

The following results will be derived for a single finger, as in Figure 3.1 and Table 3.1, since the overall effect can be obtained simply by summing the contributions of all fingers:

$$\mathbf{K}_J = \sum_{i=1}^{n_f} \mathbf{K}_{J_i}. \quad (3.23)$$

From the contact velocity constraints in Table 3.1, we can specify some, but not all, of the components of the fingertip motion when the object is displaced slightly. We need to make some assumptions about the fingertip control to determine the remaining components. One possibility is to assume that the fingertip orientation remains essentially fixed with respect to some global coordinate system. For long, multijointed fingers with point contact, this is probably a reasonable assumption. A more general assumption is that like any underconstrained elastic mechanism, the grasp will adopt a configuration that minimizes its potential energy, subject to kinematic constraints. In this case we can solve for the motion of the fingertips using Lagrange multipliers. Since the grasp is initially at equilibrium, displacing the object will increase the potential energy:

$$\Delta p.e. = \frac{1}{2}(\delta \mathbf{x}_f^T \mathcal{K}_f \delta \mathbf{x}_f) - \delta \mathbf{x}_f^T \mathbf{f}_f \quad (3.24)$$

where $-\delta \mathbf{x}_f^T \mathbf{f}_f$ represents work done against the initial grasp forces. Note that the potential energy includes the combined structural and servo stiffness. To minimize $\Delta p.e.$ subject to the constraint $\mathcal{H}(\delta \mathbf{x}_f - \delta \mathbf{x}_p) = 0$ in equation (3.10), we define the “cost function” c as

$$c = \Delta p.e. + \mathbf{l}^T \mathcal{H}(\delta \mathbf{x}_f - {}_B \mathcal{J} \delta \mathbf{x}_b) \quad (3.25)$$

where \mathbf{l} is a vector of the n Lagrange multipliers. To find the solution, we differentiate c with respect to $\delta \mathbf{x}_f$ and obtain

$$\delta \mathbf{x}_f^T \mathcal{K}_f - \mathbf{f}_f^T + \mathbf{l}^T \mathcal{H} = 0$$

or

$$\mathcal{K}_f \delta \mathbf{x}_f + \mathcal{H}^T \mathbf{l} = \mathbf{f}_f \quad (3.26)$$

Combining equations (3.10) and (3.26), we have a matrix equation expressed in fingertip coordinates:

$$\begin{bmatrix} \mathcal{K}_f & \mathcal{H}^T \\ \mathcal{H} & 0 \end{bmatrix} \begin{bmatrix} \delta \mathbf{x}_f \\ \mathbf{l} \end{bmatrix} = \begin{bmatrix} \mathbf{f}_f \\ \mathcal{H} \delta \mathbf{x}_p \end{bmatrix} \quad (3.27)$$

If \mathcal{K}_f cannot be obtained by inverting \mathcal{C}_f , due to negligible structural compliance, the equations can be solved in the finger joint space. Solving for $\delta \mathbf{x}_f$ (where $\delta \mathbf{x}_f$ is the concatenated vector of all fingertip motions), we obtain:

$$\begin{bmatrix} \delta \mathbf{x}_f \\ \mathbf{l} \end{bmatrix} = \begin{bmatrix} \mathcal{K}_f & \mathcal{H}^T \\ \mathcal{H} & 0 \end{bmatrix}^{-1} \begin{bmatrix} \mathbf{f}_f \\ \mathcal{H} \delta \mathbf{x}_p \end{bmatrix}. \quad (3.28)$$

For particular contact types with decoupled servo stiffness, the partitions of the inverse matrix in equation (3.28) can be computed symbolically in terms of \mathbf{C}_f for each finger. Appendix (A.2) shows the solution for $\delta \mathbf{x}_{f_i}$ (where $\delta \mathbf{x}_{f_i}$ is the motion of each fingertip) for the case of independent point contacts with friction, when \mathcal{K}_f is block-diagonal.

While $\delta \mathbf{x}_{f_i}$ represents the absolute motion of a fingertip, $(\delta \mathbf{x}_{f_i} - \delta \mathbf{x}_{p_i})$ represents the relative motion of the fingertip with respect to the object. Expressed in the body coordinate frame $B(xyz)$, the relative motion becomes

$${}^B \mathbf{J}_i^{-1} (\delta \mathbf{x}_{p_i} - \delta \mathbf{x}_{f_i}) = \delta \mathbf{x}_b - {}^B \mathbf{J}_i^{-1} \delta \mathbf{x}_{f_i}. \quad (3.29)$$

By comparing $\delta \mathbf{x}_{f_i}$ and $\delta \mathbf{x}_{p_i}$, it is possible for a given contact geometry and contact type (e.g. rolling contact) to determine how the contact point is moving upon the object. Figure 3.2 shows the contact coordinate systems before and after a fingertip has rolled slightly. The details of computing the motion of the contact can be complex, but solutions are discussed in [Kerr 1986] and [Ji 1987] and, for the special case in which the finger does not twist about its own axis while rolling, a first-order approximation is given in [Cutkosky 1985]. For the stiffness analysis, it suffices to

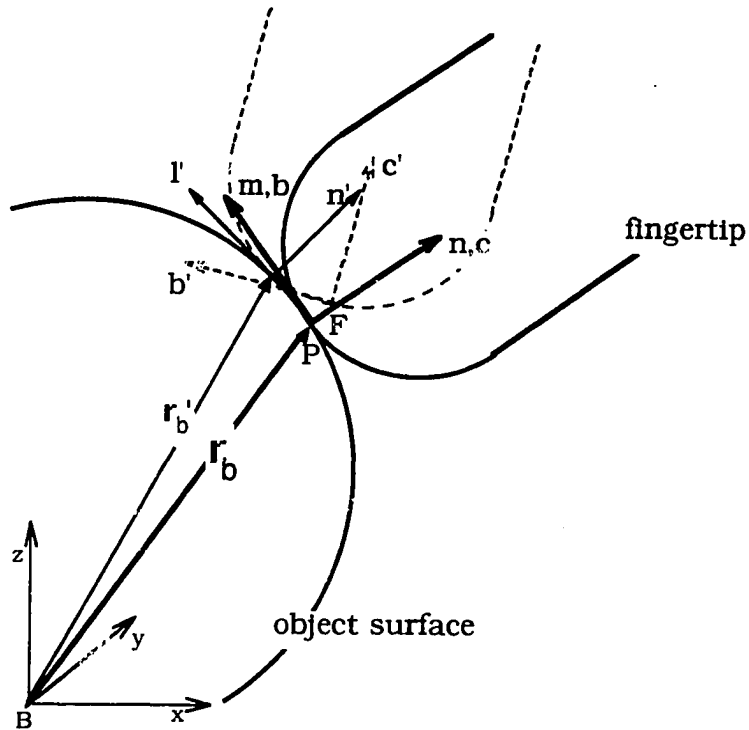


Figure 3.2: Coordinate systems for a finger rolling on a grasped object

find the change in the resultant *force* on the object as the finger rotates with respect to the object and the contact point shifts upon the object. Put another way, from equation (3.11) we know that initially $\mathbf{f}_{pi} = \mathbf{f}_{fi}$, but after infinitesimal motion the force acting at the contact becomes

$$\mathbf{f}'_{pi} = \mathbf{D}_i^T \mathbf{f}_{fi} \quad (3.30)$$

where \mathbf{D}_i is a matrix that relates the linear velocities of the new and previous contact points on the grasped object and expresses them and the angular velocity of the grasped object with respect to the fingertips, in local $P(lmn)$ coordinate frames at the new and previous contact points. Details are given in Appendix A.3. Then, in body coordinates we have

$$\mathbf{f}'_{bi} = {}_B^P \mathbf{J}_i^T \mathbf{D}_i^T \mathbf{f}_{fi} = {}_B^P \mathbf{J}_i^T \mathbf{f}_{fi} + {}_B^P \Delta \mathbf{J}_i^T \mathbf{f}_{fi}. \quad (3.31)$$

If no rolling or sliding occurs, \mathbf{D}_i will contain only rotation terms, but in general both

translations and rotations may be present. Solving for ${}^p_B \Delta J_i^T$, we have

$${}^p_B \Delta J_i^T = {}^p_B J_i^T (D_i^T - I) \quad (3.32)$$

where ${}^p_B \Delta J_i^T$ represents a differential Jacobian due to the changes in the geometry. Details are given in Appendix (A.3).

Multiplying ${}^p_B \Delta J_i^T$ by f_{f_i} gives us $K_{J_i} \delta x_b$, which represents the change in forces due to geometry effects only. Since ${}^p_B \Delta J^T$ can be expressed as a linear function of δx_b , as shown in Appendix (A.3), it is clear that ${}^p_B \Delta J^T f_f$ is a *linear* function of f_f and δx_b only. Since f_f is held constant in defining K_J in equation (3.14), the term ${}^p_B \Delta J^T f_f$ can be written as

$${}^p_B \Delta J^T f_f = \frac{\partial ({}^p_B \Delta J^T f_f)}{\partial \delta x_b} \delta x_b. \quad (3.33)$$

Therefore, we obtain the stiffness matrix due to geometry changes as follows:

$$K_{J_i} = \frac{\partial ({}^p_B \Delta J_i^T f_{f_i})}{\partial \delta x_b} \quad (3.34)$$

Finally, the effective grasp stiffness is obtained by summing K_b from section 3.4.2 and K_{J_i} for all fingers:

$$K_e = K_b + \sum_{i=1}^{n_f} K_{J_i}. \quad (3.35)$$

3.4.4 Scaling K_e by the characteristic length of the grasp

Equation (3.35) expresses the equivalent stiffness of a grasp. However, we often would like to scale a stiffness matrix according to some characteristic length of the grasp so that the linear and rotational terms are of comparable magnitude. The scaling matrix can be expressed as

$$S = \begin{bmatrix} 1 & 0 & 0 & 0 & 0 & 0 \\ 0 & 1 & 0 & 0 & 0 & 0 \\ 0 & 0 & 1 & 0 & 0 & 0 \\ 0 & 0 & 0 & 1/r_c & 0 & 0 \\ 0 & 0 & 0 & 0 & 1/r_c & 0 \\ 0 & 0 & 0 & 0 & 0 & 1/r_c \end{bmatrix} \quad (3.36)$$

where r_c is the characteristic length of the grasp. Therefore, the scaled stiffness matrix, \mathbf{K}_e^\dagger , has consistent units of Nm . \mathbf{K}_e^\dagger is related to \mathbf{K}_e by

$$\mathbf{K}_e = \mathbf{S} \mathbf{K}_e^\dagger \mathbf{S}^T. \quad (3.37)$$

For any infinitesimal displacement from its nominal position, we can compute the increment in force and moment by

$$\delta \mathbf{f} = \mathbf{K}_e \delta \mathbf{x}_b = \mathbf{S} \mathbf{K}_e^\dagger \mathbf{S}^T \delta \mathbf{x}_b. \quad (3.38)$$

3.4.5 Examples of the forward procedure

In the following examples, some of the issues that arise in computing the overall compliance of a grasp are illustrated. To reduce the algebra, Example 3.1 illustrates a grasp with structural compliance but without changes in geometry and Example 3.2 illustrates the effects of changes in grasp geometry, without structural compliance.

Example 3.1 Inserting a rivet into a hole

Figure 3.3 shows two three-joint fingers about to insert a small rivet into a chamfered hole. We wish to find \mathbf{K}_b due to servo and structural compliance. The grasp is inspired by the thumb-index finger “pinch” that people use in precision tasks with tiny objects. The grasp also approximates a two-fingered grasp between the thumb and one of the fingers of the Stanford/JPL hand, except that the base axis of the thumb has been rotated parallel to the base axes of the fingers to simplify the Jacobian. Note that while the grasp appears planar in Figure 3.3, it can manipulate the rivet along the x axis, out of the plane of the page. For realism, let us choose servo and structural compliances comparable to those listed for the Stanford/JPL hand in Table 3.2 and assume “very-soft” contacts between the fingertips and the rivet. The Jacobians and the compliance matrices are given in Appendix (A.4.1). Applying equations (3.15) through (3.22), we arrive at the object stiffness matrix at the tip of the rivet, which

is listed in Appendix (A.4.1). Let us reckon the characteristic length of this grasp as $r = 0.1m$. We can then employ equations (3.36) and (3.37) to find the scaled stiffness matrix, \mathbf{K}_b^\dagger .

$$\mathbf{K}_b^\dagger = \begin{bmatrix} 24.9 & 0 & 0 & 0 & 25.8 & 0 \\ 0 & 289.0 & 0 & 19.1 & 0 & 0 \\ 0 & 0 & 616.1 & 0 & 0 & 0 \\ 0 & 19.1 & 0 & 22 & 0 & 0 \\ 25.8 & 0 & 0 & 0 & 37 & 0 \\ 0 & 0 & 0 & 0 & 0 & 35 \end{bmatrix} \times 10^2 Nm$$

Discussion:

Looking at \mathbf{K}_b^\dagger , it is noticed that while the structural compliances are small compared to the servo compliances, (about 10%) they prevent both the grasp and fingertip compliance matrices from becoming singular. By evaluating the eigenvalues of \mathbf{K}_b , we can readily find the stiffest and softest directions. The eigenvalues are all positive, confirming that the grasp is indeed stable. Also, since \mathbf{K}_b^\dagger has full rank, the grasp is a force-closure grasp and can resist forces and moments from any direction⁴. Finally, it is observed that the stiffness matrix is decoupled in the z -direction since the grasp is symmetric about the z axis. If \mathbf{K}_b^\dagger were completely diagonal, the center of compliance of the rivet would be at the $B(xyz)$ origin.

Before leaving this example, it is worth recalling that the stability and full rank properties of this grasp stem from our assumption of “very-soft” fingertips. In fact, the choice of contact model for an example such as this requires some care. The contact areas are small since the head of the rivet is thin. However, if we had assumed point contacts with friction, the change in \mathcal{H} would result in a new stiffness matrix with a singular direction: $\vec{d} = [0 \ 0 \ 0 \ 0 \ 1 \ 0]$. In other words, the grasp could not resist moments about the y axis and would not be a force-closure grasp – which seems unrealistic. A soft-finger model (in which the fingertips are free to roll about their a

⁴However, this grasp cannot *impart* independent forces and motions in all directions, due to kinematic coupling.

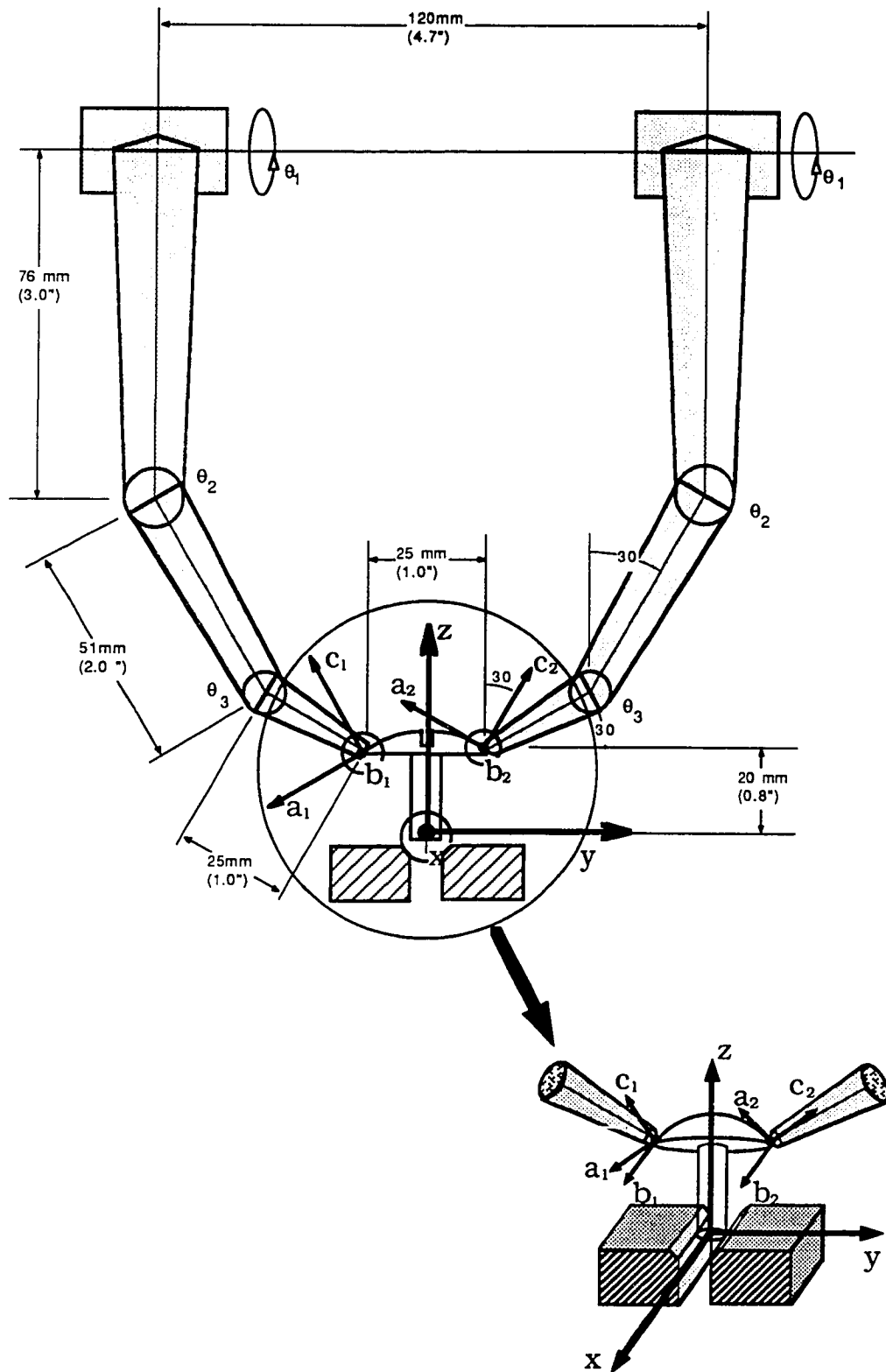


Figure 3.3: Inserting a rivet with two soft-tipped fingers

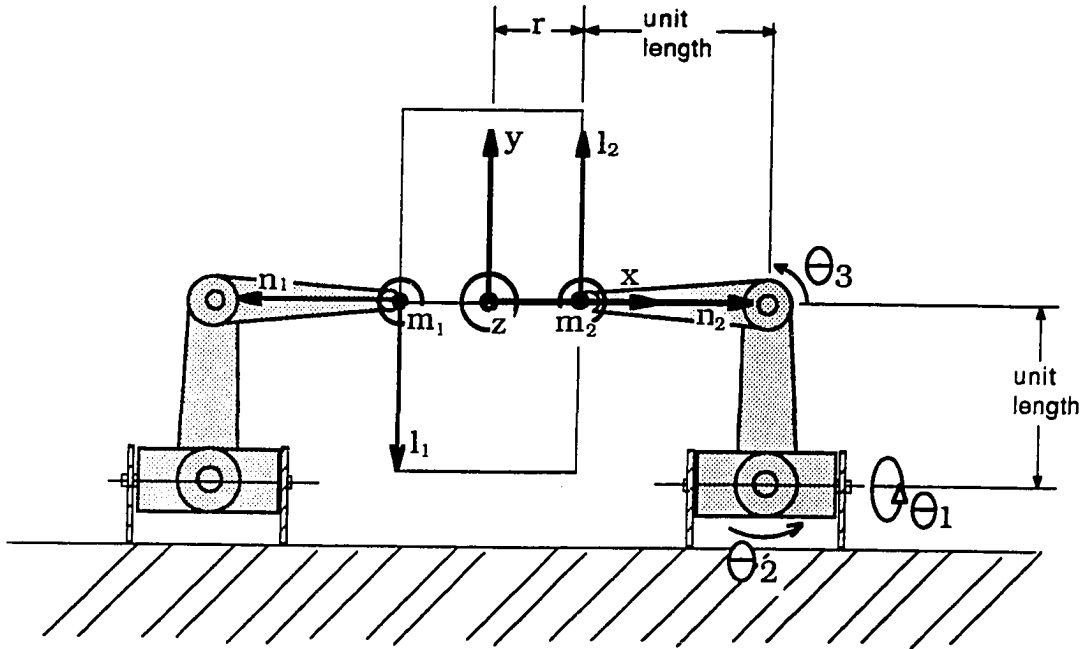


Figure 3.4: A possibly unstable grasp with point-contact fingers

and b axes, but prevented from twisting about their c axes) seems more reasonable, but can also lead to an unrealistic stiffness matrix. Part of the problem is that the surface normal (the direction of the c axis) is poorly defined at the edge of the rivet. In addition, the combination of a rotational constraint about the c axis and a lack of constraint for rotations about the a and b axes, tends to produce a grasp stiffness matrix that is unrealistically stiff with respect to rotations about the z and y axes. As a result, the best model is the “very-soft” finger in which a full 6×6 compliance matrix exists for the contact, but for which rotational compliances are much larger than translational compliances, due to the small contact area. The reader can also verify that this contact model is appropriate when grasping a small object such as a thumbtack between the thumb and index fingers, since the fingertips deform and may even partially enclose the edges of the object. As shown in [Cutkosky and Wright 1988], the very-soft finger model approaches the point-contact model in the limiting case as the contact area becomes small compared to the characteristic lengths of the fingertips or the object.

Example 3.2 *The effect of changes in grasp geometry for two point-contact fingers*

We wish to compute the effective stiffness, including the effects of changes in geometry, for the grasp shown in Figure 3.4. As in Figure 3.3, although the grasp looks planar, it can impart motions into and out of the page. For simplicity, we assume point-contact fingertips and negligible structural compliance. As a result, the grasp stiffness matrix, \mathbf{K}_b , will be singular and we will not have a force-closure grasp. The Jacobians \mathcal{J}_θ and $\mathcal{P}\mathcal{J}$ and the joint stiffness matrix \mathbf{K}_θ are given in Appendix (A.4.2). For a diagonal joint stiffness matrix, and the dimensions shown in Figure 3.4, we apply equations (3.18), (3.21) and (3.22) to obtain

$$\mathbf{K}_b = 2 \begin{bmatrix} (k_b + k_c) & 0 & 0 & 0 & 0 & -rk_c \\ 0 & k_c & 0 & 0 & 0 & 0 \\ 0 & 0 & k_a & 0 & 0 & 0 \\ 0 & 0 & 0 & 0 & 0 & 0 \\ 0 & 0 & 0 & 0 & r^2 k_a & 0 \\ -rk_c & 0 & 0 & 0 & 0 & r^2 k_c \end{bmatrix} \quad (3.39)$$

where r is one half the width of the object. (Because the links have unit length, the translational and rotational stiffness elements may appear to have the wrong dimensions, but they are N/m and Nm, respectively.) As expected \mathbf{K}_b is singular and $\vec{y}=[0\ 0\ 0\ 1\ 0\ 0]$ is the singular direction of the grasp.

We now wish to determine the effects of small changes in the grasp geometry. Following equations (3.23)–(3.34), we obtain \mathbf{K}_j :

$$\mathbf{K}_j = 2 \begin{bmatrix} 0 & 0 & 0 & 0 & 0 & 0 \\ 0 & -f_n & 0 & 0 & 0 & 0 \\ 0 & 0 & 0 & 0 & 0 & 0 \\ 0 & 0 & 0 & 0 & 0 & 0 \\ 0 & 0 & 0 & 0 & -r f_n & 0 \\ 0 & 0 & 0 & 0 & 0 & -r f_n(1+r) \end{bmatrix} \quad (3.40)$$

where f_n represents the initial normal grasp force applied at the fingertips. As in \mathbf{K}_b , linear and rotational stiffness elements may appear to have the wrong dimensions, but

this is an artifact of the unit link lengths. It is observed that \mathbf{K}_j is singular because the grasp geometry is unaffected by moving the object along the x axis or rotating it about the x axis. In addition, since the fingertips cannot rotate about their b axes, there is no change in the grasp geometry for small motions in the z direction. More importantly, the stiffness terms corresponding to rotations about the y and z axes are negative. Thus, \mathbf{K}_j tends to *destabilize* the grasp.

The effective grasp stiffness is obtained by adding \mathbf{K}_b and \mathbf{K}_j as in equation (3.35). The resulting expression for \mathbf{K}_e makes intuitive sense:

$$\mathbf{K}_e = 2 \begin{bmatrix} (k_b + k_c) & 0 & 0 & 0 & -rk_c \\ 0 & (k_c - f_n) & 0 & 0 & 0 \\ 0 & 0 & k_a & 0 & 0 \\ 0 & 0 & 0 & 0 & 0 \\ 0 & 0 & 0 & r(rk_a - f_n) & 0 \\ -rk_c & 0 & 0 & 0 & r(rk_c - f_n - rf_n) \end{bmatrix} \quad (3.41)$$

Discussion:

The effective stiffness matrix of this grasp reveals important grasp properties. For example, since \mathbf{K}_e is singular, we know that the grasp is not a force-closure grasp. Examination of the fourth row and column reveals that this is because the grasp cannot impart or resist moments about the x axis. In addition, it is found that if either

$$f_n \geq rk_a \quad \text{or} \quad f_n \geq \left(\frac{rk_c}{r+1} \right) \left(\frac{k_b}{k_b + k_c} \right),$$

\mathbf{K}_e will not be positive definite and the grasp will be unstable. We also see that for a given object size and finger stiffness, pressing harder without increasing the finger stiffness makes the grip less stable. This effect is easily demonstrated by pressing a small coin on edge between two fingers and gradually increasing the grasp force until the coin snaps over. In fact, since human muscles tend to become stiffer when larger forces are applied, there is some automatic compensation for this instability. If we purposefully tense our muscles, thereby increasing \mathbf{K}_b , we can preserve the positive definiteness of \mathbf{K}_e for large grasp forces.

3.5 Reverse stiffness computation – controlling the grasp stiffness

Given an initial grasp and a manipulation task, how should we control the finger joints so as to achieve a desired grasp stiffness?

Working backwards from equation (3.35), we have

$$\mathbf{K}_b = \mathbf{K}_e - \sum_{i=1}^{nf} \mathbf{K}_{j_i}$$

where \mathbf{K}_e is the desired grasp stiffness and \mathbf{K}_j is a function of the grasp geometry. There are then two major steps in the reverse procedure: (1) obtain \mathcal{K}_p from the desired \mathbf{K}_b , and (2) obtain C_θ or K_θ from \mathcal{K}_p . We see from equations (3.21) and (3.22) that we can expand the contact stiffness as

$$\mathcal{K}_p = \begin{bmatrix} \mathbf{K}_{p_{11}} & \mathbf{K}_{p_{12}} & \dots & \mathbf{K}_{p_{1,nf}} \\ \mathbf{K}_{p_{21}} & \mathbf{K}_{p_{22}} & \dots & \mathbf{K}_{p_{2,nf}} \\ \ddots & & & \\ \dots & & & \mathbf{K}_{p_{nf,nf}} \end{bmatrix} \quad (3.42)$$

where $\mathbf{K}_{p_{ij}}$ are the desired submatrices of \mathcal{K}_p that we wish to specify. Note that for $i \neq j$, $\mathbf{K}_{p_{ij}}$ represent coupling terms among the joints on different fingers. These terms provide us with considerably more control over \mathbf{K}_b than we could obtain from independently servoed fingers.

Equation (3.22) presents an underconstrained problem: there are many possible \mathcal{K}_p that will satisfy \mathbf{K}_b . However, there are also numerous constraints on \mathcal{K}_p imposed by the kinematics of the fingers, the contact types and the joint configurations. The reverse compliance procedure is consequently difficult, often involving both overconstraint and underconstraint in a single grasp. The problem is similar to reverse force or velocity computations, for which solutions have been presented by Kobayashi [1985] and Kerr [1986], but is more complicated due to off-diagonal terms in the stiffness matrix and due to structural compliances. However, as we shall see in the following

section, these extra terms also afford us more opportunities to achieve a desired grasp stiffness.

Before launching into an exploration of general, three-dimensional reverse compliance it is worth examining a simple case that provides us with some physical insight for what can happen.

Example 3.3 *Controlling the compliance of a planar grasp*

The dimensions and configuration of a simple, two-fingered grasp are shown in Figure 3.5. Since this is a planar problem, forces and motions are represented by three-element vectors with two linear components and one rotation: $[x, y, \phi]$. The Jacobian matrix of the left finger is

$$\mathbf{J}_{\theta_1} = \begin{bmatrix} 0 & -1 \\ 2 & 1 \\ 1 & 1 \end{bmatrix} \quad (3.43)$$

which maps joints to the cartesian coordinates $[l_1, n_1, \phi_{m_1}]$, and the right finger follows from symmetry. It will be assumed that structural compliance is confined to the fingertips and that the contact areas are small enough that the contact behaves nearly as a point contact. The symbolic \mathcal{C}_θ , \mathcal{H} and \mathcal{C}_s matrices are given in Appendix (A.4.3). If the grasp is kept symmetric, the forward and reverse compliance computations are simple enough to perform symbolically.

We want to locate the center of compliance [Whitney 1980] of the object, (the point for which the stiffness or compliance matrix becomes diagonal) at an arbitrary location, while also maintaining a stable (positive-definite) stiffness matrix and controlling the magnitude of the stiffnesses in the x , y and ϕ directions. Four different cases, of increasing complexity, are examined:

1. No coupling in the control of the joints (\mathcal{K}_θ or \mathcal{C}_θ is diagonal)
2. Coupling only between the joints on each finger (\mathcal{K}_θ or \mathcal{C}_θ is block-diagonal)
3. Full coupling among all joints

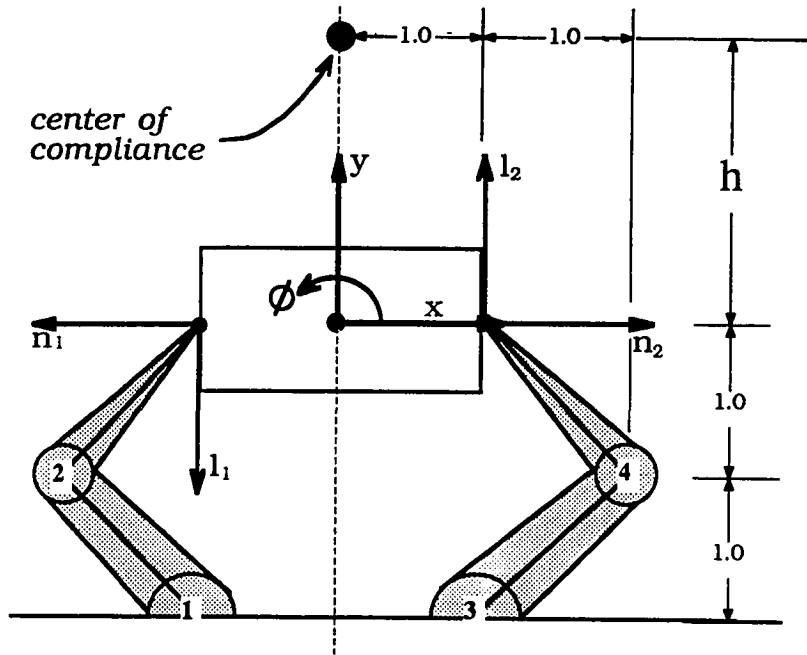


Figure 3.5: Coordinates and center of compliance for a planar grasp

4. An over-constrained case in which the lower right joint is locked

In general, the planar grasp stiffness matrix, \mathbf{K}_b , is a 3×3 symmetric matrix, resulting in 6 equations. However, since this grasp is symmetric, its stiffness will always be uncoupled with respect to forces and motions along the centerline of the grasp, provided we control the joints symmetrically. In this case, there are only 4 equations to satisfy. For the \mathcal{C}_θ , \mathcal{H} and \mathcal{C}_s matrices in Appendix (A.4.3), it can be shown that the location of the center of compliance with respect to the $B(xyz)$ origin is

$$h = \frac{C_{\theta_{24}} + C_{\theta_{22}} + 2C_{\theta_{14}} + 2C_{\theta_{12}}}{C_s + C_{\theta_{24}} + C_{\theta_{22}}} \quad (3.44)$$

where $C_{\theta_{ij}}$ are the elements of $\mathcal{C}_\theta = \mathcal{K}_\theta^{-1}$ in Appendix (A.4.3), and are controlled by adjusting servo gains.

Case 1: no coupling

With no coupling, C_θ is diagonal and $C_{\theta_{24}}$ and $C_{\theta_{12}}$ are zero so that

$$h = \frac{C_{\theta_{22}}}{C_s + C_{\theta_{22}}}.$$

As we might expect from examining the designs of Remote-Center-Compliance (RCC) devices [Whitney 1980], [Cutkosky and Wright 1985], $h \rightarrow 0$ as the structural compliance becomes very large and $h \rightarrow 1$ when structural compliance is negligible. The latter case corresponds to the instantaneous center of rotation of a linkage formed by the fingers and object in Figure 3.5. By adjusting the compliance of the second joints of the fingers we could, in theory, vary h between 0 and 1, except that there are practical upper and lower bounds on $C_{\theta_{22}}$. The lower bound is established by the maximum servo stiffness ($1/C_{\theta_{22}}$) that we can reasonably obtain while the upper bound is determined by the need to keep C_θ positive definite so that the grasp is stable.

Case 2: intra-finger coupling

If coupling between the first and second joint of each finger is allowed, we obtain another independent variable, $C_{\theta_{12}}$, that we can use in controlling \mathbf{K}_b and h . The resulting expression for h is:

$$h = \frac{C_{\theta_{22}} + 2C_{\theta_{12}}}{C_s + C_{\theta_{22}}}$$

It would now appear that we could place the center of compliance anywhere along the centerline of the grasp except that again, we are limited by achievable upper bounds on the servo stiffnesses, and by the need to keep C_θ positive definite. If we look at the limiting case in which we are trying to maximize h , (in which case C_s should approach zero) we arrive at the following bounds on h , in terms of the elements of C_θ to keep the joint compliance matrix positive definite:

$$1 - 2\sqrt{\frac{n}{C_{\theta_{22}}} - 1} < h < 1 + 2\sqrt{\frac{n}{C_{\theta_{22}}} - 1} \quad (3.45)$$

where $n = (C_{\theta_{11}} + C_{\theta_{22}})$ is the trace of C_θ .

Case 3: inter- and intra-finger coupling

In contrast with the last two cases, if coupling among the joints on different fingers is

permitted, the expression for k is given by equation (3.44), from which it is clear that we now have considerably more freedom in controlling h while keeping \mathcal{C}_θ positive definite by choosing appropriate off-diagonal terms.

Case 4: over-constraint

Suppose that the lower right joint is locked, so that we have a hand with just three joints. Can we still control \mathbf{K}_b ? If we use coupling among all the joints, we have 6 independent variables, which would seem to be enough to control the 6 independent elements of \mathbf{K}_b (the grasp is no longer symmetric). However, our intuition tells us that with only a single link on the right side, we will run into difficulties, since the tip of the link cannot move in the x direction without also moving in the y direction.

The symbolic expression for this non-symmetric grasp matrix is complicated, but some special cases are worth examining. To begin with, we *must* have structural compliance to achieve any control of \mathbf{K}_b . In addition, if we try to diagonalize \mathbf{K}_b at the origin we discover that this is only possible if the diagonal terms, k_{b11} and k_{b33} (corresponding to stiffnesses in the x and ϕ directions, respectively) are also zero. More generally, it is possible to achieve a variety of \mathbf{K}_b matrices, but our options are severely constrained. For example, if we try to place the center of compliance at a location [0 1 0] with stiffnesses in the x , y and ϕ directions of 50, 75, and 100, the resulting joint stiffness matrix,

$$\mathbf{K}_\theta = \begin{bmatrix} -100 & 0 & 100 \\ 0 & 50 & -50 \\ 100 & -50 & 50 \end{bmatrix}, \quad (3.46)$$

is not positive definite.

This raises an interesting issue: How can one be sure that the reverse compliance procedure will not produce joint stiffness matrices with negative eigenvalues, and more importantly, how can one be sure that a positive definite joint stiffness matrix will not produce an unstable \mathbf{K}_b matrix? Fortunately, it can be shown that while a positive definite \mathbf{K}_b matrix does not always produce a positive definite \mathcal{K}_θ matrix, the reverse is always true. The proof is given in Appendix (A.5). Thus, a safe approach

is to require that \mathcal{K}_θ be positive definite and to use the off-diagonal terms resulting from coupling among the joints to increase the positive definiteness of \mathcal{K}_θ .

3.5.1 An approach to reverse stiffness computation

The planar example in the last section has given us some idea of what to expect when solving for \mathcal{K}_θ to achieve a desired \mathbf{K}_b . The basic problem is to ensure that the limitations of the contacts and finger joints are reflected in \mathcal{K}_p .

The two steps of the reverse procedure will be elaborated in the following. First, we have to find a matrix \mathcal{K}_p that satisfies equation (3.22). As discussed previously, this is an underconstrained problem, and many solutions exist. However, \mathcal{K}_p must also satisfy contact and joint constraints:

1. **contact constraints:** The desired value of \mathcal{K}_p should reflect the constraints represented by \mathcal{H} . In other words, \mathcal{K}_p should have the same zero rows and columns as $\mathcal{H}^T \mathcal{H}$. This is because $\mathcal{K}_p = \mathcal{H}^T (\mathcal{H} \mathcal{C}_f \mathcal{H}^T)^{-1} \mathcal{H}$, as shown in equation (3.21).
2. **joint constraints:** To ensure that the fingers can fully control the \mathcal{K}_p matrix, we require that the null space of the product

$$\Omega = (\mathcal{C}'_s, -\mathcal{C}'_s \mathcal{H} \mathcal{K}_p \mathcal{H}^T \mathcal{C}'_s) \quad (3.47)$$

should be the same as the left null space of

$$\mathcal{B} = \mathcal{H} \mathcal{J}_\theta \quad (3.48)$$

where $\mathcal{C}'_s = \mathcal{H} \mathcal{C}_f \mathcal{H}^T$ (the structural compliance of the fingertip as seen by the object through the contact). The derivation is given in Appendix (A.6). As an example, in the over-constrained case from Example 3.3, the finger tip on the right is constrained to move in the $\pm[1 \ 1 \ 0]$ direction, which is orthogonal to the null space of Ω ($[1 \ -1 \ 0]$).

The remaining requirement, which surfaced in the over-constrained example in the last section, is that \mathcal{C}_θ should be kept positive definite so that \mathbf{K}_θ will be positive definite (or positive semidefinite for a non-force-closure grasp). In addition, it may be useful to impose other restrictions for numerical or controls reasons.

Once we have found a suitable \mathcal{K}_p matrix that satisfies the above constraints, it is straightforward to find \mathcal{K}_θ . The presence of structural compliance provides some complication but, following the derivation in Appendix (A.6), it can be shown that

$$\mathcal{K}_\theta = \mathcal{C}_\theta^{-1} = [(\mathcal{H}\mathcal{J}_\theta)^*(\mathcal{C}'_s - \mathcal{C}'_s\mathcal{H}\mathcal{K}_p\mathcal{H}^T\mathcal{C}'_s)(\mathcal{J}_\theta^T\mathcal{H}^T)^*]^{-1} - (\mathcal{J}_\theta^T\mathcal{H}^T\mathcal{C}'_s^{-1}\mathcal{H}\mathcal{J}_\theta) \quad (3.49)$$

where the superscript “*” denotes generalized inverse.

3.5.2 Examples of the reverse procedure

In this section, examples are used to illustrate the issues in computing the joint stiffness to achieve the desired grasp stiffness as closely as possible. Example 3.4 is an example of a reverse stiffness computation for the grasp in Example 3.1.

Example 3.4 Reverse compliance computation for an assembly problem

Let us return to the three-dimensional grasp of Example 3.1, and attempt to determine appropriate joint stiffnesses so as to achieve a desired stiffness for the rivet. As Whitney [1980] and others have demonstrated, it is ideal if the center of compliance of the rivet is placed at or near its tip. Therefore, a stiffness matrix which is diagonal at the $B(xyz)$ origin is desired. In this example, the changes in geometry are neglected because of small grasp forces, i.e., \mathbf{K}_J is negligible. In addition, it is desirable for the stiffness along the x and y axes to be relatively small. The desired grasp stiffness

matrix, scaled by the matrix \mathbf{S} as in Example 3.1, is therefore as follows:

$$\mathbf{K}_e^\dagger = \begin{bmatrix} 40 & 0 & 0 & 0 & 0 & 0 \\ 0 & 104 & 0 & 0 & 0 & 0 \\ 0 & 0 & 490 & 0 & 0 & 0 \\ 0 & 0 & 0 & 0.1 & 0 & 0 \\ 0 & 0 & 0 & 0 & 14 & 0 \\ 0 & 0 & 0 & 0 & 0 & 27 \end{bmatrix} \times 10^2$$

where units are in N/m.

Referring to equations (3.47) and (3.48), a concatenated grasp stiffness matrix, \mathcal{K}_p , that satisfies the criteria listed earlier in this section is constructed. The result is shown in Appendix (A.4.4). Then, applying equation (3.49), we obtain \mathcal{K}_θ :

$$\mathcal{K}_\theta = \begin{bmatrix} 37.8 & 0 & 0 & -1.8 & 0 & 0 \\ 0 & 6.6 & -0.0006 & 0 & -3.5 & 3.2 \\ 0 & -0.0006 & 6.7 & 0 & 3.2 & -3 \\ -1.8 & 0 & 0 & 37.8 & 0 & 0 \\ 0 & -3.5 & 3.2 & 0 & 6.6 & -0.0006 \\ 0 & 3.2 & -3 & 0 & -0.0006 & 6.7 \end{bmatrix}$$

which can be checked through the forward procedure. The result is nearly identical to our desired \mathbf{K}_b^\dagger matrix (see Appendix A.4.4).

Discussion:

As expected, \mathcal{K}_θ is a symmetric 6×6 matrix which, like \mathbf{K}_b^\dagger , has rank 6. In addition, although \mathcal{K}_θ is the concatenated stiffness matrix of two three-joint fingers, it is not block-diagonal. In other words, inter- and intra-finger coupling occurs to achieve the desired grasp stiffness.

Suppose that we do not permit coupling between the fingers? Then we cannot expect to achieve an arbitrary \mathbf{K}_b matrix. The problem is that we have only two soft fingers, each with a 4×4 symmetric \mathbf{K}_f matrix providing 10 independent variables. Applying equation (3.22), we have

$$\mathbf{K}_b = {}^p_B \mathcal{J}^T \mathcal{K}_p {}^p_B \mathcal{J}$$

<i>contact type</i>	no coupling	intra-finger coupling	inter-finger coupling
Point contact without friction	21	21	6
Point contact with friction	7	4	3*
Soft contact	6	3	2

*: Three fingers are required to achieve force-closure in addition to controlling all elements of \mathbf{K}_e . If two fingers are used, the non-singular subset of \mathbf{K}_e can be fully controlled.

Table 3.3: Minimum number of fingers needed to control \mathbf{K}_e with and without coupling

which yields up to 21 equations. Therefore, we have a problem with 21 equations for 20 unknowns. If we rewrite the equations in the form $\mathbf{A} \mathbf{x} = \mathbf{b}$, where \mathbf{x} represents the free variables in matrices \mathbf{K}_p , and \mathbf{A} and \mathbf{b} are the known coefficients, the necessary and sufficient conditions for a solution to exist are:

$$\det [\mathbf{A} \mid \mathbf{b}] \equiv 0 \quad \text{and} \quad \mathbf{i}_{21}^T \mathbf{y} \neq 0 \quad (3.50)$$

where \mathbf{i}_{21} is a 21×1 unit vector, with the 21st element being 1, and \mathbf{y} is a vector in the null space of augmented matrix $[\mathbf{A} \mathbf{b}]$. It can be further shown that there is no solution for this grasp if coupling is not allowed. More generally, Table 3.3 shows the *minimum* number of fingers required to fully specify the grasp stiffness for some common contact types.

3.5.3 Reverse procedure for redundant grasps

Recently, much research has been conducted on manipulators with six or more degrees of freedom because they provide more freedom in control and manipulation due to redundancy [Burdick 1988]. The reverse compliance procedure for grasps with redundant degrees of freedom is greatly simplified too. The Penrose-Moore generalized inverse [Strang 1989] can be used to find an optimal solution to these reverse kinematics problems.

We wish to find the servo compliance in the joint space, \mathcal{C}_{θ_i} , such that we can achieve the desired effective stiffness in the body coordinates, \mathbf{K}_e .

From equation (3.35), we have $\mathbf{K}_b = (\mathbf{K}_e - \sum_{i=1}^{n_f} \mathbf{K}_{j_i})$, where \mathbf{K}_e is the desired effective stiffness, and \mathbf{K}_j is the stiffness due to geometry changes, which is a function of initial grasping parameters.

We recall that equation (3.22) can also be expressed as

$$\begin{aligned} \mathbf{K}_b &= \left[{}^p \mathbf{J}_1^T \ {}^p \mathbf{J}_2^T \ \dots \ {}^p \mathbf{J}_{n_f}^T \right] \begin{bmatrix} \mathbf{K}_{p_{11}} & \mathbf{K}_{p_{12}} & \dots & \mathbf{K}_{p_{1,n_f}} \\ \mathbf{K}_{p_{21}} & \mathbf{K}_{p_{22}} & \dots & \mathbf{K}_{p_{2,n_f}} \\ & & \ddots & \\ \mathbf{K}_{p_{n_f,1}} & \dots & \mathbf{K}_{p_{n_f,n_f}} \end{bmatrix} \begin{bmatrix} {}^p \mathbf{J}_1 \\ {}^p \mathbf{J}_2 \\ \vdots \\ {}^p \mathbf{J}_{n_f} \end{bmatrix} \\ &= {}^p \mathbf{J}^T \mathcal{K}_p {}^p \mathbf{J} \end{aligned} \quad (3.51)$$

where ${}^p \mathbf{J}$ and \mathcal{K}_p are concatenated matrices of Jacobians and fingertip stiffness. We can solve for \mathcal{K}_p as

$$\mathcal{K}_p = {}^p \mathbf{J}^{T*} \mathbf{K}_b {}^p \mathbf{J}^* \quad (3.52)$$

where ${}^p \mathbf{J}^{T*}$ and ${}^p \mathbf{J}^*$ are the generalized inverses of ${}^p \mathbf{J}^T$ and ${}^p \mathbf{J}$. Recalling the definition of the Penrose-Moore inverse [Strang 1989], if $\mathbf{A}\mathbf{A}^T$ is invertible then we can define a generalized inverse $\mathbf{A}^* = \mathbf{A}^T(\mathbf{A}\mathbf{A}^T)^{-1}$ such that $\bar{\mathbf{x}} = \mathbf{A}^* \mathbf{b}$ will satisfy the equation $\mathbf{A}\bar{\mathbf{x}} = \mathbf{b}$. Moreover, $\bar{\mathbf{x}}$ is the optimal least squares solution, i.e., the vector $\bar{\mathbf{x}}$ has minimum norm. Therefore, if the matrix $({}^p \mathbf{J}^T \ {}^p \mathbf{J})$ is invertible, we can substitute the generalized inverse of ${}^p \mathbf{J}^T$ and ${}^p \mathbf{J}$ into equation (3.52) to obtain the optimal solution:

$$\mathcal{K}_p = {}^p \mathbf{J} ({}^p \mathbf{J}^T {}^p \mathbf{J})^{-1} \mathbf{K}_b ({}^p \mathbf{J}^T {}^p \mathbf{J})^{-1} {}^p \mathbf{J}^T \quad (3.53)$$

in which the Frobenius norm⁵ of the matrix \mathcal{K}_p is minimized. From a physical standpoint, this is desirable since it will minimize the control effort in achieving \mathcal{K}_p . The matrix inverse of $({}^p \mathbf{J}^T {}^p \mathbf{J})$ usually exists; hence equation (3.53) is solvable. Although there are infinitely many solutions to equation (3.51), only the matrix \mathcal{K}_p obtained in equation (3.53) gives the minimal-norm solution.

⁵Two definitions of matrix norms are often used [Golub and Van Loan 1989]. One is the Frobenius norm, or F -norm, which is defined as $\|A\|_F = [\sum_{i=1}^m \sum_{j=1}^n |a_{ij}|^2]^{1/2}$. The other is the p -norm which is defined as $\|A\|_p = \sup_{x \neq 0} \frac{\|Ax\|_p}{\|x\|_p}$. The matrix norm referred to here is the former one.

As long as \mathcal{K}_p satisfies the contact and joint space constraints discussed in Section 3.5.1, we can take the inverse of \mathcal{K}_p , in the nonsingular subspace, to obtain \mathcal{C}_f at the fingertips. Now, since

$$\mathcal{C}_f = \mathcal{J}_\theta \mathcal{C}_\theta \mathcal{J}_\theta^T + \mathcal{C}_s \quad (3.54)$$

or

$$(\mathcal{C}_f - \mathcal{C}_s) = \mathcal{J}_\theta \mathcal{C}_\theta \mathcal{J}_\theta^T \quad (3.55)$$

one can solve for \mathcal{C}_θ with the generalized inverse of \mathcal{J}_θ and \mathcal{J}_θ^T . For redundant fingers grasping an object, the generalized inverse of \mathcal{J}_θ exists. Therefore, the optimal joint servoing is

$$\mathcal{C}_\theta = \mathcal{J}_\theta^* \mathcal{C}_f \mathcal{J}_\theta^{T*} \quad (3.56)$$

where \mathcal{J}_θ^* and \mathcal{J}_θ^{T*} are the generalized left inverses of \mathcal{J}_θ and right inverse of \mathcal{J}_θ^T . The solution obtained by equation (3.56) is the solution that minimizes the F -norm. Note that if the grasp is over-constrained, the solution given by equation (3.52) is a least-squares estimate of the true solution.

3.6 Changes in stiffness, ΔK

The stiffness analysis in Sections 3.4 and 3.5 is restricted to infinitesimal motions about some initial configuration. It is also useful to understand how the stiffness itself changes in the neighborhood of a grasp configuration. This information is particularly useful when we are close to a singular configuration, for which the grasp no longer possesses the freedom to move in all directions and for which control of the stiffness in the singular directions will not be achievable.

Let us start with the changes in the joint Jacobian matrix, $\frac{\partial \mathbf{J}_\theta}{\partial \theta}$. The joint Jacobian matrix, \mathbf{J}_θ , is an $n \times m$ matrix which is defined in Section 1.3.2. The rate of change of the Jacobian matrix with respect to the joint angles, $\frac{\partial \mathbf{J}_\theta}{\partial \theta}$, is a tensor ($n \times m \times m$) which is defined such that as $d\theta \rightarrow 0$,

$$\Delta \mathbf{J}_\theta = \left(\frac{\partial \mathbf{J}_\theta}{\partial \theta} \right) d\theta = \sum_{k=1}^m \left(\frac{\partial \mathbf{J}_\theta}{\partial \theta_k} d\theta_k \right). \quad (3.57)$$

Equation (3.57) can also be re-arranged in terms of the changes in the cartesian coordinates, $d\mathbf{x}$

$$\Delta \mathbf{J}_\theta = \left(\frac{\partial \mathbf{J}_\theta}{\partial \mathbf{x}} \right) d\mathbf{x} = \sum_{k=1}^n \left(\frac{\partial \mathbf{J}_\theta}{\partial x_k} dx_k \right). \quad (3.58)$$

Since $d\mathbf{x} = \mathbf{J}_\theta d\theta$, we can equate equations (3.57) and (3.58) to obtain

$$\frac{\partial \mathbf{J}_\theta}{\partial \theta} = \frac{\partial \mathbf{J}_\theta}{\partial \mathbf{x}} \mathbf{J}_\theta. \quad (3.59)$$

If the right-inverse of the joint Jacobian matrix, \mathbf{J}_θ^* , exists (it usually exists unless the finger is over-constrained, i.e., if the matrix $\mathbf{B} = \mathbf{H}\mathbf{J}_\theta$ is of rank smaller than n) we can re-write equation (3.59) as

$$\frac{\partial \mathbf{J}_\theta}{\partial \mathbf{x}} = \frac{\partial \mathbf{J}_\theta}{\partial \theta} \mathbf{J}_\theta^*. \quad (3.60)$$

Note that the error $\Delta \mathbf{J}_\theta$ depends on such parameters as the size of the links, and the orientation of the fingers. In addition, the values of $\Delta \mathbf{J}_\theta$ computed from equations (3.57) and (3.58) will have larger errors when the configuration is nearly singular. An example is given in the following to illustrate $\Delta \mathbf{J}_\theta$ for a 2-link finger.

Example 3.5 Find $\Delta \mathbf{J}_\theta$ for a two-link manipulator

As shown in Figure 3.6, let us consider a planar point-contact finger with friction so that the number of degrees of freedom is $m = 2$ (two joints) and $n = 2$ (point contact). The joint Jacobian matrix with respect to the cartesian coordinates at the fingertip is given by

$$\mathbf{J}_\theta = \begin{bmatrix} (-l_1 s_1 - l_2 s_{12}) & -l_2 s_{12} \\ (l_1 c_1 + l_2 c_{12}) & l_2 c_{12} \end{bmatrix}$$

where $s_i = \sin \theta_i$, $c_i = \cos \theta_i$, $s_{12} = \sin(\theta_1 + \theta_2)$, and $c_{12} = \cos(\theta_1 + \theta_2)$. Differentiating the matrix \mathbf{J}_θ with respect to θ_1 and θ_2 , we have

$$\frac{\partial \mathbf{J}_\theta}{\partial \theta_1} = \begin{bmatrix} (-l_1 c_1 - l_2 c_{12}) & -l_2 c_{12} \\ (-l_1 s_1 - l_2 s_{12}) & -l_2 s_{12} \end{bmatrix}; \quad \frac{\partial \mathbf{J}_\theta}{\partial \theta_2} = \begin{bmatrix} -l_2 c_{12} & -l_2 c_{12} \\ -l_2 s_{12} & -l_2 s_{12} \end{bmatrix}.$$

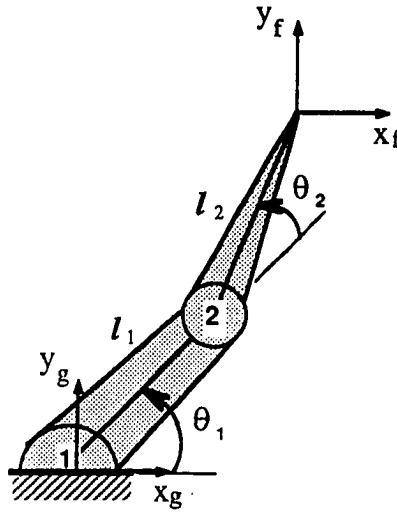


Figure 3.6: A 2-link planar manipulator

From equation (3.60), $\frac{\partial \mathbf{J}_\theta}{\partial \mathbf{x}}$ can be computed as:

$$\frac{\partial \mathbf{J}_\theta}{\partial \mathbf{x}} = \frac{\partial \mathbf{J}_\theta}{\partial \theta} \left(\frac{1}{l_1 l_2 s_2} \right) \begin{bmatrix} l_2 c_{12} & l_2 s_{12} \\ (-l_1 c_1 - l_2 c_{12}) & (-l_1 s_1 - l_2 s_{12}) \end{bmatrix}. \blacksquare$$

Once $\Delta \mathbf{J}_\theta$ is known, the matrices $\frac{\partial \mathbf{K}_p}{\partial \theta}$, $\frac{\partial \mathbf{K}_p}{\partial \mathbf{x}}$, and $\Delta \mathbf{K}_p$ can be determined according to the changes in $d\theta$ by using $\mathbf{K}_p = \mathbf{H}^T (\mathbf{B} \mathbf{C}_\theta \mathbf{B}^T)^{-1} \mathbf{H}$ defined previously. The change in the contact stiffness matrix, $\Delta \mathbf{K}_p$, is (Appendix A.7):

$$\Delta \mathbf{K}_p = \mathbf{H}^T (-2 \mathbf{B}^{-T} \mathbf{C}_\theta^{-1} \mathbf{B}^{-1} \Delta \mathbf{B} \mathbf{B}^{-1} + \mathbf{B}^{-T} \Delta \mathbf{B}^{-T} \mathbf{B}^{-T} \mathbf{C}_\theta^{-1} \mathbf{B}^{-1} \Delta \mathbf{B} \mathbf{B}^{-1}) \mathbf{H} \quad (3.61)$$

If $\mathbf{B} = \mathbf{H} \mathbf{J}_\theta$ is not an invertible square matrix, there are two possible cases: (1) redundant case – the generalized inverse of \mathbf{B} can be used in equation (3.61) to obtain the solution. (2) over-constrained case – the exact solution may not be obtainable; nevertheless, the generalize inverse of \mathbf{B} will give rise to the solution that minimizes the norms of $\delta \theta$.⁶

The changes in the grasp stiffness $\Delta \mathbf{K}_e$ can be found by knowing $\Delta \mathbf{K}_b$, if we neglect second-order and smaller terms at the contacts. The derivation is given in Appendix

⁶This is because $d\mathbf{x}_{tr} = \mathbf{B} \delta \theta$ for the components transmitted through the contacts.

A.7.

$$\Delta \mathbf{K}_b = \sum_{i=1}^{nf} {}^p_B \mathbf{J}_i^T \Delta \mathbf{K}_p {}^p_B \mathbf{J}_i. \quad (3.62)$$

The equations derived in this section can readily be extended to the concatenated forms.

3.7 Manipulation with finite motions

In the previous sections, the stiffness and compliance of a grasp for infinitesimal motions have been investigated. This analysis is sufficient for most fine manipulations with respect to an initial configuration. However, in the cases where the motion of the grasp is finite, which can happen when either the stiffnesses of the fingers are small (a very gentle grasp, for example) or the initial grasp forces are large, we need to seek a way of extending the previous analysis.

In general the cartesian stiffness matrix is orientation-dependent. For finite displacements, we no longer can assume that it is constant. However, for any finite displacement, $(\mathbf{x}_0 - \mathbf{x}_e)$, away from the equilibrium position, we can compute the corresponding force as:

$$\mathbf{f}_0 = \int_{x_e}^{x_0} \mathbf{K}_p(\mathbf{x}) d\mathbf{x} \quad (3.63)$$

where \mathbf{f}_0 is the initial or “bias” force on each finger with respect to which small variations, $\delta \mathbf{f}_p$, will subsequently be computed. If we use the Jacobian matrix obtained at the equilibrium position, we can obtain the joint torques by $\tau_0 = \mathbf{J}_\theta^T \mathbf{f}_0$. Therefore, $\Delta \theta = \mathbf{C}_\theta \tau_0$, where \mathbf{C}_θ is the compliance matrix in the joint space. The compliance matrix in the joint space is constant for a given joint servoing (if it is varying, \mathbf{C}_θ still can be obtained assuming we know how the joint servo gains are varied) and it is nonsingular. Since the equilibrium positions are known, the nominal joint positions can be obtained as $\theta_0 = \theta_e + \Delta \theta$. The nominal cartesian position of the finger can be found by $\mathbf{x}_0 = (\mathbf{J}_\theta)_0 \theta_0$. Note that there is no general inverse of the joint Jacobian involved in the above expressions.

However, the assumption of a constant Jacobian in computing the torque τ_0 may not be accurate because of the finite motion. A better approximation is to use an average Jacobian matrix, $\bar{\mathbf{J}}_\theta = \mathbf{J}_\theta + \frac{1}{2}\Delta\mathbf{J}_\theta$, using the equations derived in the previous section to compute $\Delta\mathbf{J}_\theta$ and obtain τ_0 for a more accurate result.

Another alternative is to employ numerical integration using equation (3.63) to find the nominal position, \mathbf{x}_0 . We have to integrate along the direction of $d\mathbf{x}$ for each interval. The direction of $d\mathbf{x}$ is parallel to that of the vector $\mathbf{K}_p^{-1}\mathbf{f}_0$. We can now numerically integrate for small intervals of $d\mathbf{x} = \Delta\mathbf{x}$ and keep updating the new position and $\mathbf{K}_p(\mathbf{x})$ to correct the instantaneous direction of the next $\Delta\mathbf{x}$ until we reach the value of \mathbf{f}_0 . The integration can be expressed as:

$$\mathbf{f}_0 = \sum_{i=1}^j \mathbf{K}_p(\mathbf{x}_i) \Delta\mathbf{x}_i \quad (3.64)$$

where the direction of $\Delta\mathbf{x}_i$ is parallel to that of $\mathbf{K}_p^{-1}(\mathbf{x}_i)\mathbf{f}_0$ and the integration interval is $\|\Delta\mathbf{x}_i\|$. Consequently, the nominal position is \mathbf{x}_j .

With this extension, we can immediately expand the analysis in Sections 3.4 and 3.5 to manipulation with finite movements. We now find stiffness matrices based on an initial or “nominal” position instead of the “equilibrium” position.

3.8 Experiments

A concern regarding the foregoing stiffness analysis is that it might be impractical in realistic manipulation situations due to the presence of extra joint torques due to velocity feedback, friction, ... etc. To examine the significance of such effects, experiments were conducted on a two-fingered planar manipulator. Each finger of the planar manipulator consisted of a five-bar linkage as in [Asada 1984]. The sketch of this planar manipulator and detailed information are in Appendix A.8 and Figure A.3.

In the experiments, we controlled the fingers such that the stiffness in the joint space

parameters	θ_1	θ_2	ϕ_1	ϕ_2	x	y	J_θ
Values	57°	0°	0°	83°	0.27 m	0.08 m	$\begin{bmatrix} 0.08 & 0.0 \\ -0.028 & 0.102 \end{bmatrix}$

Table 3.4: Parameters of the planar manipulator used in the experiments

was constant. This was achieved by a joint-space controller with constant gains. The applied servo stiffness in equation (3.65) was then compared with the stiffness measured from the experiments. The orientation of the planar manipulator for which the data were taken is listed in Table 3.4.

The frictions of the DC motors used to drive the finger were measured experimentally in the vicinity of the orientation listed in Table 3.4.

The commanded joint-space stiffness matrix for each finger was:

$$K_\theta = \begin{bmatrix} 1.43 & 0 \\ 0 & 1.51 \end{bmatrix} Nm. \quad (3.65)$$

This stiffness corresponds to unity position feedback gains for both motors. We note that there was also a velocity feedback term for stabilization, but since the fingertip weights were applied slowly, the velocity feedback did not significantly affect the quasistatic behavior. From the forward procedure, we expect that

$$K_p = \begin{bmatrix} 242 & -50 \\ -50 & 144 \end{bmatrix}.$$

During the experiments, weights were loaded carefully, resulting in quasistatic response, i.e., very small accelerations ($0.02g$ approximately, taking average values from Figure 3.7). The joint positions were recorded and the torques were computed as $\tau = J_\theta^T f - \tau_{friction}$, where the frictional torques, $\tau_{friction}$, are about $0.009 Nm$ and $0.003 Nm$ for motors 1 and 2 respectively. $\tau_{friction}$ was not subtracted when it was known that the torque resulting from f_i would result in zero torque on a particular motor due to the manipulator being in a decoupled configuration. A typical plot of the angles and torques is given in Figure 3.7 with K_θ from equation (3.65) and $f_{ext} = [0 \ 0.98]^T N$.

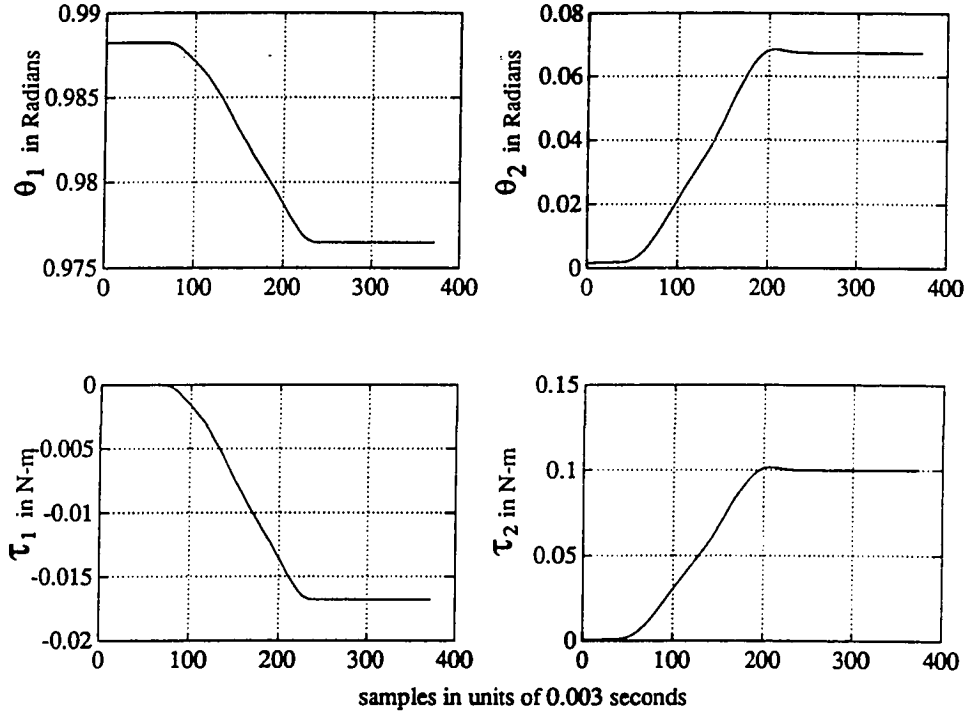


Figure 3.7: A typical plot of stiffness experiment when an external force is applied

The least squares solution [Strang 1989] of the stiffness matrix \mathbf{K}_θ can be found by the following equation:

$$\mathbf{K}_\theta = [\tau_1 \ \cdots \ \tau_{15}] [\delta\theta_1 \ \cdots \ \delta\theta_{15}]^* \quad (3.66)$$

where $\delta\theta_i$ and τ_i are from the i 'th sample and $[\delta\theta_1 \ \cdots \ \delta\theta_{15}]^*$ is the generalized inverse which leads to a least-squares best fit with the experimental results.

The data were taken by applying a weight of 100gm along the [1 0], [0 1], and $[\frac{1}{\sqrt{2}} \ \frac{1}{\sqrt{2}}]$ directions. For each direction, five runs were conducted. Average variations in the $\delta\theta$ data were 0.001 to 0.002 radians or about 0.1% to 0.2%. The experimental result for \mathbf{K}_θ was:

$$\mathbf{K}_\theta = \begin{bmatrix} 1.417 & -0.075 \\ -0.081 & 1.49 \end{bmatrix}. \quad (3.67)$$

The errors of the eigenvalues of the stiffness matrix, \mathbf{K}_θ , compared with equation (3.65), are (4.4%, 1.9%). Thus, the predicted and measured values are close despite some uncertainty in $\tau_{friction}$ and despite fingertip movements of approximately 6mm.

3.9 Summary

The stiffness or compliance of a robotic grasp represents the rate of change of grasp forces with respect to small motions of the grasped object. The stiffness depends on structural compliances in the fingers and fingertips, on servo gains at the finger joints, and on small changes in the grasp geometry that affect the way in which the grasp forces act upon the object. As such, the grasp stiffness is a useful measure of the grasp. The rank of the stiffness matrix immediately reveals whether the grasp is a force-closure grasp and can resist forces and moments from arbitrary directions. The singular directions, \vec{d} , are readily found through $\mathbf{K}_e \vec{d} = 0$. The eigenvalues of the matrix reveal the stiffest and softest directions. Generally, the stiffest directions will be those in which only structural compliance is present. Finally, the positive-definiteness of the grasp matrix is a measure of the quasistatic grasp stability. As discussed in Section 3.4.3, an unstable grasp is often one for which the contributions of changes in the grasp geometry, \mathbf{K}_J , are significant, and negative.

For controlling a hand, one needs to specify the servo gains at the finger joints for a desired grasp stiffness. For example, we may wish the grasp to have a center of compliance at a particular point. Achieving the desired stiffness may be either an over-constrained or under-constrained problem, depending on the number of fingers and the number of joints per finger. One way to check this is to look at the stiffness matrix obtained through the forward procedure – it should have full rank and no extremely stiff directions. Generally, it is useful to couple the servoing of joints on different fingers so that we can better control the off-diagonal terms of \mathbf{K}_b . In the fourth example, it is shown that without inter-finger coupling we are not able to satisfy the compliance requirements of the task.

Finally, some extensions to finite motion analysis have been discussed. The results of experiments on a two-fingered planar manipulator have been presented to explore the practicality of applications of stiffness in grasping with uncertainties. The experimental results match the predicted results closely, provided that uncertainties in

joint friction are accounted for.

Chapter 4

Friction Models and Prediction of Slipping

4.1 Introduction

When manipulating parts in multifingered robotic hands it has been found that slipping must be reckoned with since it is nearly unavoidable [Fearing 1986]. Consequently, we would like to be able to predict under what circumstances fingers will slide against a grasped object and in what directions they will start to slide. The stiffness method developed in Chapter 3 can be applied to predict the initiation of slipping. Two measures are proposed for both point-contact and soft fingers. One is the “worst-case-finger” measure that identifies the finger which is most prone to slipping. The other is a “progression-toward-friction-limit” measure that identifies the likelihood of slipping by determining how fast each finger advances toward its respective friction limit due to the infinitesimal changes of contact forces and moments when external forces are applied.

4.2 Friction models

The analysis of sliding behavior in grasping calls for accurate friction models. In this section, the contact properties and friction models are presented.

4.2.1 Coordinates and transformations

As in Section 3.3.1, a coordinate frame, $P(lmn)$, is affixed at the centroid of the pressure distribution at each contact. Each $P(lmn)$ frame moves with its associated contact and is aligned so that l and m lie in the local tangent plane and n is normal to the object surface, as shown in Figure 3.1 and 4.1.

4.2.2 Friction model for soft fingers

The Coulomb friction law

$$f_t \leq \mu f_n \quad (4.1)$$

is usually adopted when grasping with hard, point-contact fingers. The forces f_t and f_n are the tangential and normal force, respectively, and μ is the coefficient of friction. Equation (4.1) can usually be used for contacts with negligible contact areas.

When grasping with soft fingers, however, the Coulomb friction law must be extended to account for moments applied about the axis of the finger, as shown in Figure 4.1. A recurrent suggestion in the literature on grasping is to add a constraint on the moment:

$$m_n \leq \mu_t f_n \quad (4.2)$$

where μ_t is a “torsional coefficient of friction”. However, as shown in [Howe, Kao and Cutkosky 1988], this model does not give accurate results since it ignores the interaction between applied torsional and translational loads. A better solution is to think of the friction limit as constituting a surface in force/moment space.

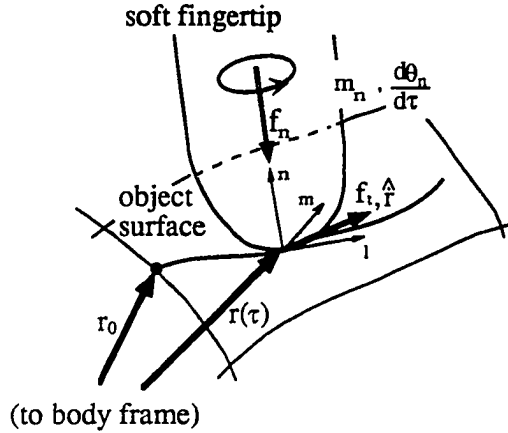


Figure 4.1: A fingertip sliding on an object sustains a tangent force, \mathbf{f}_t , and moment, m_n , when the finger has a sliding velocity, $\mathbf{v}_{slip} = [v_l, v_m, 0, 0, 0, \omega_n]^T$, with respect to the surface.

Consider a soft fingertip sliding on a grasped object. The force at the contact is given by $\mathbf{f}_p = [f_l, f_m, f_n, 0, 0, m_n]^T$. If we define a vector, $\mathbf{f}_{slip} = [f_l, f_m, 0, 0, 0, m_n]^T$, representing the tangential force and moment sustained at the contact due to friction, then the upper bound on \mathbf{f}_{slip} defines a surface in (f_l, f_m, m_n) space, as shown in Figure 4.2. If \mathbf{f}_{slip} lies inside this limit surface, no sliding occurs, but as it increases and intersects the surface, sliding begins.¹

The derivation and properties of friction limit surfaces are discussed in detail by Goyal, Ruina and Papadopoulos [1989] and are analogous to the properties of convex stress/strain-rate surfaces in classical plasticity theory [Hill 1950]. The cross section of a limit surface for the special case of an elastic finger with a Hertzian pressure distribution is also described by Jameson [1985].

The limit surfaces have two properties that are particularly useful for solving quasistatic motion problems:

1. The limit surface for a combination of contact points is a closed, convex surface and can be obtained as the Minkowski sum of the limit surfaces for the individual

¹If \mathbf{f}_{slip} were to go outside the limit surface, static equilibrium would be violated and the fingertip would accelerate with respect to the object.

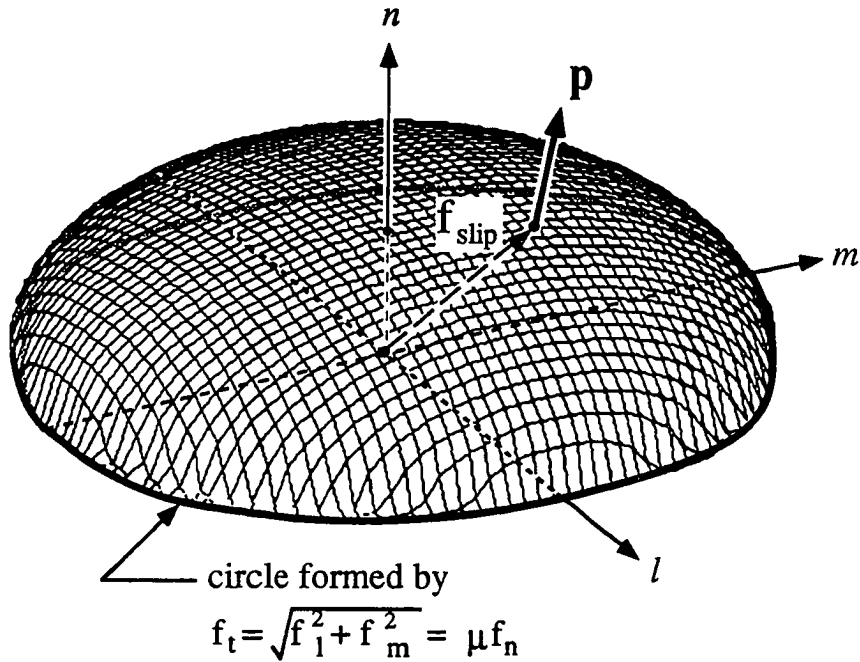


Figure 4.2: Friction limit surface in force/moment space for the fingertip in Figure 4.1. Sliding begins when f_{slip} intersects the limit surface. The direction of sliding is given by the unit normal, p .

points.

2. The unit normal, p , to the limit surface where an applied load, f_{slip} , intersects the surface, gives the instantaneous direction of sliding motion (see Figure 4.2).

As a result of these properties, the limit surface provides a (nonlinear) constraint equation relating the applied forces and moment at a contact and also relates the applied forces to the direction of sliding. In general, the limit surface for a contact depends on the details of the pressure distribution and on variations in the local coefficient of friction, and must be computed numerically. However, for special cases such as line, point and axisymmetric contacts, the limit surfaces, or good approximations to them, are easily computed [Lee and Cutkosky 1990]. In the case of axisymmetric contacts, the limit surface is represented by any cross section taken in the (f_t, m_n) plane, where f_t is the magnitude of the tangential force. The cross section can be

approximated by fitting an ellipse through the points of maximum possible tangential force, $(f_{t,max}, 0)$ and maximum moment, $(0, m_{n,max})$, as shown in Figure 4.3. The maximum tangential force is simply $f_t = \mu f_n$ and is available when no moment is applied. The maximum moment depends on the first polar moment of the pressure distribution and is available when there is no tangential force. The equation of the elliptical limit surface is then:

$$\text{soft contact : } \frac{f_t^2}{(\mu f_n)^2} + \frac{m_n^2}{m_{n,max}^2} \leq 1. \quad (4.3)$$

Before leaving this section, the accuracy of the elliptical approximation should be addressed. From experimental data with soft rubber fingertips [Howe, Kao, and Cutkosky 1988], it is found that the error is largest when the force and moment are at approximately half their maximum values. A typical maximum error is about 5% for a soft rubber fingertip with a normal force of 1.0N to 3.0N. For high contact forces (over 6.0 N) the error may be as large as 15%. These errors are acceptable when we consider that the coefficient of friction itself can vary by 30% due to changes in surface cleanliness, humidity and sliding speed, and when we recall that the entire quasistatic analysis is an approximate one in which dynamic effects are ignored.

A second observation is that for the special case of point contacts, no moment can be applied so the limit surface reduces to a circle in the (f_t, f_m) plane. In this case, $\mathbf{f}_{slip} = [f_t, f_m]^T$ and $|\mathbf{f}_{slip}| = \mu f_n$. Also, \mathbf{p} is parallel to \mathbf{f}_{slip} .

In some cases it may also be useful to employ a conservative linear approximation to the limit surface:

$$\text{soft contact (linearized model)} : f_t + A|m_n| \leq \mu f_n \quad (4.4)$$

where $A \approx (\mu f_n)/m_{n,max}$ is a proportionality constant between the torsion and shear limits. Figure 4.3 compares the decoupled, elliptical and linearized models with experimental results for a soft fingertip.

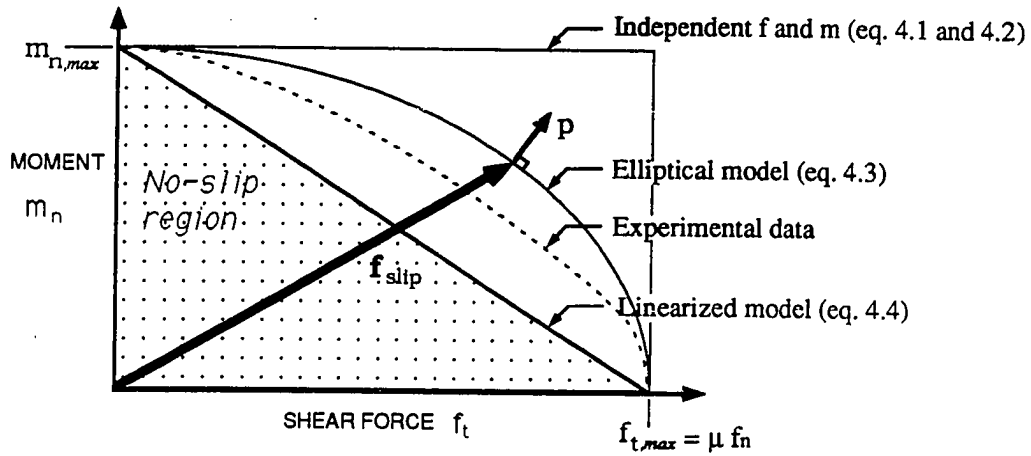


Figure 4.3: Comparison of friction models and experimental results (from [Howe, Kao and Cutkosky 1988]) for limit surface cross section in (f_t, m_n) plane. p is a unit vector, normal to the ellipse at $[f_t, m]$, where $f_t = \sqrt{f_t^2 + f_m^2}$.

4.3 Grasp compliance and contact forces

In this analysis, it is assumed that an initial set of grasp forces has been established such that the grasp is at equilibrium. The stiffness matrices from Chapter 3 then provide a relationship between changes in forces and small motions of the grasped object. When a new external force and moment, \mathbf{f}_b , is applied to the grasped object, the changes in the contact forces at the fingertips can be expressed using the results from Chapter 3 as:

$$\delta \mathbf{f}_p = -\mathcal{K}_p {}_B^P \mathcal{J} \mathbf{K}_e^{-1} \mathbf{f}_b \quad (4.5)$$

where \mathcal{K}_p is the concatenated fingertip stiffness matrix from equation (3.21), \mathbf{K}_e is the overall grasp stiffness matrix from equation (3.35), \mathbf{f}_b is the task-induced force applied to the grasped object, and ${}_B^P \mathcal{J}$ is the concatenated coordinate transformation matrix from equation (3.13). From the definition of \mathcal{K}_p , we also have:

$$\delta \mathbf{f}_p = -\mathcal{K}_p \delta \mathbf{x}_p \quad (4.6)$$

where $\delta\mathbf{f}_p$ and $\delta\mathbf{x}_p$ are concatenated vectors expressing small changes in the fingertip forces and positions. If \mathcal{K}_p is known for an initial grasp configuration, the new contact forces for small motions of the grasp can be found as $\mathbf{f}_p = \mathbf{f}_0 + \delta\mathbf{f}_p$, where \mathbf{f}_0 is the initial grasp forces.

4.4 Measures to predict the onset of sliding

The analysis of the fingertip stiffness, combined with various friction models, can be employed to predict which fingers are most likely to slip in the course of a task. The resulting slipping measures suggest strategies for controlling the grasp. For example, if a particular finger is likely to approach its friction limits during a task, it may help to soften that finger (reducing its servo stiffness) while correspondingly increasing the stiffness of other fingers.

In this section, two measures are proposed to predict the onset of sliding for both point-contact and soft fingers: (1) the “worst-case-finger” measure which is an extension of a criterion discussed by Cutkosky [1985] for a planar grasp and characterizes the absolute stability of each contact, and (2) the “progression-toward-friction-limit” measure which describes the incremental change in the stability of the contact due to task-oriented external forces. Both suggest useful strategies for controlling the initiation of sliding.

4.4.1 Worst-case-finger measure for point contacts

We are interested in knowing when a particular point-contact finger will slip. The worst-case-finger measure provides a way to know which finger is most likely to slip due to infinitesimal changes in contact forces when the grasped object is subjected to external forces. Suppose the initial force at the contact is $\mathbf{f}_p = [f_l \ f_m \ f_n \ 0 \ 0 \ 0]^T$, as shown in Figure 4.4. When a new external force is applied to the object as part of

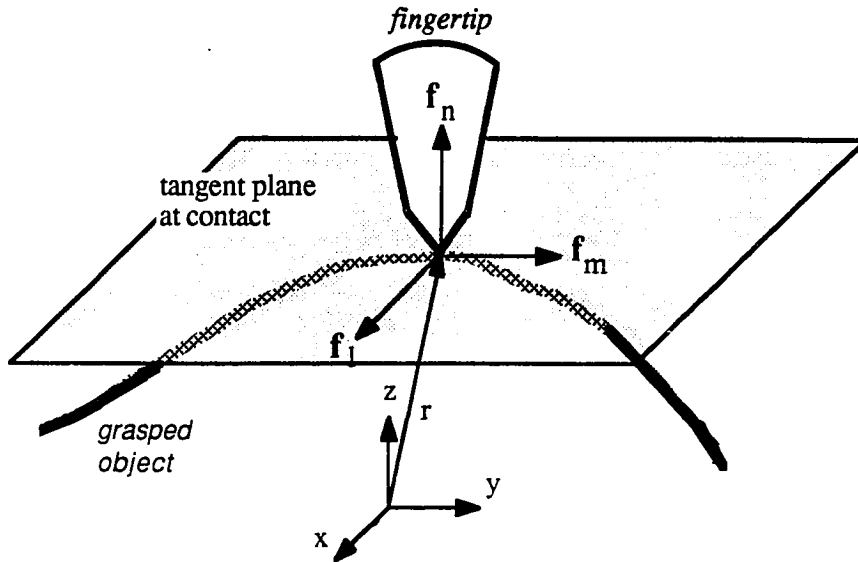


Figure 4.4: Contact coordinates and forces for a point-contact finger with Coulomb friction

the manipulation task or due to an unmodeled disturbance, the contact force changes can be determined by equations (4.5) and (4.6). Therefore, the new contact force becomes $\mathbf{f}'_p = \mathbf{f}_0 + \delta\mathbf{f}_p$, where $\delta\mathbf{f}_p = [\delta f_l \ \delta f_m \ \delta f_n \ 0 \ 0 \ 0]^T$. The tangential contact force is $f_t = \sqrt{f_l^2 + f_m^2}$. Now the resultant tangential and normal forces become

$$\begin{aligned} f_{t_i} &= \sqrt{(f_{l_i} + \delta f_{l_i})^2 + (f_{m_i} + \delta f_{m_i})^2} \\ f_{n_i} &= f_{n_i} + \delta f_{n_i} \end{aligned} \quad (4.7)$$

According to the Coulomb law of friction, $f_{t_i} = \alpha_i \mu_i f_{n_i}$ where slipping occurs as $\alpha \rightarrow 1$, or

$$\sqrt{(f_{l_i} + \delta f_{l_i})^2 + (f_{m_i} + \delta f_{m_i})^2} \geq \mu_i(f_{n_i} + \delta f_{n_i}) \quad (4.8)$$

Thus, at a given grasp configuration, the finger nearest to slipping will be the one for which α is closest to 1, or for which

$$\alpha_i = \frac{\sqrt{(f_{l_i} + \delta f_{l_i})^2 + (f_{m_i} + \delta f_{m_i})^2}}{\mu_i(f_{n_i} + \delta f_{n_i})} \quad (4.9)$$

is greatest.

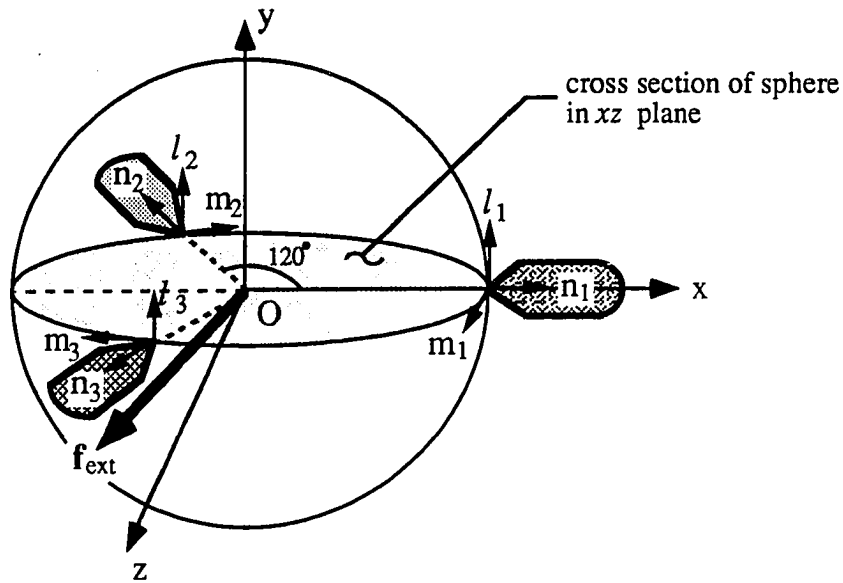


Figure 4.5: Example of “worst-case-finger” slip measure for three fingers holding a sphere

This is the so-called “worst-case-finger” measure for a grasp subject to external forces, \mathbf{f}_b , (assuming that \mathbf{f}_b is in the range space of \mathbf{K}_e). Note that this measure gives the worst-case finger for a particular external force. We can also determine a general worst-case finger by identifying the eigenvectors of the \mathbf{K}_e matrix associated with the singular eigenvalues.

Example 4.1 *Worst-case-finger measure: a rigid ball grasped by three point-contact fingers*

In order to illustrate applications of the “worst-case-finger” measure, let us consider a ball of radius R being held by three point-contact fingers equally spaced (120° apart) on a major circle as shown in Figure 4.5. The initial force applied on every finger to maintain static equilibrium is $\mathbf{f}_0 = [0 \ 0 \ f \ 0 \ 0 \ 0]^T$ with respect to the local contact coordinates, l_i, m_i and n_i . The task-induced external force is $\delta\mathbf{f} = \mathbf{f}_{ext} = [-df \ -df \ 0 \ 0 \ 0 \ 0]^T$ applied at the center of the ball, O .

Taking into consideration the contact constraints, let us assume that the stiffness

matrix of the point-contact fingers, \mathbf{K}_{p_i} , at the contact coordinates is

$$\mathbf{K}_{p_i} = \begin{bmatrix} k_{11} & k_{12} & k_{13} & 0 & 0 & 0 \\ k_{21} & k_{22} & k_{23} & 0 & 0 & 0 \\ k_{31} & k_{32} & k_{33} & 0 & 0 & 0 \\ 0 & 0 & 0 & 0 & 0 & 0 \\ 0 & 0 & 0 & 0 & 0 & 0 \\ 0 & 0 & 0 & 0 & 0 & 0 \end{bmatrix}$$

In Appendix B.1, the transformation matrices, ${}^p\mathbf{J}_i$, the effective stiffness of the grasp, \mathbf{K}_e , and the body displacement $\delta\mathbf{x}_b$ are derived. The forces at the contacts, after infinitesimal motions, are $\mathbf{f}_{p_i} = \mathbf{f}_0 + \delta\mathbf{f}_{p_i}$ with respect to the local coordinates, l_i, m_i and n_i .

The results are complex in the general case, but if we further assume that the above \mathbf{K}_{p_i} matrix is diagonal, we have a simple result:

$$\begin{aligned} \alpha_1 &= \frac{k_{22} + k_{33}}{(3f - 2df)k_{33} + 3fk_{22}} df \\ \alpha_2 &= \frac{k_{22} + k_{33}}{(3f + df)k_{33} + 3fk_{22}} df \\ \alpha_3 &= \alpha_2 \end{aligned} \quad (4.10)$$

Details are derived in Appendix B.1.

From equation (4.10), it is apparent that finger 1 is the worst-case finger, as would be expected. If $\alpha_1 \rightarrow 1$, we can find the criterion for slipping:

$$df = \frac{3f(k_{22} + k_{33})}{k_{22} + 3k_{33}}.$$

It is interesting to notice that k_{11} does not affect the measures, α_i . This is because of the decoupled \mathbf{K}_{p_i} matrix, which leads to a diagonal \mathbf{K}_b matrix. The l_i directions are decoupled from m_i and n_i . If we make k_{11} larger, the displacements along l_i directions will be smaller for the same values of $\delta\mathbf{f}_{p_i}$.

4.4.2 Worst-case-finger measure for soft fingers

The linearized friction model for soft fingers in equation (4.4) can be employed to find a conservative measure to predict the initiation of sliding motion for soft fingers. We can rewrite Equation (4.4), after infinitesimal motion, as

$$\sqrt{(f_l + \delta f_l)^2 + (f_m + \delta f_m)^2} + A|m_n + \delta m_n| < \mu(f_n + \delta f_n). \quad (4.11)$$

Following the approach of Section 4.4.1, the measure α becomes

$$\alpha_i = \frac{\sqrt{(f_{l_i} + \delta f_{l_i})^2 + (f_{m_i} + \delta f_{m_i})^2} + A|m_{n_i} + \delta m_{n_i}|}{\mu(f_{n_i} + \delta f_{n_i})} \quad (4.12)$$

where the subscript i denotes the values for the i th finger. Note that $\alpha \rightarrow 1$ as the finger starts to slip. For any given grasp, the finger closest to slipping is the finger for which α_i is closest to unity. We notice that α is a function of the friction parameters (μ and A), the initial contact forces (f_l, f_m, f_n, m_n), and the changes in the forces ($\delta f_l, \delta f_m, \delta f_n, \delta m_n$).

4.4.3 Progression-toward-friction-limit measure for point contacts

The “worst-case-finger” measure identifies the finger that is most likely to slip by indicating how far it is from its friction limit according to a dimensionless ratio, α . However, we would like to know not only how far a finger is from its friction limit, but also whether a given force applied to the grasped object will cause it to move closer to or farther from the friction limit, and how fast. In other words, we would like to know the sensitivity of the finger to slipping when forces and moments are applied to the object.

The “progression-toward-friction-limit” measure provides us with a way to predict how the force at each finger progresses toward the edge of the friction limit whenever infinitesimal motion occurs. Referring to Figure 4.6, a potential function, V , is defined

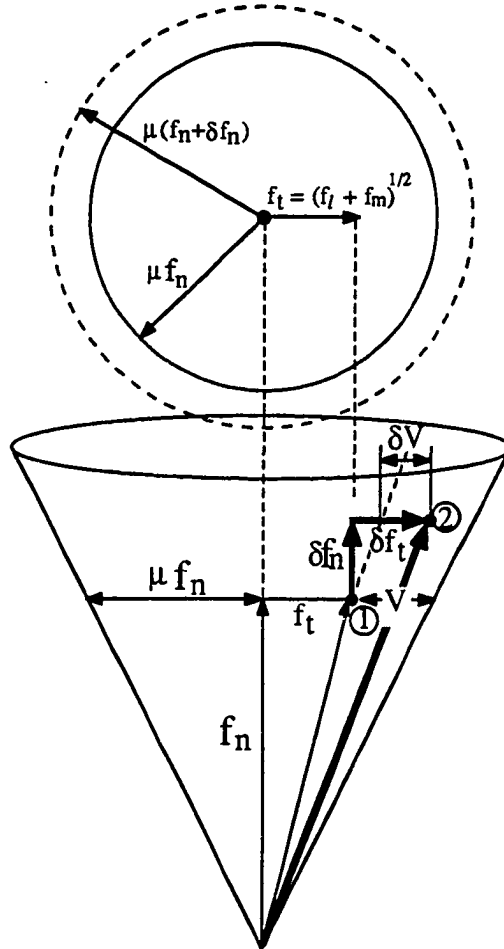


Figure 4.6: Friction cone and progression-toward-friction-limit measure for point contact fingers. Positions 1 and 2 show the states before and after the external force is applied. V is the distance from such positions to the edge of the friction cone.

which indicates how far a point-contact finger is away from the edge of the friction limit in terms of the contact forces.

$$V = \sqrt{f_l^2 + f_m^2} - \mu |f_n| \quad (4.13)$$

Depending upon the coordinate setup (in-normal or out-normal), the sign of f_n could be positive or negative. For this analysis, the magnitude of f_n is used to define V .

Therefore, we define the measure as

$$\delta V = [\sqrt{(f_l + \delta f_l)^2 + (f_m + \delta f_m)^2} - \mu |f_n + \delta f_n|] - [\sqrt{f_l^2 + f_m^2} - \mu |f_n|] \quad (4.14)$$

which gives us the magnitude of the progression toward the edge of the Coulomb friction cone after the grasped object is displaced infinitesimally. In Figure 4.6, positions 1 and 2 show the state of forces with respect to the friction cone before and after the external force is applied.

If δV is positive, the contact at the finger is moving toward the edge of the friction cone. If this measure continues to be positive, the finger will eventually exceed the slipping limits and start to slide. In Appendix B.2, we take the first order approximation to δV ,

$$\delta V \cong \left(\frac{f_l \delta f_l + f_m \delta f_m}{\sqrt{f_l^2 + f_m^2}} - \mu \delta f_n \operatorname{sgn}(f_n) \right) \quad (4.15)$$

which gives us a quantity implying how rapidly the finger force progresses toward the friction limit. The signum function of f_n , denoted as $\operatorname{sgn}(f_n)$, is defined in Appendix B.2. In equation (4.15), δf_l , δf_m , and δf_n are found using equation (4.5).

It is also useful to construct a vector measure of the rate of change of δV with respect to a chosen generalized coordinate frame $\mathbf{q} = [q_1 \ q_2 \ q_3 \ q_4 \ q_5 \ q_6]^T$. It is defined as

$$\mathbf{u} = \frac{\partial(\delta V)}{\partial \mathbf{q}} = \begin{bmatrix} \frac{\partial(\delta V)}{\partial q_1} & \frac{\partial(\delta V)}{\partial q_2} & \frac{\partial(\delta V)}{\partial q_3} & \frac{\partial(\delta V)}{\partial q_4} & \frac{\partial(\delta V)}{\partial q_5} & \frac{\partial(\delta V)}{\partial q_6} \end{bmatrix} \quad (4.16)$$

By comparing the different elements in equation (4.16), we can readily identify the most vulnerable direction with respect to the generalized coordinates, q_i .

We can also define a similar scalar measure for an induced infinitesimal motion of the object $d\mathbf{q}$.

$$dV = \frac{\partial(\delta V)}{\partial \mathbf{q}} d\mathbf{q} = \mathbf{u} d\mathbf{q}. \quad (4.17)$$

Note that dV is not necessarily the same as δV although they are both scalar measures. From dV we estimate the magnitude of the progression measure when we try to move the object in the $d\mathbf{q}$ direction, while δV is a measure with respect to the given external force.

By evaluating both the scalar and vector measures, it is possible to arrange parameters

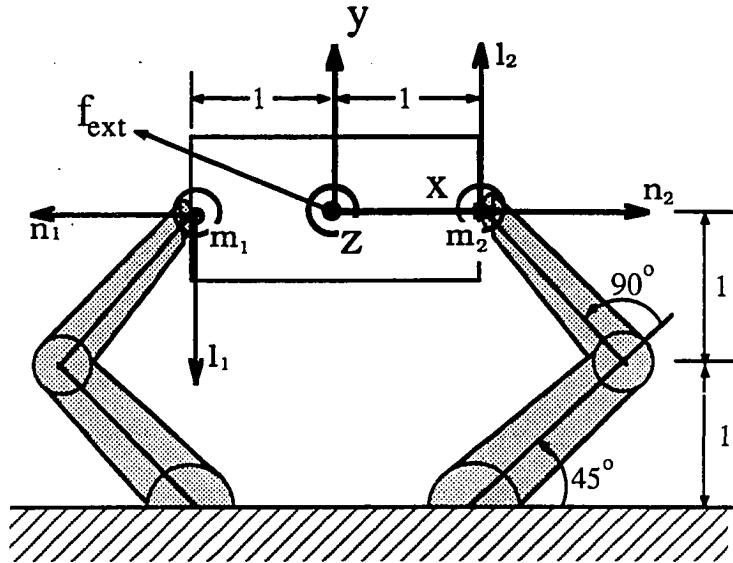


Figure 4.7: A 2D grasp example for progression-toward-friction-limit measures

of the grasp, such as the stiffness of the fingers, to improve stability and make it less vulnerable to slipping under certain task-induced forces. Suggestions to stabilize a grasp will be discussed in Section 4.5.

Example 4.2 Computing δV , u , and dV for arbitrary small motions of an object grasped by two point-contact fingers

Let us consider a 2D grasp as shown in Figure 4.7 where a rigid body is held by two point-contact fingers. In this example, a more general solution will be attempted by applying arbitrary external forces. The initial grasp forces are $f_1 = [f_n \frac{w}{2} 0]^T$, $f_2 = [f_n - \frac{w}{2} 0]^T$ applied on the fingers, where w is the weight of the rigid body. To simplify the expressions, we assume that the distance from both contact points to the center of the rigid body is 1 unit. Assume that the task-oriented external force is $\delta f = f_{ext} = [df_x df_y dm]^T$.

Using the transformations and stiffness matrices in Appendix B.3, we can easily

compute the scalar measures, δV_i , according to equation (4.15).

$$\begin{aligned}\delta V_1 &= \frac{1}{2}(dm - df_y) + \mu_1 \frac{(df_x + df_y)k_{\theta_1} + 4df_x k_{\theta_2}}{2k_{\theta_1} + 8k_{\theta_2}} \\ \delta V_2 &= -\frac{1}{2}(dm + df_y) - \mu_2 \frac{(df_x - df_y)k_{\theta_1} + 4df_x k_{\theta_2}}{2k_{\theta_1} + 8k_{\theta_2}}\end{aligned}\quad (4.18)$$

From equations (4.18), we can clearly see the symmetry of the measure ($\delta V_1 = \delta V_2$) if \mathbf{f}_{ext} has only a df_y component. If only a positive moment, dm , is applied, finger 1 will advance toward its friction limit with a positive δV_1 because of the increasing shear force.

The vector measure, \mathbf{u}_i , can be formulated by choosing the generalized coordinates $\mathbf{q} = [x \ y \ \theta_z]^T$.

$$\begin{aligned}\mathbf{u}_1 &= [-(1 - \mu_1)\frac{k_{\theta_1}}{4} \quad -(1 - \mu_1)\frac{k_{\theta_1}}{4} - k_{\theta_2} \quad (1 - \mu_1)\frac{k_{\theta_1}}{4} + k_{\theta_2}] \\ \mathbf{u}_2 &= [(1 - \mu_2)\frac{k_{\theta_1}}{4} \quad -(1 - \mu_2)\frac{k_{\theta_1}}{4} - k_{\theta_2} \quad -(1 - \mu_2)\frac{k_{\theta_1}}{4} - k_{\theta_2}]\end{aligned}\quad (4.19)$$

As expected, the vector measure is also symmetric in the y direction. Note that the elements of \mathbf{u}_i in the x and θ_z directions are of opposite sign, which means that the force/moment applied in these two directions will make one finger less vulnerable and the other finger more vulnerable.

The estimated scalar measure for motion in the direction $d\mathbf{q} = [dq_1 \ dq_2 \ dq_3]^T$ can be obtained by equations (4.17).

$$\begin{aligned}dV_1 &= \frac{k_{\theta_1}}{4}(1 - \mu_1)(-dq_1 - dq_2 + dq_3) + k_{\theta_2}(-dq_2 + dq_3) \\ dV_2 &= \frac{k_{\theta_1}}{4}(1 - \mu_2)(dq_1 - dq_2 - dq_3) - k_{\theta_2}(dq_2 + dq_3)\end{aligned}\quad (4.20)$$

4.4.4 Progression-toward-friction-limit measure for soft fingers

Following the approach of Section 4.4.3, we can look at the onset of slipping of a soft finger by constructing a potential function, V_s , using the linearized friction model

from equation (4.4):

$$V_s = \sqrt{f_l^2 + f_m^2} + A|m_n| - \mu|f_n| \quad (4.21)$$

which indicates how far a finger is from its friction limits. In addition, we can define the change in the potential function, after an external force is applied, as

$$\begin{aligned} \delta V_s &= (f'_l + A|m'_n| - \mu|f'_n|) - (f_l + A|m_n| - \mu|f_n|) \\ &= [\sqrt{(f_l + \delta f_l)^2 + (f_m + \delta f_m)^2} + A|m_n + \delta m_n| - \mu|f_n + \delta f_n|] \\ &\quad - [\sqrt{f_l^2 + f_m^2} + A|m_n| - \mu|f_n|] \end{aligned} \quad (4.22)$$

Dropping small terms, this can be simplified to

$$\delta V_s = \left(\frac{f_l \delta f_l + f_m \delta f_m}{\sqrt{f_l^2 + f_m^2}} + A(|m_n + \delta m_n| - |m_n|) - \mu \delta f_n \operatorname{sgn}(f_n) \right). \quad (4.23)$$

Like α , δV_s is a function of the friction parameters (μ and A) and the ratios of the initial grasp forces (f_l, f_m, m_n) and of how rapidly the forces change ($\delta f_l, \delta f_m, \delta f_n, \delta m_n$).

4.5 Strategies to stabilize a grasp

Equations (4.5) and (4.6), along with the measures proposed in Section 4.4, suggest methods for making a finger less likely to slip under a given set of task-induced forces. For example, given some initial grasp configuration and grasp stiffness (which are functions of finger geometry, servoing, etc.) and given some expected disturbances or task-induced forces, \mathbf{f}_b , we make the following observations:

1. If we increase \mathbf{K}_b (the grasp stiffness due to servo and structural compliance terms in \mathbf{K}_e) by increasing the servo stiffnesses, then \mathbf{K}_e^{-1} will decrease. However, \mathbf{K}_{p_i} will increase, so α_i will not change much for the same \mathbf{f}_b .
2. If we decrease \mathbf{K}_{p_i} , the stiffness of the i th finger, for just the worst-case-finger (the finger for which α_i is closest to one) then α_i will decrease for that finger.

<i>Example 4.1</i>	α_i	normal force, f	df	k_{11}	k_{22}	k_{33}
finger 1	decrease	increase	decrease	—	increase	decrease
finger 2	decrease	increase	increase	—	increase	increase
finger 3	decrease	increase	increase	—	increase	increase

Table 4.1: Changes recommended to make the 3D grasp example more resistant to slipping according to the “worst-case-finger” measure

However, in making one finger more compliant, we somewhat reduce the overall grasp stiffness, \mathbf{K}_e , resulting in larger motions of the object. More generally, if we reduce the stiffness of a finger that contributes greatly to the overall grasp stiffness, then the object moves more, which tends to destabilize the grasp. Therefore, we should increase the stiffnesses of the other fingers to keep \mathbf{K}_e more or less constant.

3. If we increase the normal force, f_n , for the worst-case-finger and adjust f_n for the other fingers so as to maintain equilibrium, then the grasp will be less vulnerable to slipping. However, this may have undesirable effects such as damaging the object or decreasing grasp stability by increasing the change in stiffness with respect to changes in grasp configuration, \mathbf{K}_j .

A solution for delaying the onset of slipping is therefore to specify \mathbf{K}_p (through appropriate control of \mathbf{K}_θ and/or adjustment of the grasp configuration) so that $\delta f_{l_i}, \delta f_{m_i}$, and δm_{n_i} for the worst-case finger are either small or in the right direction to increase δV when an external force is applied to the object.

This is most easily seen through a few examples. As in Example 4.1, the worst-case-finger measures for each finger, α_i , are found in equation (4.10). The equations suggest a few ways to stabilize the grasp. They are listed in Table 4.1.

Table 4.2 lists the variations of the grasp parameters that can improve the stability of the grasp from Example 4.2, using equations (4.18) – (4.20) and based on $\mu_1, \mu_2 \cong 0.5 - 0.7$ and a positive definite \mathbf{K}_θ matrix. We observe that increasing df_y , to some

<i>Example 4.2</i>	$\delta V_i, dV_i, u_i$	f_n	df_x	df_y	dm	k_{θ_1}	k_{θ_2}	dq_1	dq_2	dq_3
finger 1	dec	–	dec	inc	dec	cond	dec	inc	inc	dec
finger 2	dec	–	inc	inc	inc	cond	inc	dec	inc	inc

“dec”: *decrease*

“inc”: *increase*

“cond”: *conditional, may increase or decrease depending on the actual grasp parameters and task requirements*

Table 4.2: Changes recommended to make the 2D grasp example more resistant to slipping according to the “progression-toward-friction-limit” measures

extent, will always stabilize both fingers because it compensates for the weight of the object, resolved as tangential forces on both fingers. On the other hand, changes in df_x and dm tend to stabilize one finger but destabilize the other. Equation (4.20) suggests that to ensure a “robust” grasp in this problem, we should make the fingers more compliant in the direction of the contact tangent plane and stiffer in the normal directions.

Example 4.3 Application of the slipping measures and recommendations to stabilize a 3D grasp with soft contacts

The grasp in Figure 4.8 shows two four-joint fingers grasping a rectangular block. The dominant task-related forces are represented as a resultant force, f_b , at the center of the block as shown in Figure 4.8. For simplicity we assume that the joint stiffness matrix of each finger is diagonal. For the purposes of the example we have chosen stiffness values typical of a robotic hand so that the matrix for the left finger becomes:

$$\mathbf{K}_{\theta_1} = \begin{bmatrix} 2 & 0 & 0 & 0 \\ 0 & 2 & 0 & 0 \\ 0 & 0 & 2 & 0 \\ 0 & 0 & 0 & 1.25 \end{bmatrix} Nm \quad (4.24)$$

The matrix for the right finger, \mathbf{K}_{θ_2} , is identical to \mathbf{K}_{θ_1} since the grasp is assumed to be symmetrical. Following the methods in Chapter 3 the scaled fingertip stiffness

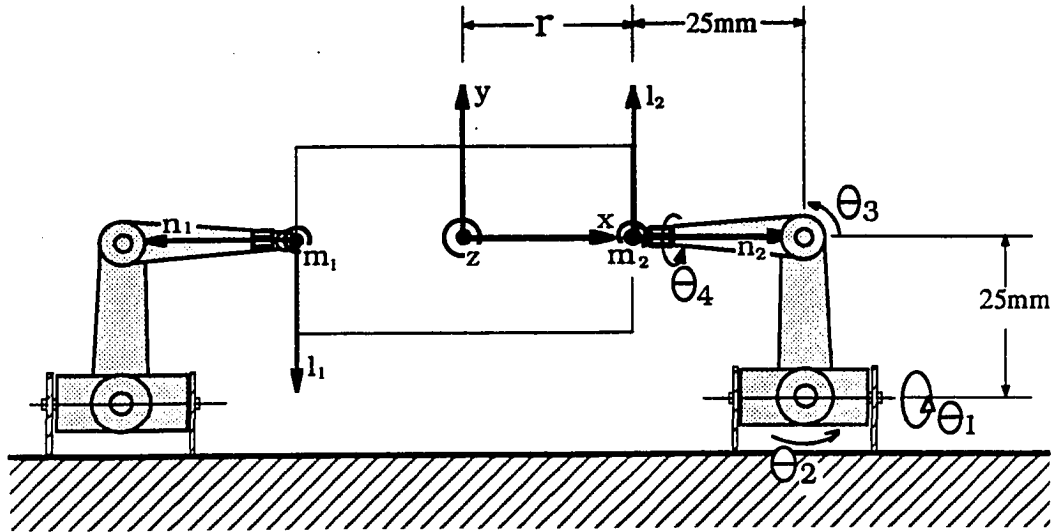


Figure 4.8: Example of two four-joint soft-contact fingers grasping a rectangular block

matrix, with $r_c = 25\text{mm}$, becomes:

$$\mathbf{K}_{p_1}^\dagger = \begin{bmatrix} 3200 & 0 & 3200 & 0 & 0 & 0 \\ 0 & 5200 & 0 & 0 & 0 & 2000 \\ 3200 & 0 & 6400 & 0 & 0 & 0 \\ 0 & 0 & 0 & 0 & 0 & 0 \\ 0 & 0 & 0 & 0 & 0 & 0 \\ 0 & 2000 & 0 & 0 & 0 & 2000 \end{bmatrix} \text{Nm} \quad (4.25)$$

$\mathbf{K}_{p_2}^\dagger$ follows from symmetry. We observe that the stiffnesses are zero for rotations about the l and m axes since the contact is a soft finger contact. (For point contacts the stiffness for rotations about the n axis would be zero as well).

Choosing a task induced force $\mathbf{f}_b = [0.5 \ 0.5 \ 0 \ 0.2 \ 0 \ 0]^T$ and an initial grasping force of $\mathbf{f}_{p_1} = [-1 \ 0 \ -2 \ 0 \ 0 \ 0]^T$ and $\mathbf{f}_{p_2} = [1 \ 0 \ -2 \ 0 \ 0 \ 0]^T$, we find $\delta\mathbf{f}_{p_1} = [0.25 \ 0 \ 0.5 \ 0 \ 0 \ 0.1]^T$ and $\delta\mathbf{f}_{p_2} = [-0.25 \ 0 \ 0 \ 0 \ 0 \ -0.1]^T$. The results are summarized in Table 4.3, assuming a coefficient of friction $\mu = 0.7$ and a typical value of $A = 3.0$ in equation (4.4), corresponding to a contact patch of approximately 1.0cm diameter. As Table 4.3 shows, finger 1 (the left finger) is clearly the worst-case-finger, which matches our intuition. Since there are only two fingers in this example, the effects of any moment

Measures	left finger	right finger
Worst-case-finger	$\alpha_1 = 1.0$	$\alpha_2 = 0.75$
Progression-to-slipping	$\delta V_1 = 0.4$	$\delta V_2 = 0.05$

Table 4.3: Slipping measures for Example 4.3 in Figure 4.8

Worst-case	α	df_l	$ m_n $	f_b	grasp force	K_θ
finger 1	decr	decr	decr	decr	incr	decr
finger 2	decr	decr	decr	decr	incr	incr
Progression-to-slip	δV	df_l	$ m_n $	f_b	grasp force	K_θ
finger 1	decr	incr	decr	decr	incr	decr
finger 2	decr	decr	decr	decr	incr	incr

Table 4.4: Changes recommended to make the grasp more resistant to slipping

about the n -axis are large.

Applying the strategies listed earlier in this section, we can make the grasp less vulnerable to slipping by decreasing K_θ for the left finger and slightly increasing K_θ for the right finger so as to keep K_θ more or less constant. Another possibility is to increase the grasp force (but this may introduce other problems since increasing the grasp force can make a grasp subject to instabilities). The strategies for making the grasp less vulnerable to slipping are summarized in Table 4.4.

The linearized friction model in equation (4.4) and δV_s in (4.22) demonstrate that both fingers are progressing towards their friction limits because of the change in m_n (although one finger is progressing considerably faster than the other). A measure that did not include both torsion and shear would not give this result.² ■

²If point contacts were assumed, we would obtain $\alpha_1 = 0.71$, $\alpha_2 = 0.54$, $\delta V_1 = 0.1$ and $\delta V_2 = -0.25$ which would not predict the slipping behavior correctly for this case.

4.6 Critical configurations

The “*critical configuration*” of a grasp is defined as one such that two or more fingers slip at the same time. It is a function of the effective stiffness, the external force, the contact constraints, and the orientation of the grasp. Formally, the critical configuration is at

$$\alpha_i = \alpha_{i+1} = \cdots = \alpha_n = 1 \quad \text{for } (n - i) \geq 1 \quad (4.26)$$

The analysis of the critical configuration is useful in securing a grasp so that it can accommodate a maximum task-induced force before slipping. In the extreme case, all fingers will slide at the same time instead of one finger sliding first. However, this may not be always achievable. For example, in Example 4.1, if we apply an external force along the y direction, all three fingers will eventually slip simultaneously. However, only fingers 2 and 3 can slide at the same time if we apply a force along the $+x$ direction. In both cases, however, we achieve a “critical configuration”.

In Example 4.4, we discuss the critical configuration of a two-degree-of-freedom manipulator.

Example 4.4 *Critical configurations of two-degree-of-freedom fingers: prediction and experiment*

The fingers used for conducting these experiments are depicted in Figure 4.9, which also shows the initial orientation of the grasp. The manipulator was located at the U. C. Berkeley robotics laboratory and is described in [Murray and Sastry 1989]. External forces were applied to the grasped object by pulling on a string attached at various points on the object. The external force was gradually increased until one or both fingers started to slip, at which point the direction of the force and the geometry of the grasp were recorded.

The theoretical results depend on the joint stiffness matrix, the grasp geometry, the contact type, and the coefficient of friction between the fingertip material and the

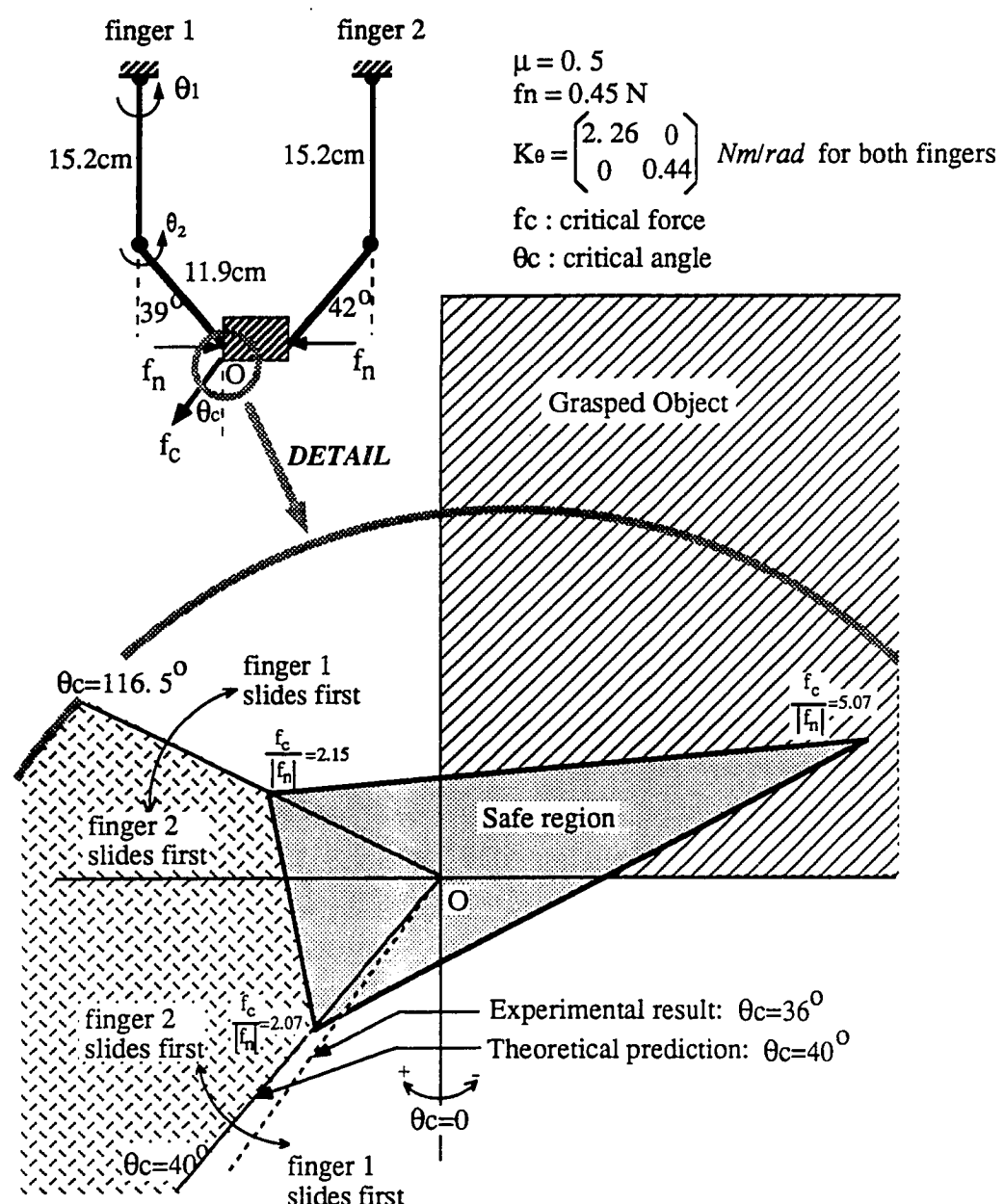


Figure 4.9: Polar plot ($f_c/|f_n|$ radial, θ_c angular) of onset of slipping with respect to the external force showing predicted and experimental critical angles at which both fingers slip simultaneously

object surface. The coefficient of friction between the rubber fingertip and the object surface was measured by the apparatus used in [Howe, Kao, and Cutkosky 1988] and was found to have a value between 0.5 and 0.6, although a certain amount of viscoelastic creep is apparent over a long period of time.

Figure 4.9 summarizes the predicted versus the experimental results for the slipping analysis performed with the grasp configuration shown and with the joint stiffness,

$$\mathbf{K}_\theta = \begin{bmatrix} 2.26 & 0 \\ 0 & 0.44 \end{bmatrix} \text{Nm/rad.}$$

where joint 2 has a smaller stiffness value due to a smaller motor. The enlargement in Figure 4.9 is a polar plot of force direction and magnitude as a function of the onset of slipping. At the center of this polar plot is a triangular “safe region” in which the magnitude of the external force is too small to produce slipping at either finger. Outside this triangular region, either the left or the right finger will start to slip. As the polar plot shows, the theoretical analysis predicts that if the external force, \mathbf{f}_c , is applied between $\theta_c = 40^\circ$ and $\theta_c = 116.5^\circ$, the right finger, finger 2, will slip first. For all other angles of external force, finger 1 will start to slip first. The angles $\theta_c = 40^\circ$ and $\theta_c = 116.5^\circ$ are called the *critical angles* at which both fingers will slip simultaneously. Under these conditions, the experimental results show that finger 2 slipped first between the angles of $\theta_c = 36^\circ$ and $\theta_c = 116.5^\circ$, which corresponds very closely with the theoretical predictions.

4.7 Summary

In this chapter, friction models and limit surfaces have been examined. Early work in grasping tended to focus on the kinematics of finger-object contacts, and adopted point-contact models with Coulomb friction. For soft fingertips, this leads to inaccurate results. Various friction models have been discussed and compared with experimental data. An elliptical approximation can be used to analyze friction with soft fingers. The experimental results also suggest a simpler, linear model that is

adequate for predicting the onset of slipping.

Two measures for predicting the onset of slipping have been proposed. The measures are computed for each fingertip and depend not only on the local finger stiffness and contact type but also on the overall grasp stiffness and configuration. The first measure singles out a "worst-case" finger that is most prone to slipping. The second measure predicts whether a given set of external forces and moments will cause individual fingers to become more or less likely to slip, and measures how fast each finger is progressing toward the friction limit.

The results of the analysis suggest strategies for controlling the fingers of a hand to make them less vulnerable to slipping in the presence of task-induced forces. Finally, the "critical configuration" of a grasp has been defined and illustrated by an example and experiments.

Chapter 5

Quasistatic Manipulation With Sliding

5.1 Introduction

Increasingly, it has been recognized that sliding is an important part of dexterous manipulation [Peshkin 1986, Fearing 1986, Brock 1987]. With industrial robots and passive grippers, the goal was to avoid slipping so that the location of the part would not be lost. However, when people handle objects, they often take advantage of slipping to achieve desired motions of the part. As an example, consider the process of picking up a tool such as a screwdriver or a hammer with the fingertips and then switching to a wrap grasp for working. During this manipulation process the fingers briefly slide upon the tool handle as it is brought against the palm to achieve a more powerful grasp. Hence, it is important to model such manipulations, and to suggest control strategies for accomplishing them.

In this chapter, a method for modeling dexterous manipulation with sliding objects is developed. The approach combines compliance and friction limit surfaces. The method is useful both for describing how a grasp will behave in the presence of

external forces (e.g., when and how each fingertip will slide) and for planning how to control the fingers so that the grasped object will follow a desired trajectory. The approach is discussed in the context of a single sliding finger in this chapter. Extensions to multiple fingers are covered in Chapter 6. For each sliding finger, the trajectories are characterized by a transient and steady-state solution. The underlying approach is discussed and illustrated with several examples. Experimental results are also presented.

5.2 Analytic form of sliding trajectory of a single finger

In this section, the background material from the previous chapters on kinematics, grasp stiffness and friction limit surfaces is combined to obtain a set of differential equations that govern the quasistatic sliding motion of a fingertip with respect to an object.

Problem statement:

A single compliant fingertip presses against the surface of a rigid object. The problem is to find a relationship between forces and the sliding motions of the fingertip. This relationship will allow us to compute a trajectory for a given sequence of forces or, conversely, to compute a sequence of forces that must be applied to achieve a desired trajectory. In both cases, it is the *relative* motion of the fingertip and object with respect to each other that will be found.

Assumptions:

1. The fingertip is either pointed, or locally spherical and the contact area is small enough that soft-finger contact kinematics [Salisbury 1985, Kerr 1986] apply (no moments transmitted about axes parallel to the contact plane).

2. The grasped object is rigid and the surface is locally smooth and continuous. If the fingertip comes to a discontinuity in the surface, the problem must be stopped and re-started with new initial conditions.
3. The grasp kinematics and geometries are known so that the location of the contact point can be computed as a function of the configuration of the finger and the object.
4. The fingertip stiffness can be characterized by a matrix, as in Chapter 3, that relates variations in the forces and moments applied through the contact to compliant deflections of the fingertip. The variations are with respect to some initial forces and are sufficiently small that the instantaneous linear stiffness relationship of equation (4.6) is accurate. Also, the stiffness matrix is continually updated using the known finger kinematics.
5. The normal force, f_n , applied by the fingertip is known and is controllable.
6. The elements of $\mathbf{f}_{slip} = [f_l, f_m, 0, 0, 0, m_n]^T$ are sufficiently small that the compliant deflections associated with them can be expressed by $\mathbf{K}_p^{-1}\mathbf{f}_{slip}$. (This assumption is explained further in the next section).
7. Velocity- and acceleration-dependent terms (e.g., inertial forces) are sufficiently small that a quasistatic analysis is applicable.

5.2.1 Minimum power principle with Coulomb friction

A starting point for the quasistatic sliding analysis is that the fingertip must be, at all times, in static equilibrium. However, where constraint forces are present, the equations of equilibrium may be inconvenient to use. As an alternative, Peshkin [1988] proposes a “minimum power principle” which is a generalization of static equilibrium for quasistatics. In the minimum power formulation, forces are separated into constraint and nonconstraint forces [Peshkin 1988]. Motion along the constrained directions is defined by the constraints. Motion along the unconstrained directions

is governed by the minimum power principle. The restrictions for the principle to apply include quasistatic motion with no inertial terms, and sliding friction where the magnitude of the force is independent of speed. This approach to modeling the sliding of objects in a plane can be adapted to describe the sliding of fingertips along the surface of a grasped object.

The instantaneous power of a system of particles can be expressed as:

$$P_v = - \sum_i \mathbf{f}_{xc_i} \cdot \mathbf{v}_i \quad (5.1)$$

where \mathbf{v}_i is the velocity of particle i and \mathbf{f}_{xc_i} are the forces acting on each particle, excluding constraint forces (which simply predefine the motion with respect to the constrained directions). The magnitude of \mathbf{v} is small, and constant, since only quasistatic motions are considered. The power will be minimized for a particular direction of the velocity vector, which is found by taking

$$\nabla(\mathbf{f} \cdot \mathbf{v}) = \frac{\partial P_v}{\partial \mathbf{v}} = 0 \quad (5.2)$$

From equation (5.2), it can be shown that the forces have to be velocity-independent to satisfy equilibrium.

An essential element in extending this sliding analysis to a compliant grasp is that variations in the fingertip forces can be represented as stiffness multiplied by displacement. When the finger is sliding, $\mathbf{f}_p = \mathbf{f}_{slip}$ is on the limit surface, using either the point-contact or elliptical friction model. The expression for the power, as a function of the instantaneous velocity of the finger with respect to the object is:

$$P_v = -(\mathbf{f}_{slip}) \cdot \mathbf{v} - \mathbf{K}_p \delta \mathbf{x}_p \cdot \mathbf{v} + \mathbf{f}_0 \cdot \mathbf{v} \quad (5.3)$$

where \mathbf{f}_{slip} is the force/moment on the limit surface, and \mathbf{f}_0 is the initial force acting on the finger so that, from equation (4.6), $\mathbf{f}_p = \mathbf{f}_0 - \mathbf{K}_p \delta \mathbf{x}_p$. Applying the minimum power principle to this system, once can obtain the governing equation of motion for sliding, subject to compliance:

$$\frac{\partial P_v}{\partial \mathbf{v}} = -\mathbf{f}_{slip} - \mathbf{K}_p \delta \mathbf{x}_p + \mathbf{f}_0 \cdot \frac{\mathbf{v}}{|\mathbf{v}|} = 0. \quad (5.4)$$

To satisfy static equilibrium, it is required that the gradient of the j th component of equation (5.3) be equal to the total force, \mathbf{f}_j , resulting from the components of \mathbf{f}_0 , $\mathbf{K}_p \delta \mathbf{x}_p$ and \mathbf{f}_{slip} in that direction. With a treatment similar to that in [Peshkin 1988], we can write

$$f_j = \frac{d}{dv_j}(\mathbf{f} \cdot \mathbf{v}) = \mathbf{f}_{slip,j} + \sum_{l=1}^3 v_l \frac{d}{dv_j}(\mathbf{K}_p \delta \mathbf{x}_p)_l + (\mathbf{K}_p \delta \mathbf{x}_p)_j - \mathbf{f}_0 \cdot \frac{\mathbf{v}}{|\mathbf{v}|}$$

which requires that

$$\sum_{l=1}^3 v_l \frac{d}{dv_j}(\mathbf{K}_p \delta \mathbf{x}_p)_l = 0 \quad (5.5)$$

to satisfy force equilibrium in the directions of motion. This requirement is clearly satisfied since \mathbf{K}_p and $\delta \mathbf{x}_p$ are independent of \mathbf{v} . Thus, the minimum power principle can be applied to compliant grasps.

5.2.2 Curves and parameterization

As in previous chapters, small changes in the position and orientation of the contact $P(lmn)$ frame with respect to the body $B(xyz)$ frame are given by $\delta \mathbf{x}_p$. For this section, it is convenient to decompose $\delta \mathbf{x}_p$ into a position vector, $\delta \mathbf{r} = \mathbf{r} - \mathbf{r}_e = [\delta r_l, \delta r_m, \delta r_n]^T$ and a vector of orientations, $[\delta \theta_l, \delta \theta_m, \delta \theta_n]^T$, representing infinitesimal angle changes. The coordinate frames and vectors, \mathbf{r} and \mathbf{r}_e , are shown in Figure 5.1.

All varying quantities are expressed in terms of an independent parameter, τ . Due to the quasistatic nature of the analysis, and the fact that friction forces depend only on the directions of motion and not the speeds, τ is not directly correlated with time. As a result, we can speak only of the *relative* magnitudes of different velocities. For example, we can tell if a finger is sliding twice as fast in the X direction as in the Y direction. If we happen to know how τ varies as a function of time (perhaps because the velocities of the fingers or the object are given as the input to a problem), we can of course obtain the time dependence of all terms. However, this is not necessary to obtain plots of the motions of the contacts and the object.

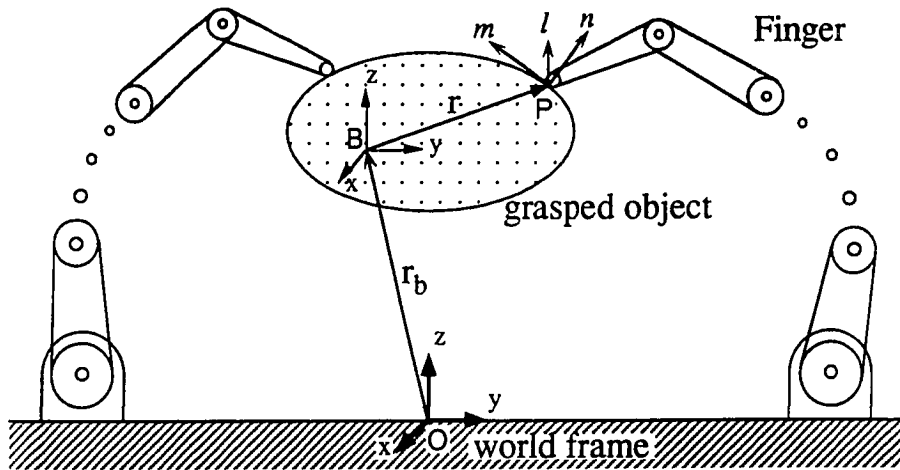


Figure 5.1: Coordinate systems and vectors for a finger/object contact sliding on the surface of a grasped object

The vector \mathbf{r} , describing the contact location with respect to the object, varies as the contact moves and therefore $\mathbf{r}(\tau)$ traces a curve on the surface of the grasped object, as shown in Figure 5.2. In this analysis it is assumed that $\mathbf{r}(\tau)$ is locally continuous and differentiable (C^2). (Discontinuities will be handled by stopping the problem and re-starting it with a new set of initial conditions.) $s(\tau)$ is defined as the length along the curve, $\mathbf{r}(\tau)$, starting from \mathbf{r}_0 at $\tau = 0$. In other words, $s(\tau) = \int_0^\tau \|\frac{d\mathbf{r}}{d\tau}\| d\tau$. In addition, $\hat{\mathbf{r}}(\tau)$ is defined to be the unit tangent along $\mathbf{r}(\tau)$. Therefore, $\hat{\mathbf{r}}(\tau)$ corresponds to the instantaneous direction of motion along $\mathbf{r}(\tau)$. It can be shown from elementary differential geometry [DoCarmo 1986] that

$$\hat{\mathbf{r}} = \frac{d\mathbf{r}}{d\tau} \frac{d\tau}{ds}. \quad (5.6)$$

Note that since $\hat{\mathbf{r}}(\tau)$ is expressed in the moving $P(lmn)$ frame, and must lie in the local tangent plane, it has no n component and can be written as a 2×1 vector:

$$\hat{\mathbf{r}} = \begin{bmatrix} dr_l/d\tau \\ dr_m/d\tau \end{bmatrix} \frac{d\tau}{ds}. \quad (5.7)$$

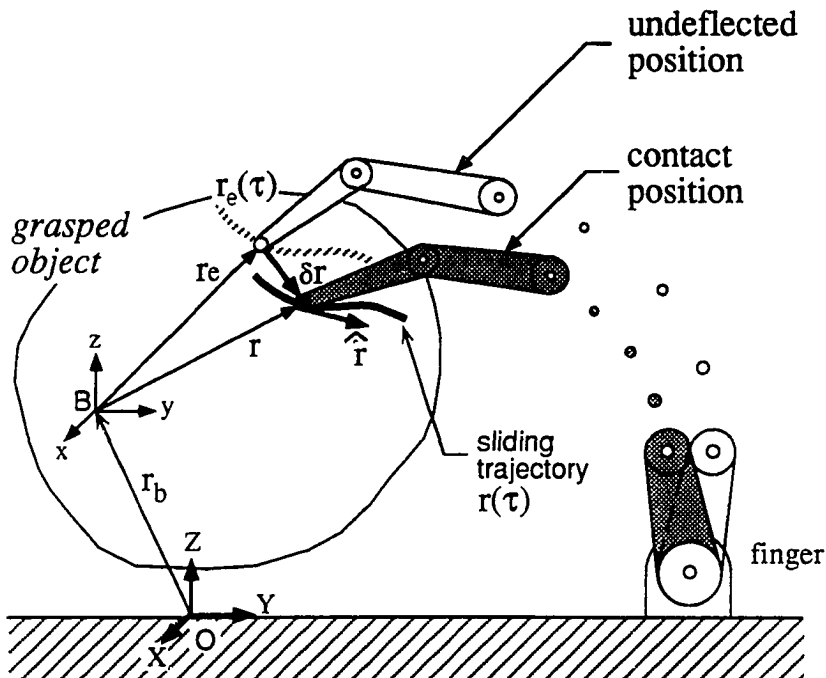


Figure 5.2: Trajectory and motion vectors for a compliant finger sliding on the surface of an object

5.2.3 Limit surface constraints for soft and point contact fingers

In this section, a special form of the limit surface equations from Section 4.2.2 is developed, which will be useful for sliding soft-contact and point-contact fingertips.

First, we recall that for approximately axisymmetric pressure distributions, the limit surface will be axisymmetric. Since the limit surface is axisymmetric, the projection of \mathbf{p} on the (l, m) plane is parallel to $\mathbf{f}_t = [f_l, f_m]^T$, which means that the tangential force is parallel to the linear component of the sliding velocity. Since the instantaneous direction of linear motion is given by $\hat{\mathbf{r}}$, \mathbf{f}_t can be written as $f_t \hat{\mathbf{r}}$. Secondly, from Section 4.2.2, we know that the unit normal to the limit surface, \mathbf{p} , is parallel to the instantaneous direction of motion and the direction cosines of \mathbf{p} are related to m_n and \mathbf{f}_t by the equation of the ellipsoid. The relationships are summarized in Figure 5.3.

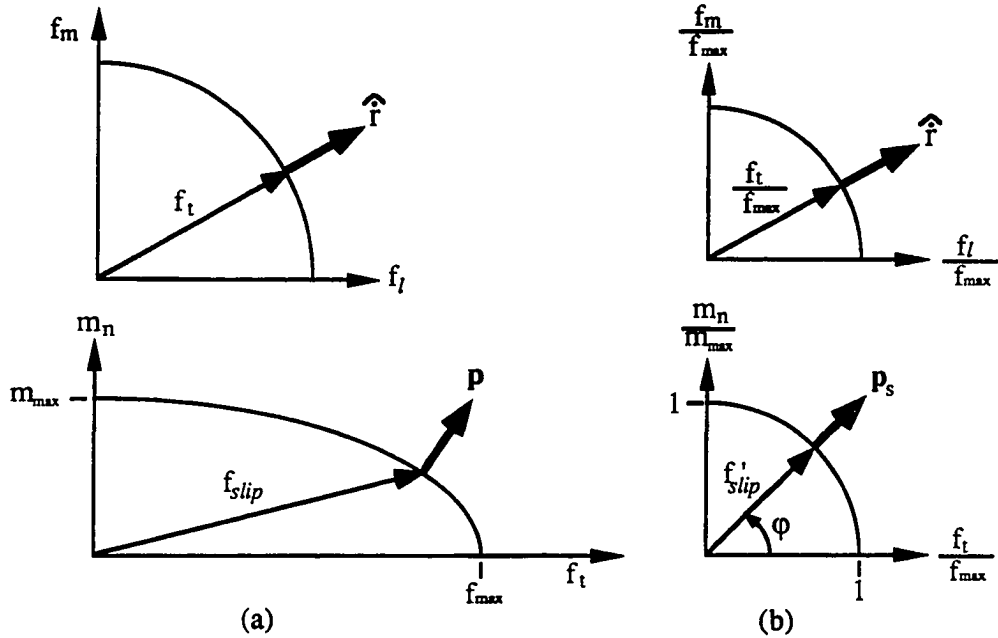


Figure 5.3: Projections of (a) ellipsoidal and (b) normalized spherical limit surfaces onto different planes showing the relationships between the force/moment and the unit normal

We can normalize the limit surface such that the ratio of the linear and angular components of p is dimensionless. There are at least two ways to normalize the limit surfaces. One is to plot $(f_l, f_m, m_n/R)$ instead of (f_l, f_m, m_n) , where R is the radius of the contact area. The other approach is to plot nondimensionalized limit surfaces with $(\frac{f_l}{f_{max}}, \frac{f_m}{f_{max}}, \frac{m_n}{m_{max}})$, in which case the ellipsoidal limit surface becomes an unit sphere. It can be shown that the first approach results in the same normalized elliptical surface for different contact radii when the contact pressure is uniform. The second approach gives rise to a dimensionless spherical limit surface. The latter approach will be used since it does not explicitly involve the contact radius, R . The direction of the unit normal of the spherical limit surface, p_s , is parallel to the direction of the normalized force/moment vector, f'_{slip} , as shown in Figure 5.3. Therefore, we have expressions that relate the relative magnitude of the normalized rotational component to the magnitude of the normalized translational components for a given tangential

force, f_t , and moment, m_n :

$$\cot \psi = \left(\frac{f_t}{\mu f_n} \right) / \left(\frac{m_n}{m_{max}} \right) = \frac{(\sqrt{dr_l^2 + dr_m^2}/d\tau)/m_{max}}{(d\theta_n/d\tau)/\mu f_n} \quad (5.8)$$

Expressing this relationship in the l and m directions, we have:

$$\cot \psi_l = \frac{(dr_l/d\tau)/m_{max}}{(d\theta_n/d\tau)/\mu f_n} = \left(\frac{m_{max}}{\mu f_n} \right) \frac{f_l}{m_n} \quad (5.9)$$

$$\cot \psi_m = \frac{(dr_m/d\tau)/m_{max}}{(d\theta_n/d\tau)/\mu f_n} = \left(\frac{m_{max}}{\mu f_n} \right) \frac{f_m}{m_n} \quad (5.10)$$

It is obvious from equations (5.8) – (5.10) that $\cot \psi = \sqrt{\cot \psi_l^2 + \cot \psi_m^2}$. By defining

$$\lambda = \frac{m_{max}}{\mu f_n} \quad (5.11)$$

(where λ has units of length) we can rewrite equation (5.8) to (5.10) as

$$\frac{\sqrt{dr_l^2 + dr_m^2}/d\tau}{d\theta_n/d\tau} = \lambda \cot \psi = \left(\frac{m_{max}}{\mu f_n} \right)^2 \frac{f_l}{m_n} \quad (5.12)$$

$$\frac{dr_l/d\tau}{d\theta_n/d\tau} = \lambda \cot \psi_l = \left(\frac{m_{max}}{\mu f_n} \right)^2 \frac{f_l}{m_n} \quad (5.13)$$

$$\frac{dr_m/d\tau}{d\theta_n/d\tau} = \lambda \cot \psi_m = \left(\frac{m_{max}}{\mu f_n} \right)^2 \frac{f_m}{m_n} \quad (5.14)$$

In summary, equations (4.3), (5.12), (5.13), and (5.14) provide constraint equations among $(\frac{f_l}{f_{max}}, \frac{f_m}{f_{max}}, \frac{m_n}{m_{max}})$ and $(\frac{dr_l}{d\tau}, \frac{dr_m}{d\tau}, \frac{d\theta_n}{d\tau})$ for a given value of f_n .

5.2.4 Equations of sliding motion

A fingertip presses against the surface of an object with a force, \mathbf{f}_p , which can be broken into a normal component and a frictional component:

$$\mathbf{f}_p = f_n \mathbf{e}_3 + \mathbf{f}_{slip} \quad (5.15)$$

where $\mathbf{e}_3 = [0, 0, 1, 0, 0, 0]^T$ and $\mathbf{f}_{s,ip} = [f_l, f_m, 0, 0, 0, m_n]^T$ as defined in Section 4.2.2. For small variations in \mathbf{f}_p about an initial value, \mathbf{f}_0 , we can also use equation (4.6) to express \mathbf{f}_p as

$$\mathbf{f}_p = \mathbf{f}_0 - \mathbf{K}_p \delta \mathbf{x}_p. \quad (5.16)$$

Due to the action of $\delta \mathbf{f}_p$ on the fingertip, there is a small difference between the actual and the undeflected or nominal position and orientation. We define \mathbf{r}_e as the undeflected position such that $\mathbf{r}_e - \mathbf{r} = \delta \mathbf{r}$. Thus as the finger becomes increasingly stiff, $\mathbf{r} \rightarrow \mathbf{r}_e$. Similarly, there is a small angular displacement, $\delta \rho$, due to changes in moments applied at the contact. (However, due to the kinematics of soft-contact fingertips, only δm_n and $\delta \theta_n$ are non-zero.)

An assumption is now made that will simplify the following derivation. It is assumed that the elements of $\mathbf{f}_{s,ip}$ are sufficiently small that the compliant deflections associated with them can be accurately expressed by $\mathbf{K}_p^{-1} \mathbf{f}_{s,ip}$. In practice, this is generally true when manipulating objects that are considerably larger than the point and soft contact fingertips themselves, for the following reasons: (i) the contact areas are small in comparison to the object size and therefore the moments, m_n , are small and the deflections associated with them are very small; (ii) the product μf_n is small, unless the fingers are squeezing hard upon the object, and therefore the tangential forces are not large enough to produce large deflections for practical values of \mathbf{K}_p ; (iii) when μf_n is large, \mathbf{K}_p must generally be large also (to maintain grasp stability) and therefore the deflections are still small. In experiments with a two-fingered manipulator we have found that $\mathbf{K}_p^{-1} \mathbf{f}_{s,ip}$ consistently produces small deflections, corresponding to no more than a few degrees of joint motion.

With this assumption, equation (5.15) can be combined with equation (5.16) to obtain:

$$\mathbf{f}_p = \underbrace{f_{n,0} \mathbf{e}_3}_{\mathbf{f}_0} + \underbrace{\delta f_n \mathbf{e}_3 + \mathbf{f}_{s,ip}}_{\delta \mathbf{f}_p} = \mathbf{f}_0 - \mathbf{K}_p \delta \mathbf{x}_p. \quad (5.17)$$

(If the assumption that $\mathbf{K}_p^{-1} \mathbf{f}_{s,ip}$ is small did not hold, then initial values of f_l , f_m and m_n would have to be accounted for, along with the initial value of f_n .)

Matching the δf_p terms on each side of equation (5.17), we obtain

$$\mathbf{H} \left(\delta f_n \mathbf{e}_3 + \mathbf{f}_{slip} + \mathbf{K}_p \begin{bmatrix} \delta \mathbf{r} \\ \delta \rho \end{bmatrix} \right) = 0 \quad (5.18)$$

where premultiplication by the contact constraint matrix, \mathbf{H} , from Section 3.3.2, simply strips out the all-zero equations in the θ_l and θ_m components. Recalling the limit surface constraint that the tangential components of \mathbf{f}_{slip} are parallel to $\hat{\mathbf{r}}$, we can write equation (5.18) as:

$$\begin{bmatrix} 0 \\ 0 \\ \delta f_n \\ \vdots \\ 0 \end{bmatrix} + \begin{bmatrix} f_t \hat{\mathbf{r}} \\ 0 \\ \vdots \\ m_n \end{bmatrix} + \mathbf{H} \mathbf{K}_p \begin{bmatrix} \delta \mathbf{r} \\ \delta \rho \end{bmatrix} = 0 \quad (5.19)$$

Equation (5.19) contains the basic equations for instantaneous quasistatic motion of a single sliding fingertip. It includes two linear, time-varying, inhomogeneous differential equations in $dr_l/d\tau$ and $dr_m/d\tau$ and two linear, time-varying constraint equations in f_n and m_n . If \mathbf{K}_p is not diagonal, the equations are coupled. These four equations can be solved numerically, subject to the constraint equations (5.12), (5.13) and (5.14) from the limit surface. We also note that equation (5.19) does not specify the fingertip orientations about the l and m axes, which will instead be determined by the kinematics and control of the finger, and do not play a direct role in the relationship between sliding forces and motions.

5.2.5 Solving for sliding trajectories

There are three kinds of manipulation problems in solving for the relative¹ sliding motion of the fingertip with respect to the planar object using equations (5.19) and (5.12), (5.13) and (5.14).

¹It makes no difference whether we assume that the fingertip slides with respect to the object, or the object slides with respect to the fingertip. In the following sections and examples, the expressions are formulated in terms of a fingertip sliding with respect to the object.

- **The planning problem:** – Given a desired trajectory, $\mathbf{r}(\tau)$, of the fingertip, find the trajectory along which one must drive $\mathbf{r}_e(\tau)$ and $\rho_e(\tau)$ (the commanded position and orientation) and find the corresponding forces, \mathbf{f}_{slip} . In this case, since $\mathbf{r}(\tau)$ and consequently $d\mathbf{r}(\tau)/d\tau$, are known, there are 4 coupled, linear time-varying equations and three constraint equations for 7 unknowns ($\delta r_l, \delta r_m, \delta \theta_n, f_l, f_m, m_n, \delta r_n$).
- **The prediction problem:** – Given a nominal trajectory, $\mathbf{r}_e(\tau)$, find the forces, \mathbf{f}_{slip} , and the actual fingertip trajectory, $\mathbf{r}(\tau)$, that results. As in the previous case, there are 7 unknowns ($r_l, r_m, r_n, \theta_n, f_l, f_m, m_n$) and 7 equations, of which two are now first-order differential equations.
- **The applied-force problem:** – Given a set of forces, $\mathbf{f}(\tau)$, applied to the object, find the family of solutions for $\mathbf{r}(\tau)$ and $\mathbf{r}_e(\tau)$, and solve for the unique solution if the initial conditions and the relationship between τ and s are known².

5.2.6 Analytic solutions for a point-contact finger sliding on a plane

In this section the special case of a point-contact finger sliding on a planar object surface is considered. The point-contact model is a reasonable approximation where the contact diameter is an order of magnitude smaller than the average spacing between fingers [Cutkosky and Wright 1988], as when manipulating a football with the fingertips.

For point contacts, m_n is always zero, and for a planar object f_n and δr_n are constant so that the last two equations in (5.19) can be dropped. In addition, the friction limit surface equations reduce to $f_t = \mu f_n$ and $\mathbf{f}_{slip} = f_t \hat{\mathbf{r}}$.

²This relation gives us the relative magnitude of the sliding trajectory.

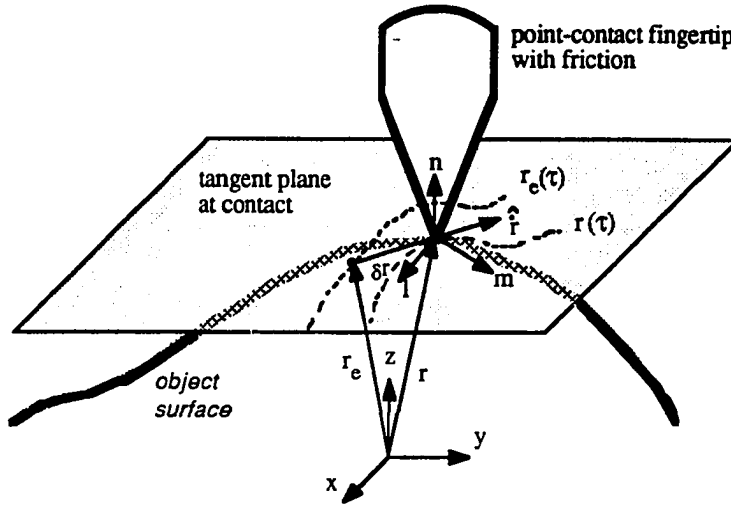


Figure 5.4: Coordinate system and trajectory for a point-contact fingertip sliding on a surface

Equation (5.19) is now reduced to:

$$\begin{bmatrix} f_t \ dr_l/d\tau \\ f_t \ dr_m/d\tau \end{bmatrix} \frac{d\tau}{ds} + \mathbf{K}_p \begin{bmatrix} r_l - r_{e,l} \\ r_m - r_{e,m} \end{bmatrix} = 0 \quad (5.20)$$

where $f_t = \sqrt{f_l^2 + f_m^2}$ and \mathbf{K}_p is now a 2×2 matrix representing the fingertip stiffness in the (l, m) plane.

For the planar point-contact case, $r(\tau)$ and $r_e(\tau)$ become two-element vectors in the (l, m) plane. Substituting μf_n for f_t , we can write equation (5.20) in a more convenient form:

$$\frac{dr(\tau)}{d\tau} + \Xi r(\tau) = \Xi r_e(\tau) \quad (5.21)$$

where $\Xi = [\mu f_n \frac{d\tau}{ds}]_{r(\tau)}^{-1} \mathbf{K}_p$. The relationships among $r_e(\tau)$, $r(\tau)$ and \hat{r} for a point-contact finger are shown in Figure 5.4. Equation (5.21) is the governing equation for the fingertip while it is sliding.

At the start of the problem ($\tau=0$) the fingertip may be subject to an initial tangential force, $\mathbf{f}_0 = [f_{l_0}, f_{m_0}]^T$, which produces an initial displacement, $\delta\mathbf{r}_0 = (\mathbf{r}(\tau_0) - \mathbf{r}_e(\tau_0))$, and

$$\mathbf{f}_0 = -\mathbf{K}_p \delta\mathbf{x}_0 \quad \text{or} \quad \mathbf{r}(\tau_0) = \mathbf{r}_e(\tau_0) - \mathbf{K}_p^{-1} \mathbf{f}_0 \quad (5.22)$$

for $|f_0| \leq \mu f_n$. Equation (5.21), together with the initial condition (5.22) represents a first-order time-varying inhomogeneous differential equation system:

$$\begin{cases} \frac{d\mathbf{r}(\tau)}{d\tau} + \Xi \mathbf{r}(\tau) = \Xi \mathbf{r}_e(\tau) \\ \mathbf{r}(\tau_0) = \mathbf{r}_e(\tau_0) + \mathbf{K}_p^{-1} \mathbf{f}_0 \end{cases}. \quad (5.23)$$

For such time-varying systems, a state-transition matrix $\Phi(\tau, \tau')$ can be defined such that

$$\mathbf{r}(\tau) = \Phi(\tau, \tau') \mathbf{r}(\tau'), \quad \text{for } \tau, \tau' \in [c, d] \quad (5.24)$$

where τ' can be any point in the interval, $[c, d]$, of definition for the differential equation. Many properties and results regarding the state-transition matrix are summarized in [Kailath 1980]. The complete solution for equations (5.21) and (5.22) is

$$\mathbf{r}(\tau) = \Phi(\tau, \tau_0) \mathbf{r}(\tau_0) + \int_{\tau_0}^{\tau} \Phi(\tau, t) \Xi(t) \mathbf{r}_e(t) dt. \quad (5.25)$$

Again, τ_0 can be any state in the interval but we choose it to be the initial state. Its reference point depends upon the simulation implementation.

For time-varying systems, closed form solutions usually do not exist and numerical computation is required to determine $\Phi(\tau, \tau_0)$.

However, when Ξ and $d\tau/ds$ are constant, equation (5.21) can be treated as a linear time-invariant system:

$$\mathbf{r}(\tau) = \underbrace{e^{-\Xi\tau} \mathbf{r}(\tau_0)}_{\text{transient}} + \underbrace{\Xi \int_{\tau_0}^{\tau} e^{-\Xi(\tau-t)} \mathbf{r}_e(t) dt}_{\text{steady-state}} \quad (5.26)$$

where t is a dummy integration variable. Equation (5.26) enables us to solve the sliding problem in an analytical form. Whenever \mathbf{K}_p , μ , f_n , and $d\tau/ds$ do not vary significantly, the results from the approximate solution are very close to those derived from lengthy numerical simulations. Concerning \mathbf{K}_p , it has been found in experiments with a two fingered manipulator that as long as the manipulator is not operated near a kinematic singularity, one can assume that \mathbf{K}_p is constant for motions that introduce a few degrees of motion in the finger joints. Moreover, under cartesian stiffness control [Salisbury 1980] the position and force servo gains may be continually adjusted to

achieve a constant endpoint stiffness. In the case where Ξ can not be regarded as constant, equation (5.26) can be used infinitesimally for simulation purposes.

The transient and steady-state solutions of equation (5.26) correspond to the homogeneous and particular solutions, respectively. From the form of these equations we expect that the initial conditions will only affect the transient term which is a decaying exponential. In fact, for any positive definite grasp stiffness matrix, K_p , the transient response resulting from the homogeneous solution of equation (5.21) is always decaying, resulting in a stable sliding trajectory.

5.3 Examples of single-finger sliding manipulation

In this section the sliding analysis for a single finger, as outlined in Sections 5.2.5 and 5.2.6, is illustrated with several examples.

Examples 5.1, 5.2, and 5.3 involve a point-contact finger sliding on a planar surface and their purpose is to illustrate the trajectory planning, to clarify the nature of transient and steady-state solutions, and to show how the approach can be used for piece-wise continuous trajectories with different static and kinetic coefficients of friction. Experimental results are presented for comparison with the analytic solution. Example 5.5 is a three-dimensional problem involving a soft-contact fingertip sliding on a curved surface. The finger is assumed to have a stiffness comparable to that of a finger of the Stanford/JPL hand. Although the problem is three-dimensional, the choice of a spherical object results in minimum kinematic overhead.

5.3.1 Planning and predicting trajectories for a point-contact finger

For the examples in this section, a simplified point-contact robotic finger is used which is modeled as having a diagonal stiffness matrix with equal stiffnesses in each

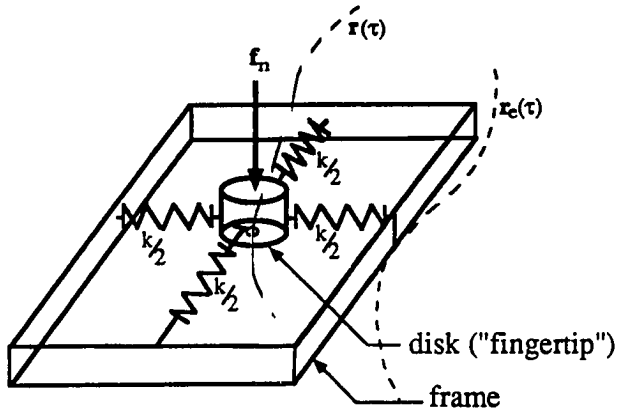


Figure 5.5: Schematic of idealized fingertip for sliding. In experiments, the frame is moved by a robot arm.

direction:

$$\mathbf{K}_p = \begin{bmatrix} k & 0 \\ 0 & k \end{bmatrix}.$$

A physical implementation of such a fingertip can be approximated by suspending a small disk with four springs and dragging the disk over the surface of an object as shown in Figure 5.5. The frame holding the springs is analogous to the base of a compliant finger, while the suspended disk is analogous to the fingertip under cartesian stiffness control. A version of the idealized “finger” in this example has been built and experiments have been carried out to verify the theoretical results.

Example 5.1 Find r_e so that r will follow a circular path

For this example, we wish to find a trajectory along which to drive the equilibrium position, $r_e(\tau)$, of the “finger” (i.e., to move the frame holding the springs) so that the fingertip, $r(\tau)$, will slide along a circular arc of radius R . This is a straightforward problem since the unit tangent, \hat{r} , can easily be found once $r(\tau)$ is known. $r_e(\tau)$ follows directly from equation (5.21).

Due to symmetry, the diagonal elements of \mathbf{K}_p are identical and equation (5.26) can be written for the point contact finger as

$$\delta r(\tau) = -\zeta \dot{r}(s) \quad (5.27)$$

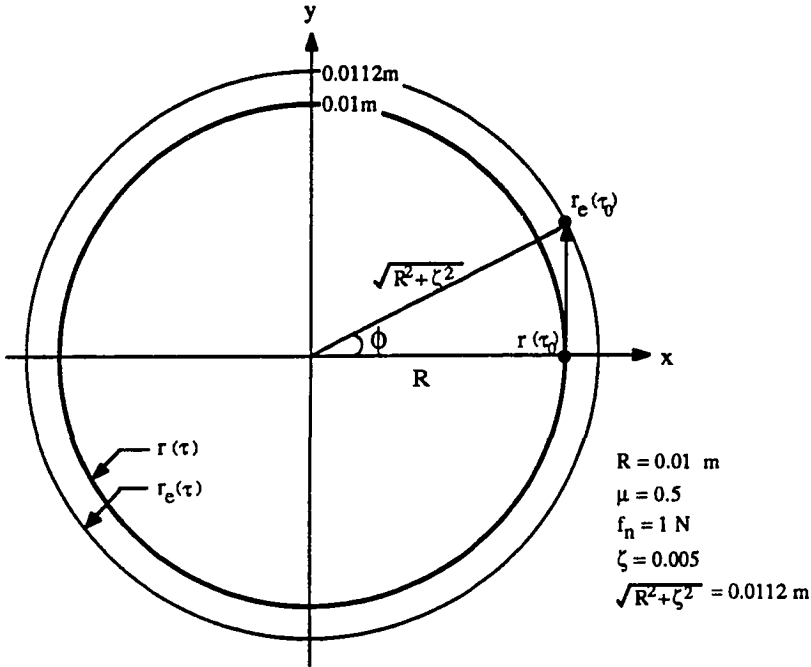


Figure 5.6: The required locus of $r_e(\tau)$ to obtain a circular trajectory of $r(\tau)$

where $\zeta = (\mu f_n)/k$. If we parameterize $r(\tau)$ with respect to the angle τ , we have

$$r(\tau) = \begin{bmatrix} R \cos(\tau) \\ R \sin(\tau) \end{bmatrix} \quad \text{and}, \quad \dot{r}(s) = \begin{bmatrix} -\sin(\tau) \\ \cos(\tau) \end{bmatrix}$$

for a circular arc of radius R . From Equation (5.27),

$$r_e(\tau) = \begin{bmatrix} R \cos \tau - \zeta \sin \tau \\ R \sin \tau + \zeta \cos \tau \end{bmatrix}$$

which means that the equilibrium positions of the finger must follow a circle of radius $\sqrt{R^2 + \zeta^2}$ and with a lead angle of $\phi = \cos^{-1}(R/\sqrt{R^2 + \zeta^2})$ with respect to the disk curve, $r(\tau)$, as shown in Figure 5.6.

Example 5.2 Steady-state and transient response of a continuous circular motion

We assume the same fingertip as in Example 5.1 but we now move $r_e(\tau)$ in a continuous circle of radius R and solve for $r(\tau)$.

From Equation (5.21), we rewrite the expression for this decoupled case as:

$$\frac{d\mathbf{r}(\tau)}{d\tau} + \xi(\tau)\mathbf{r}(\tau) = \xi(\tau)\mathbf{r}_e(\tau) \quad (5.28)$$

As in Example 5.1, $d\tau/ds = 1/\|\mathbf{r}(\tau)\|$. Therefore, $\xi = k(\mu f_n \frac{d\tau}{ds}|_{\mathbf{r}(\tau)})^{-1}$ is time-varying. However, since $k/\mu f_n$ is large, the variation in $d\tau/ds$ does not significantly affect $e^{-\xi\tau}$ and we can treat ξ as a constant, in which case equation (5.28) can be solved to obtain

$$\mathbf{r}_h(\tau) = \begin{bmatrix} c_1 e^{-\xi\tau} \\ c_2 e^{-\xi\tau} \end{bmatrix}$$

and

$$\begin{aligned} \mathbf{r}_p(\tau) &= \xi \int_0^\tau e^{-\xi(\tau-t)} \mathbf{r}_e(t) dt \\ &= \begin{bmatrix} \frac{R\xi}{1+\xi^2} [\xi(\cos \tau - e^{-\xi\tau}) + \sin \tau] \\ \frac{R\xi}{1+\xi^2} [\xi \sin \tau - (\cos \tau - e^{-\xi\tau})] \end{bmatrix} \end{aligned}$$

Also,

$$|\dot{\mathbf{r}}(s)| = \left| \frac{d\mathbf{r}(\tau)}{d\tau} \frac{d\tau}{ds} \right| = 1.$$

At steady state, $\tau \rightarrow \infty$; therefore, $\left| \frac{d\mathbf{r}_p(\tau)}{d\tau} \right| = \frac{R\xi}{\sqrt{1+\xi^2}}$ and we have

$$\left. \frac{d\tau}{ds} \right|_{\tau \rightarrow \infty} = \frac{\sqrt{1+\xi^2}}{R\xi}.$$

The approximate solution obtained if one assumes that $\frac{d\tau}{ds} \cong \frac{d\tau}{ds}|_{\tau \rightarrow \infty}$ for all τ gives good accuracy in spite of the fact that the transient response is described by a time-varying differential equation (i.e., $\frac{d\tau}{ds}|_{\mathbf{r}(\tau)}$ is not strictly constant). Now we apply the initial conditions. For instance, if the disk is initially at $(R, 0)$, and $\mu f_n = 0.5N$, $k = 100N/m$, $R = 0.01m$, and $\mathbf{r}_e(\tau) = (\cos 29^\circ, \sin 29^\circ)$ when sliding starts, we can solve for

$$\mathbf{r}(\tau) = \begin{bmatrix} 0.0107 e^{-\sqrt{3}\tau} \\ -0.00397 e^{-\sqrt{3}\tau} \end{bmatrix} + 0.0075 \begin{bmatrix} \cos \tau + \frac{1}{\sqrt{3}} \sin \tau - e^{-\sqrt{3}\tau} \\ \sin \tau - \frac{1}{\sqrt{3}} \cos \tau + \frac{1}{\sqrt{3}} e^{-\sqrt{3}\tau} \end{bmatrix}$$

where $\tau \in [0, \infty)$, and $\mathbf{r}(\tau) = (R, 0)$. The fingertip is stretched until $\tau = 29^\circ$, when it starts to slide. The above results are plotted for comparison with a numerical simulation in Figure 5.7. In the numerical simulation, equation (5.28) is used directly,

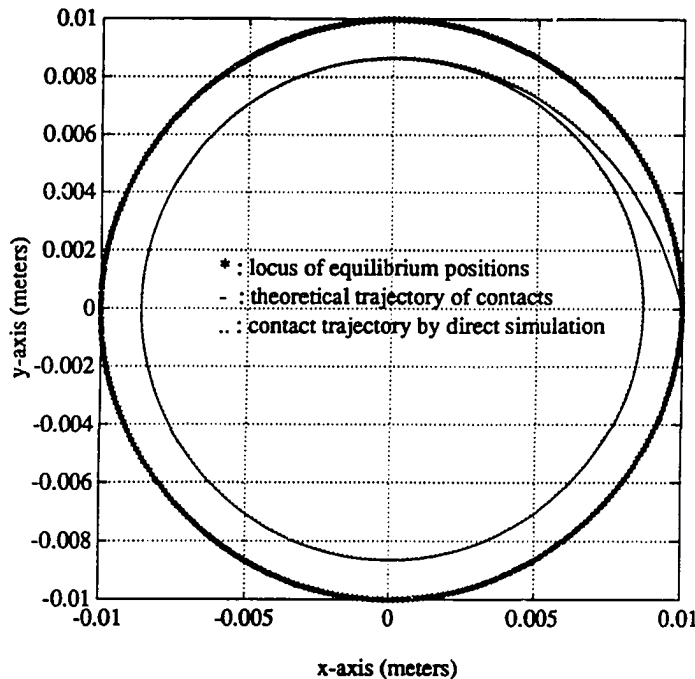


Figure 5.7: Theoretical and numerical solutions for $\mathbf{r}(\tau)$ if $\mathbf{r}_e(\tau)$ is a circle

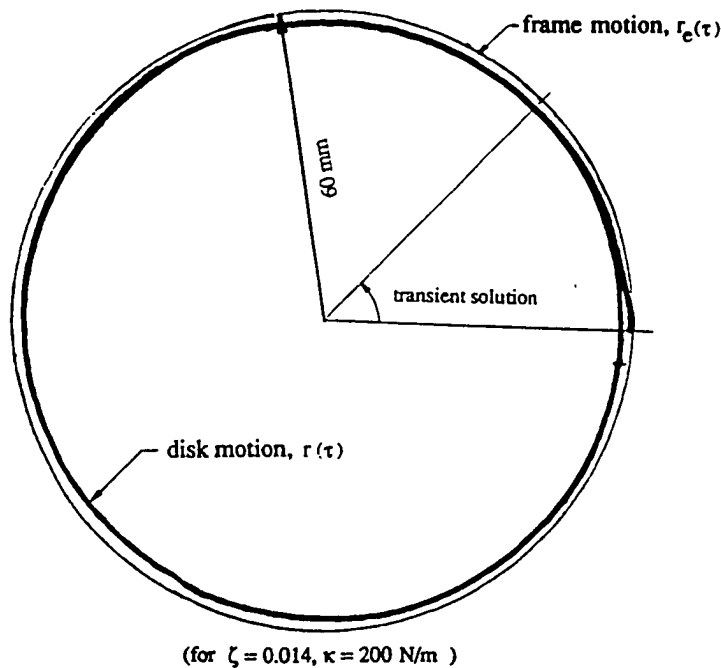


Figure 5.8: Experimental results for $\mathbf{r}(\tau)$ obtained by moving the frame, $\mathbf{r}_e(\tau)$, in a circle

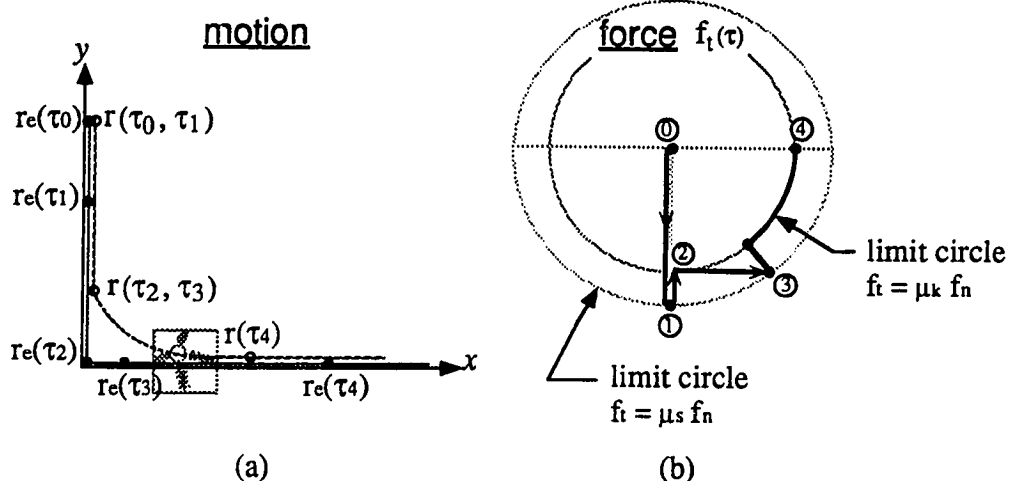


Figure 5.9: (a) Diagram of motion of frame, r_e , and disk, r (b) Tangential force trajectory $f_t(\tau)$

moving the fingertip in 1mm steps. The experimental results are shown in Figure 5.8. The disk trajectory was generated by attaching a plotter pen to the disk. ■

Example 5.3 *Transient response of a point-contact finger moving on a discontinuous planar path*

In the following example we align the contact l and m axes with the body x and y axes, respectively. The robot finger (i.e., the frame) is moved along a trajectory, $r_e(\tau)$, consisting of two straight lines as shown in Figure 5.9. Assume that $f_n = 2.5N$, $k = 85N/m$ and that the static and kinetic coefficients of friction are $\mu_s = 0.45$ and $\mu_k = 0.367$, respectively. What is the locus, $r(\tau)$, of the sliding disk?

As Figures 5.9(a) and (b) show, the problem can be decomposed into several stages:

- At τ_0 the frame, r_e , and disk, r , both start at the position $[0 \ 40]^T mm$ (numerical values are plotted in Figure 5.10). The frame starts moving in the $-y$ direction and the tangential force on the stationary disk builds as $k(r - r_e)$ increases.
- At τ_1 , when $r_e = [0 \ 26.8]^T$, the tangential force is equal to $\mu_s f_n$ and the disk starts to slide in the $-y$ direction.

- At τ_2 the frame reaches the origin and stops. If μ_k were equal to μ_s , the disk would stop at $\mathbf{r} = [0 \ 13.2]^T$, but instead the disk continues sliding until $f_t = \mu_k f_n$ at $\mathbf{r} = [0 \ 10.8]^T$.
- The frame next starts moving in the $+x$ direction and the tangential force gradually increases until f_t again reaches the limit $\mu_s f_n$, which occurs when $\mathbf{r}_e = [7.6 \ 0]^T$ at τ_3 .
- At τ_3 the tangential force is

$$\mathbf{f} = -\mathbf{K}_p(\mathbf{r}(\tau_3) - \mathbf{r}_e(\tau_3)) = \begin{bmatrix} 0.646 \\ -0.918 \end{bmatrix} N$$

and the initial direction of motion is therefore

$$\hat{\mathbf{r}}(\tau_3) = \begin{bmatrix} 0.575 \\ -0.818 \end{bmatrix}.$$

From this point on, the motion of the disk is governed by equation (5.21) and follows an exponentially decaying curve while the frame moves steadily along the x axis. Since $\mathbf{r}(\tau_3) = [0 \ 10.8]^T$, we can numerically simulate equation (5.21) to obtain the locus of $\mathbf{r}(\tau)$. Alternatively, since we know that $\frac{d\tau}{ds} = 1$ at the steady-state, we can write the approximate analytic solution of equation (5.28) as:

$$\mathbf{r}(\tau) = \begin{bmatrix} c_1 \\ c_2 \end{bmatrix} e^{-\xi \tau} + \xi \int_0^\tau e^{-\xi(\tau-t)} \mathbf{r}_e dt \quad (5.29)$$

where $\xi \cong k/(\mu_k f_n)$ and $[c_1 \ c_2]^T$ is the initial condition, $\mathbf{r} = [0 \ 10.8]^T$.

- At some point, τ_4 , the y component of the motion of $\mathbf{r}(\tau)$ can be considered negligible, so that we approach the steady-state motion, $\hat{\mathbf{r}}(\infty) = [1 \ 0]^T$.

The analytic solution of equation (5.29) is plotted in Figure 5.10 for comparison with experimental results. The experimental plot was obtained by fastening a plotter pen to the disk while a robot dragged the frame. The results are close because the object surface was a sheet of clean copier paper – a material which is designed to have predictable friction properties! ■

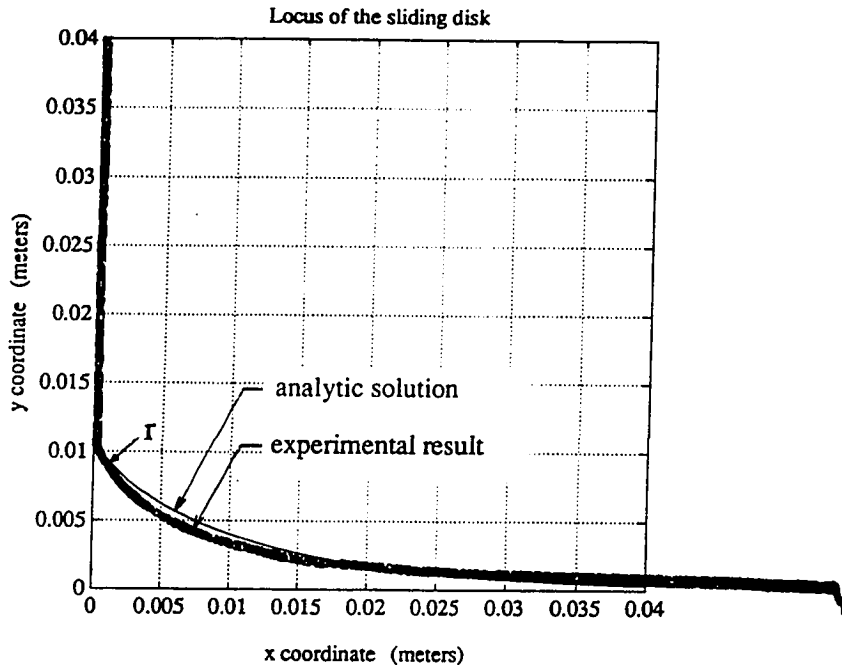


Figure 5.10: Comparison of analytic solution and experimental results for the disk trajectory in Example 5.3

Example 5.4 *Solve for $\mathbf{r}(\tau)$ given a series of applied forces*

If we apply a series of forces to the finger we must check at each instant whether the forces are large enough for sliding. While the fingertip is not sliding, it simply deflects with respect to its equilibrium position, as a function of the stiffness:

$$\delta\mathbf{r}(\tau) = -\mathbf{K}_p^{-1}\mathbf{f}. \quad (5.30)$$

While the finger slides, the motion is governed by equation (5.21) or, for the frame/disk problem, by equation (5.27). Sliding is parallel to the force applied. Therefore, the magnitude and direction of $\zeta\dot{\mathbf{r}}(s)$ are available from the force trajectory while the finger is sliding. The family of curves for $\mathbf{r}(\tau)$ can be found once the force trajectory is given. In addition, we can uniquely define $\mathbf{r}(\tau)$ and $\mathbf{r}_e(\tau)$ if we are given $\frac{d\tau}{ds}|_{\mathbf{r}(\tau)}$.

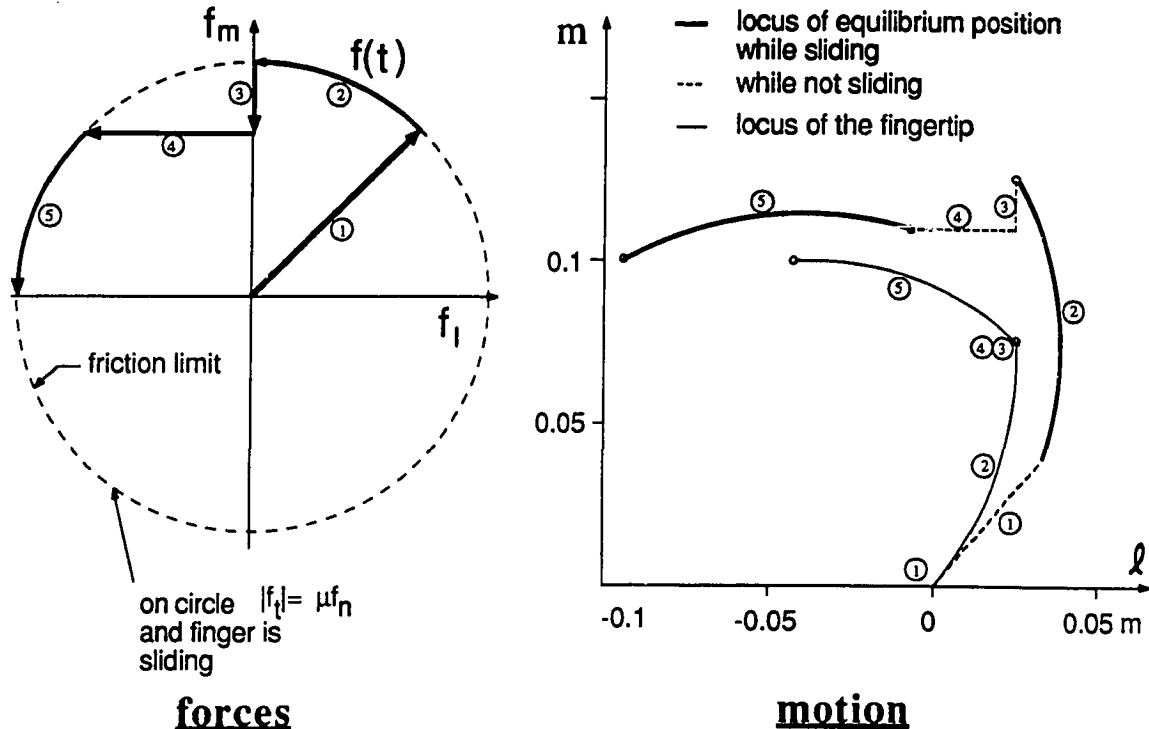


Figure 5.11: Given a force trajectory, find the trajectories of $\mathbf{r}(\tau)$ and $\mathbf{r}_e(\tau)$. The left half shows the sequence of forces. The right half shows the resulting motions.

Consider the following sequence of forces applied to the simplified fingertip of Examples 5.1 and 5.2:

$$\mathbf{f}(\tau) = \begin{cases} \left[\frac{2\sqrt{2}}{\pi} \mu f_n \tau, \frac{2\sqrt{2}}{\pi} \mu f_n \tau \right]^T & \text{if } 0 \leq \tau \leq \pi/4 \\ [\mu f_n \cos \tau, \mu f_n \sin \tau]^T & \text{if } \pi/4 \leq \tau < \pi/2 \\ \left[-\frac{\mu f_n}{\sqrt{2}} \tan \tau, \frac{\mu f_n}{\sqrt{2}} \right]^T & \text{if } \pi/2 < \tau \leq 3\pi/4 \\ [\mu f_n \cos \tau, \mu f_n \sin \tau]^T & \text{if } 3\pi/4 \leq \tau \leq \pi \end{cases}$$

The above sequence is plotted in the left half of Figure 5.11 with respect to friction limitations (represented by a limit circle) for a given normal force and coefficient of friction. While the applied tangential force is inside this circle there is no sliding; while it is on the circle, quasistatic sliding takes place. (The force cannot go outside the circle without violating static equilibrium.) During the first phase, the tangential force gradually builds until sliding begins. While the fingertip is sliding, in phases 2 and 5, τ increases linearly with the counterclockwise angle about the force plot.

The disk and frame trajectories can be found analytically from equations (5.27) and (5.30) (See Appendix C.1). The results are plotted in the right half of Figure 5.11 for comparison with the force trajectory. The plot is for $c_1 = c_2 = 1$ and $\zeta = 0.5$. The constants c_1 and c_2 depend on $d\tau/ds$ of the curve, which is determined by the rate of change of force. Physically, if we make the rate of change smaller (i.e., the force changes direction more gradually) the trajectories of both the fingertip and the finger equilibrium positions (i.e., the positions of the frame) will be enlarged because the fingertip will slide further during each interval. ■

5.3.2 A three dimensional grasp with a soft finger

Example 5.5 Sliding a soft finger on a spherical surface

In this example a simple three-dimensional trajectory for a soft-contact fingertip is considered. The goal is to trace an arc of constant latitude on the surface of a spherical object, as shown in Figure 5.12. The spherical object has a radius of $R = 7\text{cm}$. For convenience, both the $O(XYZ)$ and $B(xyz)$ coordinate frames are located at the center of the sphere. The location of the contact point is given by $\mathbf{r}(\tau)$ which is uniquely defined by the angles ϕ and θ , as indicated in the figure. The desired trajectory is an arc at $\theta = 45^\circ$ over the range $0^\circ \leq \phi \leq 90^\circ$. The question is: what should the commanded trajectory of the fingertip, $\mathbf{r}_e(\tau)$ and $\rho_e(\tau)$ be or, equivalently, what should the fingertip forces, \mathbf{f}_p , be?

Let us establish a local $P(lmn)$ coordinate system as shown in Figure 5.12, that travels with the contact, while keeping l pointed in the direction of motion so that $\mathbf{r} = [R, 0, 0]^T$ and $\dot{\mathbf{r}} = [1, 0]^T$ in the local coordinates. A convenient choice of the independent parameter is $\tau = R\phi$, in which case τ is also equal to s , the arc length along $\mathbf{r}(\tau)$.

Using typical values for a soft rubber fingertip and smooth object, we assume that $\mu = 1.0$, $f_n = 2N$, and $m_{max} = 7 \times 10^{-3}\text{Nm}$ [Howe, Kao and Cutkosky 1988]. Using

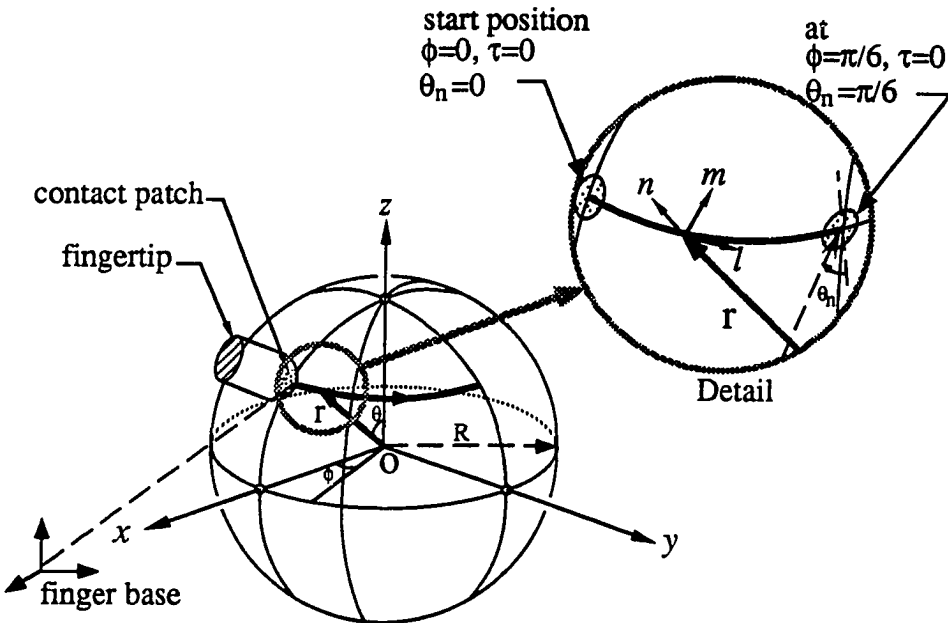


Figure 5.12: Coordinate setup for a soft-contact finger sliding along an arc on a spherical surface

the results of Section 5.2.3, we have

$$\lambda = \left(\frac{m_{max}}{\mu f_n} \right) = 3.5 \times 10^{-3} m$$

The fingertip is provided with a stiffness matrix comparable to the stiffnesses measured for the Stanford/JPL hand (as in Example 3.1 in Section 3.4.5). Two cases are considered. In the first case the fingertip stiffness matrix is assumed to be constant in local $P(lmn)$ coordinates for the duration of the arc. This is a reasonable assumption for small motions about an initial configuration or when \mathbf{K}_p is held constant by control. The second case assumes simple cartesian stiffness control so that the fingertip stiffness is constant in the world $O(XYZ)$ space. Consequently, as the fingertip slides along the sphere, the actual stiffness in $P(lmn)$ coordinates varies continuously. The stiffness matrices for the two cases are given in Appendix C.2. Although the detailed joint-to-contact kinematics will not be concerned with here, we note that they are presented by Okada [1979, 1982] for the case of four-jointed fingers manipulating a spherical object.

For this problem, equation (5.19) becomes:

$$\begin{bmatrix} f_l \\ 0 \\ 0 \\ \vdots \\ m_n \end{bmatrix} + \begin{bmatrix} 0 \\ 0 \\ \delta f_n \\ \vdots \\ 0 \end{bmatrix} + \mathbf{H} \mathbf{K}_p \mathbf{H}^T \begin{bmatrix} \delta r_l \\ \delta r_m \\ \delta r_n \\ \vdots \\ \delta \theta_n \end{bmatrix} = 0 \quad (5.31)$$

We now need to apply the constraint equations from the limit surface. First, let us rewrite equation (5.8) as:

$$f_l^2 + \frac{m_n^2}{\lambda^2} = (\mu f_n)^2. \quad (5.32)$$

Due to the kinematic configuration of the finger, there is actually some rotation about the n axis when the contact traces an arc of constant latitude. Since the base of the finger is located at a distance of $2R$ from O , the ratio between the necessary linear and rotational velocities is $dr_l/d\tau = R d\theta_n/d\tau$. Applying equation (5.9), we have

$$\frac{dr_l/d\tau}{d\theta_n/d\tau} = R = \lambda^2 \frac{f_l}{m_n}.$$

(Equation (5.10) adds nothing since there is no motion in the m direction.) Using these equations we can solve for:

$$f_l = \frac{R}{\lambda} \frac{\mu f_n}{\sqrt{\frac{R^2}{\lambda^2} + 1}} \text{ and } m_n = \frac{\mu f_n \lambda}{\sqrt{\frac{R^2}{\lambda^2} + 1}} \quad (5.33)$$

which can be substituted into equation (5.31) to obtain $\mathbf{r}_e(\tau)$. The results are plotted in Figure 5.13, where we have transformed $\mathbf{r}_e(\tau)$ back to the $O(XYZ)$ coordinates to make the trajectories clearer.

Several observations can be made from the plots. First, the commanded trajectory, $\mathbf{r}_e(\tau)$, lies slightly inside the spherical surface so that the appropriate bias forces will be generated, based on the \mathbf{K}_p matrix. In addition, when examining the projections of the curves in the (XZ) plane, we see that $\mathbf{r}_e(\tau)$ for the constant \mathbf{K}_p case is slightly below $\mathbf{r}(\tau)$, due to coupling in the \mathbf{K}_p matrix, but is level since \mathbf{K}_p , f_n and the friction properties are constant and consequently, $\delta \mathbf{r}$ is constant. By contrast, the curve for the varying \mathbf{K}_p case shows some variation in the Z direction. The plots also give an

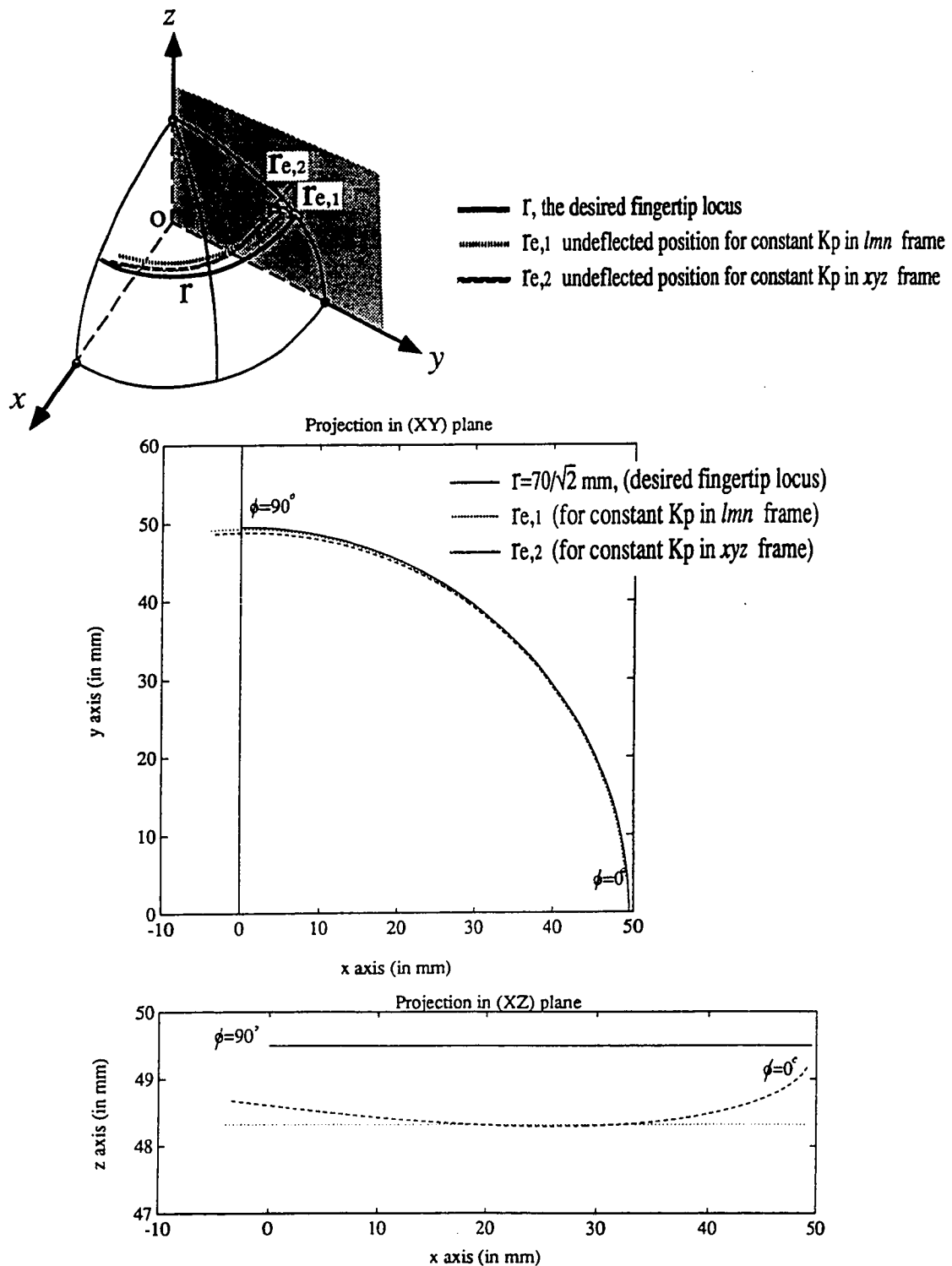


Figure 5.13: Results for a soft finger sliding on a spherical surface – three-dimensional perspective plot and magnified projections on the (XY) and (XZ) planes

idea of the amount of error associated with assuming a constant \mathbf{K}_p matrix. The error is of course most evident near the endpoints of the curve, when the variation in \mathbf{K}_p is largest. The maximum error in $|\delta\mathbf{r}|$ is about 14%.

5.4 Summary

The problem of manipulating a grasped object with one sliding finger has been investigated. The approach draws on the stiffness matrices of fingers and grasped objects presented in Chapter 3, and the friction limit surface presented in Chapter 4. The stiffness matrices correlate fingertip forces with displacements. As a result, one can describe the force on each fingertip in terms of the trajectory of a fingertip and the trajectory of its undeflected positions. The limit surface yields the relationships between the contact force/moment and the direction of sliding which results in a first-order differential equation governing the motions of the finger and the grasped object. The equation of motion is expressed in terms of an independent geometric parameter since quasistatic motion is assumed. The solution of the differential equation has a transient solution, due to initial grasp forces, and a steady-state solution.

Several simple examples are illustrated using the approach discussed in this chapter. The examples explore planning problems (computing how to drive the fingers so as to achieve a desired trajectory) and prediction problems (predicting how the fingers will respond when forces or motions are applied to the grasped object). The analytic results are compared with experiments in which an idealized fingertip is manipulated by a robot arm.

Chapter 6

Motions of Sliding Manipulation

6.1 Introduction

In this chapter the sliding motions of a multifingered grasp are discussed. The motions are solved for by formulating equations of force equilibrium, constitutive equations (stiffness and friction relationships), and equations of geometric compatibility (motion constraints). Two categories of sliding motion problems are discussed: controlling the fingers to achieve a prescribed motion; and predicting the motions that will result when forces are applied. The instantaneous motions of sliding fingers can be thought of as a vector space consisting of two components: rigid-body (RB) motions and non-rigid-body (NRB) motions. The properties of the RB and NRB motions are investigated and their use in motion planning is explored. The approaches are illustrated with several examples of sliding for multifingered grasps with point or soft contacts.

6.2 Extensions to multifingered manipulation

The necessary condition for static equilibrium is the same as that discussed in Chapter 5, i.e.,

$$\mathbf{f}_{total} = \nabla(\mathbf{f} \cdot \mathbf{v}) = \frac{\partial P_v}{\partial \mathbf{v}}. \quad (6.1)$$

The gradient of the work done over the \mathbf{v} -space is the total force, if all forces are velocity independent. However, since the equilibrium conditions do not completely determine the fingertip forces, grasp stiffness matrices are needed to determine \mathbf{f}_t , when motions and/or forces are applied to the grasped object, as discussed in Section 4.3. In considering the forces on the object it is useful to recognize that once sliding occurs, the force and moment at each finger have to be on the friction limit surface (Chapter 4) to maintain equilibrium. The total external force on the body becomes the sum of the external forces, the non-sliding contact forces and the kinetic friction forces.

The first step is to determine which fingers are sliding. For those that are not sliding, the fingertip stiffness matrices relate the contact forces to compliant motions of the contact, using equation (5.16). For sliding fingers, the sliding force/torque is governed by the friction limit surface for the contact, and the fingertip motion is governed by the results of Section 5.2.4.

In the case of multifingered sliding grasps, we need to express the sliding motions of different fingers with respect to a common coordinate frame. Thus, equation (5.19) can be transformed to the $B(xyz)$ coordinate system as:

$$\mathbf{H}_B^P \mathbf{J}^T \mathbf{H}^T \left(\begin{bmatrix} f_t \dot{\mathbf{r}} \\ 0 \\ \vdots \\ m_n \end{bmatrix} + \begin{bmatrix} 0 \\ 0 \\ \vdots \\ 0 \end{bmatrix} + \mathbf{H} \mathbf{K}_p \begin{bmatrix} \delta \mathbf{r} \\ \vdots \\ \delta \rho \end{bmatrix} \right) = 0 \quad (6.2)$$

where \mathbf{H} again serves to remove the all-zero equations corresponding to moments

about the contact l and m axes. Equations (6.2) for each finger can then be concatenated for the entire grasp:

$$\mathcal{H}_B^P \mathcal{J}^T \mathcal{H}^T \begin{pmatrix} |f_{t_1}| \hat{\mathbf{r}}_1 \\ 0 \\ m_{n_1} \\ \vdots \\ |f_{t_2}| \hat{\mathbf{r}}_2 \\ 0 \\ m_{n_2} \\ \vdots \\ \vdots \end{pmatrix} + \begin{pmatrix} 0 \\ 0 \\ \delta f_{n_1} \\ 0 \\ \vdots \\ 0 \\ 0 \\ \delta f_{n_2} \\ 0 \\ \vdots \\ \vdots \end{pmatrix} + \mathcal{H} \mathcal{K}_p \begin{pmatrix} \delta \mathbf{r}_1 \\ \delta \rho_1 \\ \vdots \\ \delta \mathbf{r}_2 \\ \delta \rho_2 \\ \vdots \\ \vdots \end{pmatrix} = 0 \quad (6.3)$$

where \mathcal{H} , and \mathcal{K}_p are the concatenated stiffness and contact constraint matrices introduced in Sections 3.3.3 and 3.4.2.

In addition to force equilibrium and the constitutive relationships due to friction and stiffness at each fingertip, we have a velocity compatibility equation for each finger:

$$\mathbf{H}_i \mathbf{v}_i = \mathbf{H}_i^P \mathbf{J}_i \mathbf{v}_b - \mathbf{H}_i \mathbf{v}_{slip,i} \quad (6.4)$$

where \mathbf{v}_i is the absolute velocity of the fingertips, \mathbf{v}_b is a 6-element vector of the linear and rotational velocity of the body, and $\mathbf{v}_{slip,i}$ is the relative sliding velocity between the fingertips and the object surface.¹ As discussed in Sections 1.3 and 3.3.2, \mathbf{J}_i^P is a cartesian transformation between the (x, y, z) coordinate system of the object and the (l, m, n) system at the i -th contact (hence $\mathbf{J}_i^P \mathbf{v}_b$ is the velocity of the grasped rigid body at the contact location) and \mathbf{H}_i is the contact constraint matrix.

Concatenating the geometry compatibility equation, (6.4), over all fingers we can write:

$$\mathcal{H} \mathcal{V} = \mathcal{H}_B^P \mathcal{J} \mathbf{v}_b - \mathcal{H} \mathcal{V}_{slip} \quad (6.5)$$

¹For cases such as point contact, where there is incomplete kinematic coupling between the fingertip and object, the undetermined elements of \mathbf{v}_i can be found from the grasp compliance matrix, as discussed in Section 3.4.3.

where the product $(\mathcal{H}_B^P \mathcal{J})$ is a $\sum n_i \times 6$ matrix and n_i is the number of linear and angular velocity components transmitted through the i 'th contact.

As in the single-finger analysis, there are essentially two types of problems: (1) controlling the fingers to achieve a prescribed motion, and (2) predicting the motions that will result when forces are applied. Examples of such problems are discussed in Sections 6.4.1 and 6.4.2.

6.3 RB and NRB motions of sliding manipulation

Equation (6.4) represents the velocity compatibility constraints of each finger, i . In analyzing general problems of sliding manipulation, it is conceptually helpful to break the elements of \mathcal{V} and \mathcal{V}_{slip} for all sliding fingertips into rigid-body and non-rigid-body components. Therefore, it is proposed that the velocities, \mathcal{V} and \mathcal{V}_{slip} , of a grasp be partitioned into these two components – the rigid-body motion (RB) and non-rigid-body (NRB) motions, denoted as $_{RB}\mathcal{V}$ and $_{NRB}\mathcal{V}$. The concept of RB and NRB motions has been applied in other disciplines, such as the theory of elasticity [Timoshenko and Goodier 1970], except that in such applications it is typically the NRB component (the deformation) that is of interest. The RB component of the velocities results in net rigid-body motion of the grasped object while the NRB component results in internal relative motions but *no* net rigid-body motion. In the next section, the NRB space will be defined formally.

6.3.1 RB and NRB vector spaces

The NRB vector space is defined as follows:

Definition 6.1 *The NRB motion is a vector space of motions with no rigid-body component.*

In the context of grasping analysis, the NRB motion in Definition 6.1 represents a vector space of motion in the null space of the rigid body motion of the fingers and object.

To simplify notation, we define $\mathcal{J}_c = (\mathcal{H}_B^P \mathcal{J})$ where \mathcal{J}_c represents those partitions of the cartesian transformation matrices seen through the contacts. Equation (6.5) is then rewritten by breaking \mathcal{V} and \mathcal{V}_{slip} into RB and NRB components:

$$\mathcal{J}_c \mathbf{v}_b = \mathcal{H}(\mathbf{v}_{RB} + \mathbf{v}_{RB\text{slip}}) + \mathcal{H}(\mathbf{v}_{NRB} + \mathbf{v}_{NRB\text{slip}}) \quad (6.6)$$

Inverting equation (6.5), we obtain

$$\mathbf{v}_b = \mathcal{J}_c^* \mathcal{H}(\mathcal{V} + \mathcal{V}_{slip}) \quad (6.7)$$

where $\mathcal{J}_c^* = (\mathcal{H}_B^P \mathcal{J})^*$ is the generalized inverse of \mathcal{J}_c . The generalized inverse is usually expressed as the left-inverse [Strang 1989], $(\mathcal{H}_B^P \mathcal{J}^T \mathcal{H}^T \mathcal{H}_B^P \mathcal{J})^{-1} \mathcal{H}_B^P \mathcal{J}^T \mathcal{H}^T$, but for convenience we choose the weighted pseudo-inverse, $(\mathcal{H}_B^P \mathcal{J}^T \mathcal{H}^T \mathcal{W} \mathcal{H}_B^P \mathcal{J})^{-1} \mathcal{H}_B^P \mathcal{J}^T \mathcal{H}^T \mathcal{W}$ where \mathcal{W} is a positive-definite and symmetric weighting matrix defined in Appendix D.1, chosen so that angular components are normalized by the characteristic length of the grasp. The choice of the pseudo-inverse is such that the optimal solution, among all solutions of $\mathcal{J}_c \mathbf{v}_b = \mathcal{H}(\mathcal{V} + \mathcal{V}_{slip})$, is the one that has the minimum weighted norm. This corresponds to the case in which

$$\mathcal{H}(\mathbf{v}_{NRB} + \mathbf{v}_{NRB\text{slip}}) = 0 \quad (6.8)$$

since, from Definition 6.1, the NRB components are in the null space of \mathcal{J}_c . Details are given in Appendix D.2. Consequently, we can rewrite equation (6.5) by grouping the RB and NRB components:

$$\mathcal{H}(\mathbf{v}_{RB} + \mathbf{v}_{NRB}) = \mathcal{H}_B^P \mathcal{J}_i \mathbf{v}_b - \mathcal{H}(\mathbf{v}_{RB\text{slip},i} + \mathbf{v}_{NRB\text{slip},i}) \quad (6.9)$$

Equation (6.7) can also be rewritten using results of equation (6.8):

$$\mathbf{v}_b = \mathcal{J}_c^* \mathcal{H}(\mathbf{v}_{RB} + \mathbf{v}_{RB\text{slip}}) + \mathcal{J}_c^* \mathcal{H}(\mathbf{v}_{NRB} + \mathbf{v}_{NRB\text{slip}}) \quad (6.10)$$

$$= \mathcal{J}_c^* \mathcal{H}(\mathbf{v}_{RB} + \mathbf{v}_{RB\text{slip}}) \quad (6.11)$$

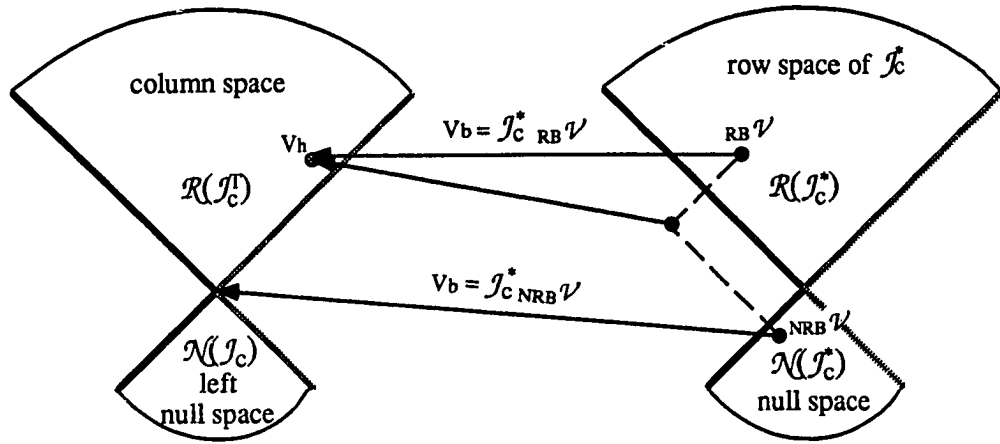


Figure 6.1: Geometric visualization of the solution spaces

Examining equation (6.10), we see that \mathbf{v}_b is in the column space of \mathcal{J}_c^* , $\mathcal{R}(\mathcal{J}_c^*)$, and, in order for the NRB motions never to contribute to \mathbf{v}_b , ${}_{NRB}\mathcal{V}$ and ${}_{NRB}\mathcal{V}_{slip}$ must lie in the null space of \mathcal{J}_c^* , $\mathcal{N}(\mathcal{J}_c^*)$. Furthermore, the sum of ${}_{NRB}\mathcal{V}$ and ${}_{NRB}\mathcal{V}_{slip}$ is not only in the null space but identically zero. These relationships can easily be visualized using Figure 6.1. We also note that the null space of \mathcal{J}_c^* is a subspace of $\mathcal{R}^{\Sigma n_i}$.

An analogy between the NRB and RB components of the finger velocities can be drawn with internal and external components of the grasp forces, as defined in the literature on dexterous manipulation (e.g., [Kerr and Roth 1986]). Just as the internal grasp forces do not contribute to the resultant force on the object, the non-rigid-body components of \mathcal{V} and \mathcal{V}_{slip} do not contribute to the resultant motion of the grasped object. The analogy should not be carried too far however, since, as will be shown in Example 6.3, a grasp with purely internal grasp forces (no resultant) can result in rigid-body sliding motions of the object.

6.3.2 Compatibility equations of sliding motion

The results of Section 6.3.1 are summarized for the following sections:

$$\mathcal{H}\mathcal{V} = \mathcal{H}_{\text{B}}^{\text{P}}\mathcal{J}\mathbf{v}_b - \mathcal{H}\mathcal{V}_{\text{slip}} \quad (6.12)$$

$$\mathbf{v} = {}_{\text{NRB}}\mathbf{v} + {}_{\text{RB}}\mathbf{v} \quad (6.13)$$

$$\mathcal{H}({}_{\text{RB}}\mathcal{V} + {}_{\text{NRB}}\mathcal{V}) = \mathcal{H}_{\text{B}}^{\text{P}}\mathcal{J}\mathbf{v}_b - \mathcal{H}({}_{\text{RB}}\mathcal{V}_{\text{slip}} + {}_{\text{NRB}}\mathcal{V}_{\text{slip}}) \quad (6.14)$$

$$\mathcal{H}({}_{\text{NRB}}\mathcal{V} + {}_{\text{NRB}}\mathcal{V}_{\text{slip}}) = 0 \quad (6.15)$$

$$\mathcal{H}_{\text{RB}}\mathcal{V} = \mathcal{H}_{\text{B}}^{\text{P}}\mathcal{J}\mathbf{v}_b - \mathcal{H}_{\text{RB}}\mathcal{V}_{\text{slip}} \quad (6.16)$$

To explore the motion of a multifingered grasp, we first define a couple of additional terms.

Definition 6.2 *The common rigid body motion of the fingers, \mathbf{v}_h , is defined such that ${}_{\text{RB}}\mathcal{V} = {}_{\text{B}}^{\text{P}}\mathcal{J}\mathbf{v}_h$.*

In other words, ${}_{\text{RB}}\mathcal{V}$ can be expressed in terms of an equivalent rigid body motion at $B(xyz)$. It is as if the fingers were attached to an imaginary object moving with velocity \mathbf{v}_h .

Definition 6.3 *Following Definition 6.2, we define $\mathbf{v}'_b = (\mathbf{v}_b - \mathbf{v}_h)$, where \mathbf{v}_b is the motion of the grasped rigid body and \mathbf{v}'_b is the net rigid body motion of the object with respect to the fingertips.*

Substituting \mathbf{v}_h into equation (6.14), we have

$$\mathcal{J}_c\mathbf{v}_h + \mathcal{H}_{\text{NRB}}\mathcal{V} = \mathcal{J}_c\mathbf{v}_b - \mathcal{H}({}_{\text{RB}}\mathcal{V}_{\text{slip}} + {}_{\text{NRB}}\mathcal{V}_{\text{slip}}).$$

Rewriting in terms of \mathbf{v}'_b , we have

$$\mathcal{H}_{\text{NRB}}\mathcal{V} = \mathcal{J}_c\mathbf{v}'_b - \mathcal{H}\mathcal{V}_{\text{slip}} \quad (6.17)$$

Equation (6.15) relates the *sum* of $_{\text{NRB}}\mathcal{V}$ and $_{\text{NRB}}\mathcal{V}_{\text{slip}}$ subject to contact constraints. However, their individual values are yet to be found. To simplify notation, we define $\mathcal{W}_c = \mathcal{H}^T \mathcal{W} \mathcal{H}$ which represents the relevant partitions of the weighting matrix, \mathcal{W} , subject to the contact constraints. Before deriving the NRB solutions, let us define a function “ g ”.

Definition 6.4 *A function “ g ”, the weighted norm of the NRB vector, is defined as*

$$g \triangleq \frac{1}{2} \|_{\text{NRB}}\mathcal{V}^T \mathcal{H}^T \mathcal{W} \mathcal{H} _{\text{NRB}}\mathcal{V} \| = \frac{1}{2} ({}_{\text{NRB}}\mathcal{V}^T \mathcal{W}_c {}_{\text{NRB}}\mathcal{V}) \quad (6.18)$$

It is useful to minimize a weighted norm, g , instead of $\|_{\text{NRB}}\mathcal{V}\|^2$, since the velocity term $_{\text{NRB}}\mathcal{V}$ includes both linear and angular components. The matrix \mathcal{W} is a weighting matrix (Appendix D.1) that scales the rotational components such that they can be brought to compare with the linear components. From Definition 6.4 and equation (6.15) we have

$$g \triangleq \frac{1}{2} ({}_{\text{NRB}}\mathcal{V}^T \mathcal{W}_c {}_{\text{NRB}}\mathcal{V}) = \frac{1}{2} ({}_{\text{NRB}}\mathcal{V}_{\text{slip}}^T \mathcal{W}_c {}_{\text{NRB}}\mathcal{V}_{\text{slip}}) \quad (6.19)$$

where the “1/2” coefficient is for convenience in the following section.

6.3.3 Solution of the NRB motion of grasps by minimization

In this section, it will be shown that the solution of NRB motions can be obtained by minimizing g , the weighted norm of $_{\text{NRB}}\mathcal{V}$ (or $_{\text{NRB}}\mathcal{V}_{\text{slip}}$). Furthermore, the result is consistent with the solution obtained by equations (6.10) and (6.11). The solution also results in the smallest (weighted) NRB motions.

Theorem 6.1 *The RB and NRB motions of a grasp can be obtained by minimizing the function “ g ”, i.e., by finding the solution to*

$$\frac{\partial g}{\partial \mathbf{v}'_b} = \frac{\partial}{\partial \mathbf{v}'_b} \left(\frac{1}{2} {}_{\text{NRB}}\mathcal{V}^T \mathcal{W}_c {}_{\text{NRB}}\mathcal{V} \right) = 0 \quad (6.20)$$

Proof: Substituting equation (6.17) into g , we have

$$g = \frac{1}{2}_{\text{NRB}}\mathcal{V}^T\mathcal{H}^T\mathcal{W}\mathcal{H}_{\text{NRB}}\mathcal{V} = \frac{1}{2}(\mathcal{J}_c\mathbf{v}'_b - \mathcal{H}\mathcal{V}_{\text{slip}})^T\mathcal{W}(\mathcal{J}_c\mathbf{v}'_b - \mathcal{H}\mathcal{V}_{\text{slip}}) \quad (6.21)$$

Differentiating equation (6.21) with respect to \mathbf{v}'_b , we obtain

$$\begin{aligned} \frac{\partial g}{\partial \mathbf{v}'_b} &= (\mathcal{J}_c\mathbf{v}'_b - \mathcal{H}\mathcal{V}_{\text{slip}})^T\mathcal{W}\mathcal{J}_c \\ &= (\mathcal{J}_c\mathbf{v}_b - \mathcal{J}_c\mathbf{v}_h - \mathcal{H}\mathcal{V}_{\text{slip}})^T\mathcal{W}\mathcal{J}_c \\ &= {}_{\text{NRB}}\mathcal{V}^T\mathcal{H}^T\mathcal{W}\mathcal{J}_c = (\mathcal{J}_c^T\mathcal{W}\mathcal{H}_{\text{NRB}}\mathcal{V})^T \end{aligned} \quad (6.22)$$

Recall from the definition of NRB motion and equation (6.10) that ${}_{\text{NRB}}\mathcal{V}$ must lie in the null space of \mathcal{J}_c^* . By the definition of the weighted generalized inverse in Section 6.3.1, $\mathcal{J}_c^*\mathcal{H}_{\text{NRB}}\mathcal{V} = ({}_{\text{B}}^P\mathcal{J}^T\mathcal{H}^T\mathcal{W}\mathcal{H}_{\text{B}}^P\mathcal{J})^{-1} {}_{\text{B}}^P\mathcal{J}^T\mathcal{H}^T\mathcal{W}\mathcal{H}_{\text{NRB}}\mathcal{V} = 0$. It is obvious that $\mathcal{J}_c^T\mathcal{W}\mathcal{H}_{\text{NRB}}\mathcal{V} = 0$ because $({}_{\text{B}}^P\mathcal{J}^T\mathcal{H}^T\mathcal{W}\mathcal{H}_{\text{B}}^P\mathcal{J})$ is non-singular. This leads to

$$\frac{\partial g}{\partial \mathbf{v}'_b} = (\mathcal{J}_c^T\mathcal{W}\mathcal{H}_{\text{NRB}}\mathcal{V})^T = 0 \quad (6.23)$$

Consequently, minimizing g does result in a solution that satisfies the NRB criterion; therefore, RB and NRB solutions can be obtained by minimizing “ g ”.

■

Equation (6.22) can also be written as

$$\mathcal{J}_c^T\mathcal{W}(\mathcal{J}_c\mathbf{v}'_b - \mathcal{H}\mathcal{V}_{\text{slip}}) = 0 \quad (6.24)$$

which can be used to solve for \mathbf{v}'_b and the RB and NRB components of the motions once the weighting matrix is chosen. In equation (6.24), \mathbf{v}'_b can be solved for (subject to undetermined constants representing the magnitude of $\mathbf{v}_{\text{slip},i}$) because the directions of $\mathbf{v}_{\text{slip},i}$ are known from the grasp forces and limit surfaces. We can pre-multiply the equation $\mathbf{v}'_b = \mathbf{v}_b - \mathbf{v}_h$ by the matrix \mathcal{J}_c and substitute the result into equation (6.12) to obtain the following equations:

$$\mathcal{H}_{\text{RB}}\mathcal{V} = \mathcal{H}(\mathcal{V} + \mathcal{V}_{\text{slip}} - {}_{\text{B}}^P\mathcal{J}\mathbf{v}'_b) \quad (6.25)$$

$$\mathcal{H}_{\text{RB}}\mathcal{V}_{\text{slip}} = \mathcal{J}_c\mathbf{v}'_b \quad (6.26)$$

Equations (6.25) and (6.26) can be used to find the RB solution of the sliding motion. The NRB motions are then obtained by $_{\text{NRB}}\mathcal{V} = \mathcal{V} - {}_{\text{RB}}\mathcal{V}$ and $_{\text{NRB}}\mathcal{V}_{\text{slip}} = \mathcal{V}_{\text{slip}} - {}_{\text{RB}}\mathcal{V}_{\text{slip}}$. Equation (6.16) consists of a set of simultaneous equations for \mathbf{v}_b resulting from each finger. Substituting the results into equation (6.11) and equating the expressions, we can solve for the remaining unknowns. This procedure will be illustrated in Example 6.4.

Before proceeding to the example we observe that in the derivation of equation (6.22), we arrived at $_{\text{NRB}}\mathcal{V}^T \mathcal{H}^T \mathcal{W} \mathcal{J}_c = 0$ which will bring us to the next theorem:

Theorem 6.2 *For a sliding manipulation of an object grasped by “nf” fingers, the RB and NRB motions, as defined in Definition 6.1 and equation (6.13), are orthogonal in the weighted space, i.e.,*

$$_{\text{NRB}}\mathcal{V}^T \mathcal{W}_{c \text{ RB}} \mathcal{V} = {}_{\text{NRB}}\mathcal{V}_{\text{slip}}^T \mathcal{W}_{c \text{ RB}} \mathcal{V}_{\text{slip}} = 0 \quad (6.27)$$

Proof: From Definition 6.2 and equation (6.23),

$$_{\text{NRB}}\mathcal{V}^T \mathcal{W}_{c \text{ RB}} \mathcal{V} = {}_{\text{NRB}}\mathcal{V} \mathcal{H}^T \mathcal{W} (\mathcal{J}_c \mathbf{v}_h) = ({}_{\text{NRB}}\mathcal{V} \mathcal{H}^T \mathcal{W} \mathcal{J}_c) \mathbf{v}_h = 0$$

In addition, using equations (6.15) and (6.16), we can show that

$$\begin{aligned} {}_{\text{NRB}}\mathcal{V}^T \mathcal{W}_{c \text{ RB}} \mathcal{V} &= (-\mathcal{H} {}_{\text{NRB}}\mathcal{V}_{\text{slip}})^T \mathcal{W} (\mathcal{J}_c \mathbf{v}_b - \mathcal{H} {}_{\text{RB}}\mathcal{V}_{\text{slip}}) \\ &= {}_{\text{NRB}}\mathcal{V}_{\text{slip}}^T \mathcal{W}_{c \text{ RB}} \mathcal{V}_{\text{slip}} - \mathbf{v}_b^T (\mathcal{J}_c^T \mathcal{W} \mathcal{H} {}_{\text{NRB}}\mathcal{V}_{\text{slip}}) \\ &= {}_{\text{NRB}}\mathcal{V}_{\text{slip}}^T \mathcal{W}_{c \text{ RB}} \mathcal{V}_{\text{slip}} \end{aligned}$$

Therefore,

$${}_{\text{NRB}}\mathcal{V}^T \mathcal{W}_{c \text{ RB}} \mathcal{V} = {}_{\text{NRB}}\mathcal{V}_{\text{slip}}^T \mathcal{W}_{c \text{ RB}} \mathcal{V}_{\text{slip}} = 0 \quad \blacksquare$$

For a sliding manipulation with given fingertip velocities, the squared norm of the fingertip velocities is the sum of squared norms of the RB and NRB components that are transmitted through contacts, using the orthogonality property in Theorem 6.2.

Assume that E is the squared norm of the fingertip velocities. E can be derived by applying equation (6.27):

$$\begin{aligned} E = \frac{1}{2}\mathcal{V}^T \mathcal{W}_c \mathcal{V} &= \frac{1}{2}(\mathbf{_{RB}}\mathcal{V} + \mathbf{_{NRB}}\mathcal{V})^T \mathcal{W}_c (\mathbf{_{RB}}\mathcal{V} + \mathbf{_{NRB}}\mathcal{V}) \\ &= \frac{1}{2}(\mathbf{_{RB}}\mathcal{V}^T \mathcal{W}_c \mathbf{_{RB}}\mathcal{V}) + \frac{1}{2}(\mathbf{_{NRB}}\mathcal{V}^T \mathcal{W}_c \mathbf{_{NRB}}\mathcal{V}) + \mathbf{_{NRB}}\mathcal{V}^T \mathcal{W}_c \mathbf{_{RB}}\mathcal{V} \\ &= \frac{1}{2}(\mathbf{_{RB}}\mathcal{V}^T \mathcal{W}_c \mathbf{_{RB}}\mathcal{V}) + \frac{1}{2}(\mathbf{_{NRB}}\mathcal{V}^T \mathcal{W}_c \mathbf{_{NRB}}\mathcal{V}) \end{aligned}$$

That is,

$$E = \frac{1}{2}(\mathbf{_{RB}}\mathcal{V}^T \mathcal{W}_c \mathbf{_{RB}}\mathcal{V}) + g \quad (6.28)$$

Physically, the solution obtained by minimizing the function “ g ” is a solution that minimizes the weighted norm of NRB motions and therefore maximizes the overall RB motions.

In some cases it may be useful to formulate the related equations in the joint space. Suppose that the joint motions corresponding to the RB and NRB motions at the fingertips are $\mathbf{_{RB}}\dot{\theta}_i$ and $\mathbf{_{NRB}}\dot{\theta}_i$:

$$\frac{1}{2}\mathcal{V}^T \mathcal{W}_c \mathcal{V} = \frac{1}{2}[\mathbf{_{RB}}\dot{\theta}_i (\mathcal{J}_\theta^T \mathcal{W}_c \mathcal{J}_\theta) \mathbf{_{RB}}\dot{\theta}_i] + \frac{1}{2}[\mathbf{_{NRB}}\dot{\theta}_i (\mathcal{J}_\theta^T \mathcal{W}_c \mathcal{J}_\theta) \mathbf{_{NRB}}\dot{\theta}_i] \quad (6.29)$$

$$= \frac{1}{2}[\mathbf{_{RB}}\dot{\theta}_i \mathbf{Q}^T \boldsymbol{\Lambda} \mathbf{Q} \mathbf{_{RB}}\dot{\theta}_i] + \frac{1}{2}[\mathbf{_{NRB}}\dot{\theta}_i \mathbf{Q}^T \boldsymbol{\Lambda} \mathbf{Q} \mathbf{_{NRB}}\dot{\theta}_i] \quad (6.30)$$

The matrix $(\mathcal{J}_\theta^T \mathcal{W}_c \mathcal{J}_\theta)$ in equation (6.29) is a symmetric matrix since \mathcal{W}_c is symmetric; therefore, it has real eigenvalues and orthogonal eigenvectors. Hence, the NRB component of the joint motions, $\mathbf{_{NRB}}\dot{\theta}_i$, is found such that the weighted quadratic function of $\mathbf{_{NRB}}\dot{\theta}_i$ (by the eigenvalues of $\mathcal{J}_\theta^T \mathcal{W}_c \mathcal{J}_\theta$ or the matrix $\boldsymbol{\Lambda}$) in the virtual eigenspace (transformed by the orthogonal eigenvectors of $\mathcal{J}_\theta^T \mathcal{W}_c \mathcal{J}_\theta$ or the matrix \mathbf{Q}) is minimized. The orthogonality property mentioned in Theorem 6.2 is preserved under such an orthogonal transformation by the eigenvectors, \mathbf{Q} .

It is noticed that although the velocities of the fingers are assumed throughout the analysis, they can be zero without affecting the correctness of the results. This generalizes the solution to the cases of combined sliding and non-sliding fingers in practical grasping problems.

6.4 Examples of multi-fingered sliding manipulation

Several examples of sliding manipulation are discussed using the criteria and theorems proposed in this chapter.

6.4.1 Achieving a prescribed motion

If the motion of the object v_b is prescribed, as may happen in planning a manipulation task, the instantaneous motions of the fingers may be solved for independently. Equation (4.6) applies to the non-sliding fingers and the results of the single finger analysis apply to the sliding fingers.

As an illustration, let us consider the “twirling” problem of rotating an object between two fingers discussed in [Fearing 1986]. With the approach that the method in Chapters 5 and 6 provides, some of Fearing’s original assumptions can be relaxed and the exact trajectories that the fingers will follow can be computed. It is also observed that the presence of coupling in the grasp stiffness matrix of the Stanford/JPL hand could account for the buildup of “yawing” motions (and eventual failure of the twirling task) that Fearing observed in experiments.

Example 6.1 “Twirling” an object between a stationary and a moving finger

Consider the problem of repeatedly turning over a pen using the thumb, index and middle fingers of a hand. This is the “twirling” problem posed by Fearing [1986]. To simplify the problem, Fearing first considers the planar manipulation of a wedge-shaped object grasped between a moving finger (finger 1) and a stationary finger (finger 2), as shown in the upper half of Figure 6.2. The fingers have small contact radii so that rolling effects can be ignored. A local coordinate system is established such that the y axis is always along the line between the two contacts. (In this example, the x and y coordinates correspond to Fearing’s θ and r coordinates, respectively.)

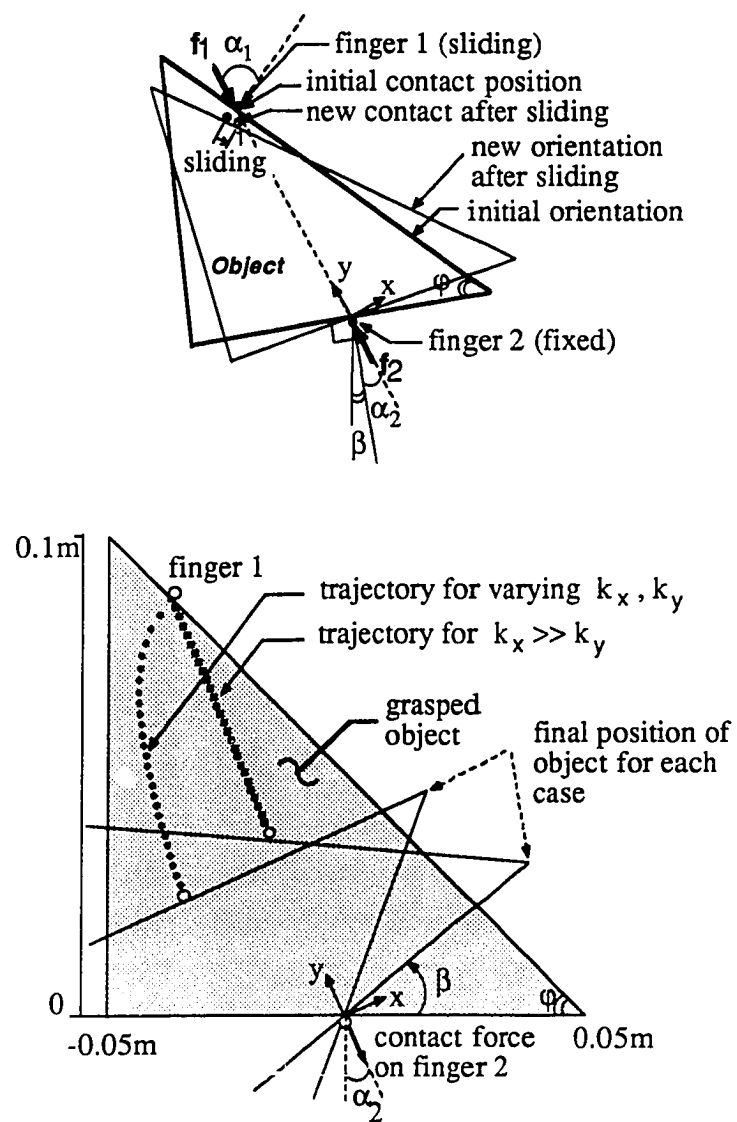


Figure 6.2: The “twirling” motion: manipulating a wedge-shaped object between a sliding and stationary finger. Upper half shows forces and coordinates. Lower half shows the trajectory of finger 1.

Finger 2 is fixed, but finger 1 has a decoupled stiffness matrix:

$$\mathbf{K}_1 = \begin{bmatrix} k_x & 0 \\ 0 & k_y \end{bmatrix}.$$

To maintain equilibrium, the grasp force applied by finger 1 must lie along the line between the two contacts as shown in Figure 6.2. Thus, $\mathbf{f}_1 = [0, -f_1]^T$. Whenever \mathbf{f}_1 is outside the friction cone (i.e., when the angle between the surface normal and the grasp force direction is too large) finger 1 will slide and the grasped object will pivot, or “twirl” with respect to finger 2.

First, the initial equilibrium position of finger 1 is found such that $\mathbf{f}_1 = \mathbf{K}_1(\mathbf{r}_1 - \mathbf{r}_{e_1})$. If the initial distance between the two fingers is d , the initial equilibrium position of finger 1 is

$$\mathbf{r}_{e_1} = \mathbf{K}_1^{-1}\mathbf{f}_1 + \mathbf{r}_1 = \begin{bmatrix} 0 \\ (-f_1/k_y + d) \end{bmatrix}.$$

which represents a point in the region between the two fingers.

Since finger 1 is outside its friction cone, it begins to slide. Finger 1 is constrained to slide along the surface of the grasped object and therefore the instantaneous direction of sliding is

$$\hat{\mathbf{r}} = \begin{bmatrix} \cos(\psi + \alpha_2) \\ -\sin(\psi + \alpha_2) \end{bmatrix}$$

where ψ is the angle between the two polyhedral surfaces and α_2 is the angle between the surface normal and \mathbf{f}_2 at finger 2. The new position of \mathbf{r} can be found from

$$\mathbf{r}_1 = \mathbf{r}_{e_1} - \mu_1 f_{n_1} \mathbf{K}_1^{-1} \hat{\mathbf{r}} = \begin{bmatrix} -\mu_1 f_{n_1} \frac{\cos(\psi + \alpha_2)}{k_x} \\ d - \frac{f_1 - \mu_1 f_{n_1} \sin(\psi + \alpha_2)}{k_y} \end{bmatrix} \quad (6.31)$$

where $f_{n_1} = f_1 \cos(\psi + \alpha_2)$. Equation (6.31) must be updated continually if \mathbf{K}_p or any of the other parameters changes with configuration.

The motion of finger 1 causes the object to twirl counterclockwise. Eventually, the contact force at finger 1 falls within the friction cone and sliding ceases. This is shown as the final position in the lower half of Figure 6.2. Note that if $k_x \rightarrow \infty$, to match Fearing’s assumption, identical results (i.e., finger 1 moves in a straight

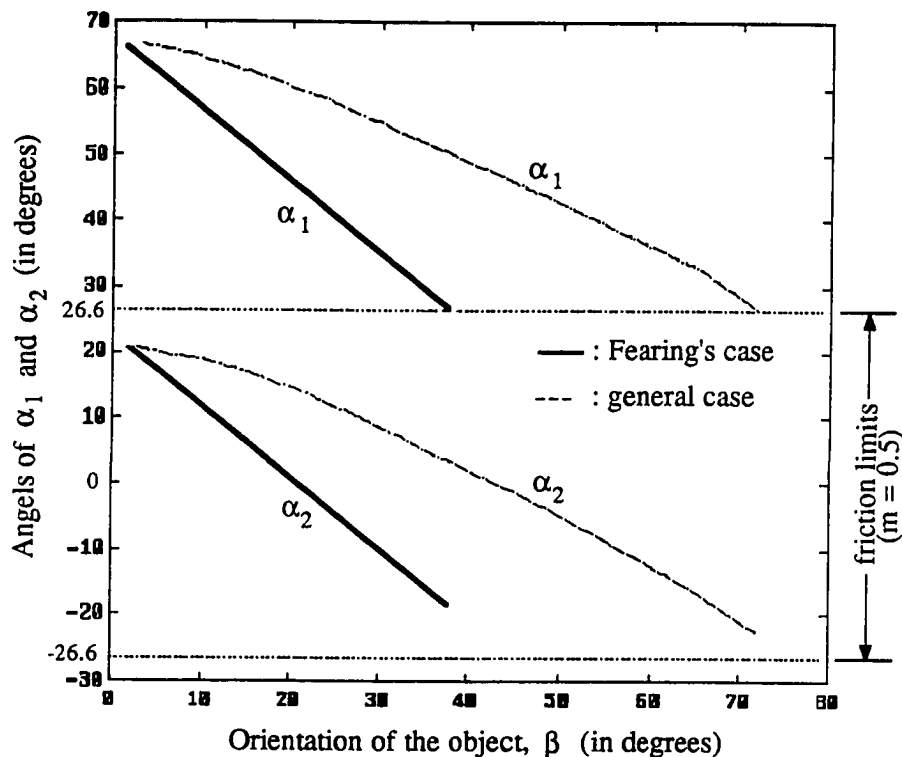


Figure 6.3: Trajectory of the angles α_1 and α_2 of the “twirling” motion

line) are obtained. The results of the angles α_1 and α_2 are shown in Figure 6.3. In Fearing’s case, both α_1 and α_2 are linear functions of the orientation parameter, β . However, this sliding analysis allows for arbitrary (and varying) stiffness matrices. In such more general cases, the trajectories for α_1 and α_2 are not linear, as shown in Figure 6.3. In informal experiments involving the twirling of a triangular object between two fingers, concave trajectories like those in the second curve of Figure 6.2 are easily obtained.

The results of the sliding analysis also provide an intriguing explanation for the “yawing” motion (rotations out of the plane of the paper) that Fearing [1987] observed, which eventually caused his twirling task to fail when performed on the Stanford/JPL hand. Since the stiffness matrix at the fingertips is generally not diagonal (unlike this example) there is coupling between motions in the twirling plane and in the direction perpendicular to the plane. Hence, as the object rotates in the twirling plane, “yawing” motions gradually develop. ■

6.4.2 Applying forces

We now consider the motions that result from applying forces to an object. For applied forces, the motions of the fingers are no longer decoupled. The motion of non-sliding fingers is governed by equation (4.6), and the motion of sliding fingers is determined according to their limit surfaces and equations (6.3), (6.9), and (6.24). The motion of the body is then determined by the sliding and non-sliding fingers.

The analysis of such problems can be illustrated with some planar examples involving soft fingers sliding on a card. The planar geometry keeps the kinematics simple so that analytic solutions may be obtained. The first example is a very simple one for which equation (6.4), the point-contact friction limit ($f_t \leq \mu f_n$) and force equilibrium suffice to determine the trajectory. The second two examples involve soft fingers with friction limit surfaces and make use of equations (6.9) and (6.24).

Example 6.2 *Two point contact fingers sliding on a surface with a given external force*

Suppose that we have two point contact fingers with identical diagonal stiffness matrices at the contacts:

$$\mathbf{K}_{p_i} = \begin{bmatrix} k_x & 0 \\ 0 & k_y \end{bmatrix}.$$

An external force with constant direction is initially applied at one of the contacts, and in a direction perpendicular to the line joining the contacts, as shown in Figure 6.4.

In Figure 6.4, finger 2 is the “worst-case” finger (see section 4.4.1) and will slide first. Once it slides, the configuration of the grasp will change and the magnitude of the external force must be adjusted to maintain static equilibrium. The paper continues to pivot about the contact point of finger 1 until the force on finger 2 reaches its friction limit. At this point, both fingers slide, which means that this is a *critical configuration* as defined in Section 4.6. Since this is a symmetric grasp, both fingers will subsequently slip at the same rate and the paper will simply translate after it reaches the critical configuration. An (x, y) coordinate system that moves with the

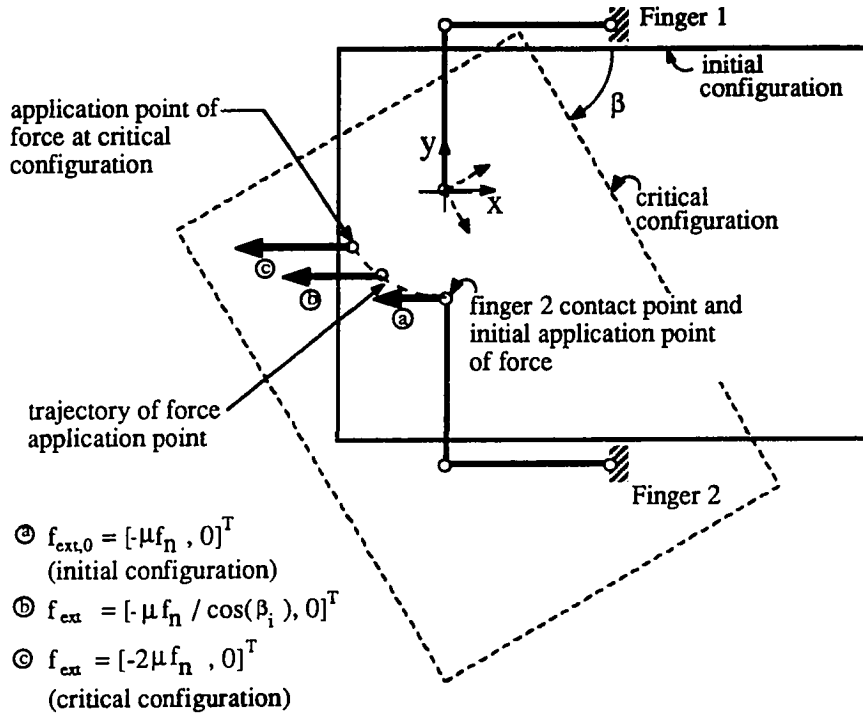


Figure 6.4: Two fingers sliding on a sheet of paper

paper is established and is located at the contact of finger 1. From static equilibrium, the external force is initially $\mathbf{f}_0 = [-\mu f_n, 0]^T$, as shown in position 1 of Figure 6.4. Assume that there is no internal force between the fingers. The initial motion of the object can be obtained from the force equilibrium and equation (6.4) and the motion constraint of finger 1. As expected, we obtain $\mathbf{v}_b = [-1, 0]^T$ units, which shows that the paper initially pivots about finger 1, and $\mathbf{v}_1 = [0, 0]^T$ and $\mathbf{v}_2 = [1, 0]^T$ with respect to the local (xy) coordinates.

Once the paper has started to move, the equations must be reevaluated. It can be found that if the paper has rotated clockwise by an angle, β , $\mathbf{f} = [-\mu f_n / \cos \beta, 0]^T$, $\mathbf{v}_b = [-1, 0]^T$, $\mathbf{v}_1 = [0, 0]^T$ and $\mathbf{v}_2 = [-\cos \beta, \sin \beta]^T$. Eventually, the critical configuration is reached, as shown in Figure 6.4 where the paper has rotated $\beta = 60^\circ$. For this configuration, the contact force at each finger is $\mathbf{f}_1 = \mathbf{f}_2 = [\mu f_n, 0]^T$ and the external force is $\mathbf{f} = [-2\mu f_n, 0]^T$.

The reader can experimentally verify this example by resting two fingers on a piece of paper and pulling with the other hand, grasping the paper near one of the contacts. Initially, the finger nearest to the applied force will slide and the object will pivot about the other finger. After the paper rotates somewhat, both fingers start to slide and the paper then translates in the direction of the applied force. Friction between the table top and the paper does not interfere with the results because the paper is flexible and the table/paper friction simply adds to the finger/paper friction at each contact. ■

Example 6.3 Sliding a card with two soft fingers (symmetric case)

Consider a sheet of paper or a business card manipulated by two fingers as shown in Figure 6.5. The rectangular sheet is supported by a smooth table top, with little friction. Also, since the paper is thin, the supporting points are concentrated immediately beneath the fingers and simply add to the finger contact forces. The fingers have soft contacts that can sustain both tangential forces and moments. No external forces are applied to the paper and, therefore, the finger forces in the plane are purely internal grasp forces. If the fingers move in a symmetrical fashion, it is obvious that only rotations of the paper are possible – no other motions of the paper will produce forces that satisfy symmetry and static equilibrium. The reader can verify this experimentally by manipulating a business card on a smooth table top with the thumb of each hand. (Using the thumbs results in larger contact areas and more noticeable friction torques). If no rigid-body motion is made with the thumbs (i.e., the hands are not moved in unison), only rotations of the card are possible.

Force equilibrium:

The equations of equilibrium for this example reduce to:

$$f_1 - f_2 = 0$$

and

$$rf_1 + rf_2 - m_1 - m_2 = 0.$$

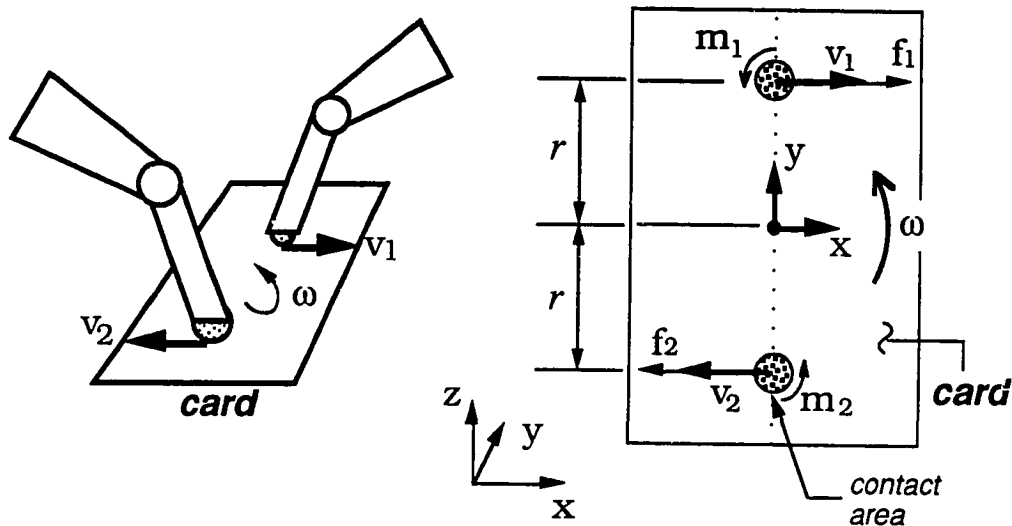


Figure 6.5: Perspective and plan view of two soft fingers manipulating a business card with linear and rotational sliding. v_i are the velocities of the fingertips, m_i are the forces and torques applied to the card by the fingertips.

This is a statically indeterminate problem (2 equations and 4 unknowns) but from symmetry², we can conclude that $f_1 = f_2 = f$ and $m_1 = m_2 = m = rf$.

Constitutive equations:

If we return to the limit surface in Figure 4.3, it can be seen that $m = fr$ determines a line with slope r that intersects the limit surface at a unique point. Using the dimensionless spherical limit surface discussed in Section 5.2.3, we can obtain the relation between the force/moment and direction of the unit normal, \mathbf{p}_s . From equations (5.8) and (5.12), we know that the ratio of the linear and rotational velocities is $\lambda \cot \psi$, where λ has units of length.

The question is: what is the magnitude of ω_z , the rotational velocity of the paper? Since the problem is quasistatic, we can only express the magnitude of ω_z in terms of the linear velocity of the fingers, v_i .

²It is not actually necessary to use symmetry, since inspection of the limit surfaces for each fingertip would reveal that if the normal and tangential forces are equal then the moments must be equal too.

Geometric Compatibility:

The instantaneous relative velocity of each fingertip with respect to the paper has the direction given by equation (5.12). The absolute velocities of the contact points on the card can be written as $\mathbf{v}_i = [v_{x_i}, v_{y_i}, \omega_{z_i}]^T$ and are equal to ${}^P_B\mathbf{J}_i \mathbf{v}_b$,³ the velocity of the grasped card transformed to the contact point, minus $\mathbf{v}_{slip,i}$, the relative velocity of the fingertip with respect to the card. Thus, for the upper fingertip we can write equation (6.4) as:

$$\mathbf{H}^P_B \mathbf{J}_1 \mathbf{v}_b = \mathbf{H}(\mathbf{v}_1 + \mathbf{v}_{slip,1}) \quad \text{or:} \quad \begin{bmatrix} -\omega_z r \\ 0 \\ \omega_z \end{bmatrix} = \begin{bmatrix} v \\ 0 \\ 0 \end{bmatrix} + c \begin{bmatrix} \lambda \cos \psi \\ 0 \\ \sin \psi \end{bmatrix}$$

where $\lambda = m_{max}/\mu f_n$, as defined in equation (5.11), ω_z is the unknown angular velocity of the paper and c is a constant corresponding to the unknown magnitude of $\mathbf{v}_{slip,i}$. In this planar soft-finger example, \mathbf{H} is simply a 3×3 identity matrix. Eliminating c and solving for ω_z , we obtain:

$$\omega_z = \frac{-v \sin \psi}{(r \sin \psi + \lambda \cos \psi)} = \frac{-v}{(r + \lambda \cot \psi)} \quad (6.32)$$

where, since $0 \leq \psi \leq \pi/2$, the minus sign indicates that the card rotates clockwise. The result agrees with intuition and with qualitative experiments in manipulating a business card with two soft fingers. When r is small ($r \ll \lambda \cot \psi$) and the fingers are close together, $\omega \cong -(v \tan \psi)/\lambda$. In other words, ω_z is small, and directly related to the ratio of the maximum linear and rotational friction force. The reader can verify this experimentally by bringing two fingers close together and sliding them. The fingers slide considerably with respect to the card, but the card does not rotate much. On the other hand, when r is large ($r \gg \lambda \cot \psi$), $\omega \cong -v/r$, which corresponds to the case in which the card simply pivots between two point-contact fingers. ■

Example 6.4 Manipulating a card with two sliding soft fingers (nonsymmetric case)

³where ${}^P_B\mathbf{J}$ is now a planar 3×3 cartesian transformation matrix

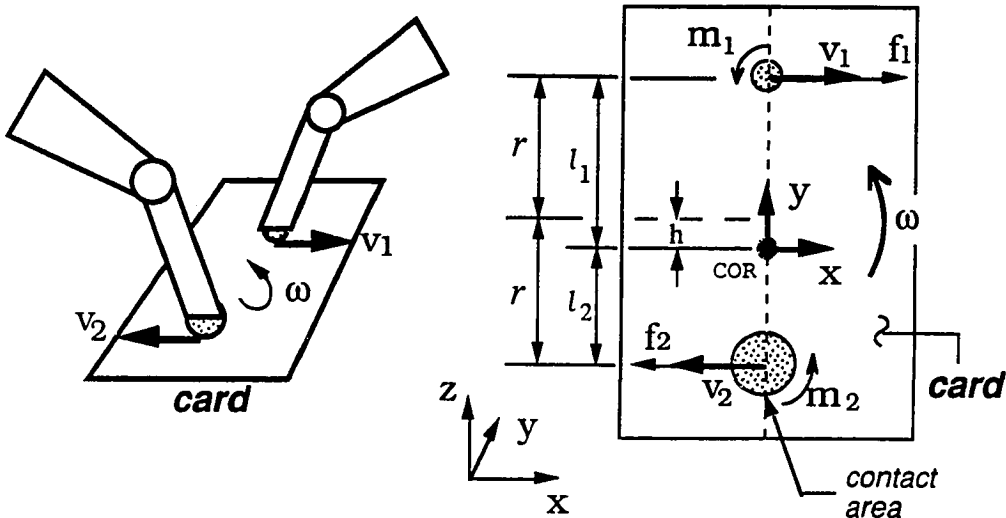


Figure 6.6: Perspective and plan view of two soft fingers manipulating a business card with linear and rotational sliding. The equation of motion is formulated with respect to a coordinate frame at the center of rotation (COR).

Let us re-consider the task of two fingers manipulating a card with linear and rotational sliding, as shown in Figure 6.6. This example is similar to Example 6.3 except that (1) no assumptions about the symmetry are made, (2) the reference coordinates are at the (as yet undetermined) center of rotation (COR). We assume that the distance between the two contact centroids is $2r$ and the distance between the center and COR is h , as shown in Figure 6.6.

Even though no symmetry is assumed, we can show by contradiction that the object can not move in the y direction and $f_{y_1} = 0$ (see Appendix D.3). Since the reference frame is at the COR, we know that the velocity of the card is given by $\mathbf{v}_b = [0 \ 0 \ \omega]^T$. The problem is now to solve for both ω and the COR location, h . The equations can be formulated in the same manner as those in Example 6.3.

Referring to Figure 6.6, the equations of equilibrium for the unsymmetric case are:

$$f_1 - f_2 = 0$$

$$-f_1l_1 - f_2l_2 + m_1 + m_2 = 0$$

where $l_1 = r + h$ and $l_2 = r - h$. The constitutive equations are

$$f_i = \mu_i f_{n,i} \frac{1}{\sqrt{1 + l_i^2}}, \quad m_i = m_{max,i} \frac{l_i}{\sqrt{1 + l_i^2}} \quad \text{for } i = 1, 2$$

where $\mu_i f_{n,i}$ and $m_{max,i}$ are the semiaxes of the elliptical cross-sections of the limit surfaces. The normalized unit normal, \mathbf{p}_s , is parallel to the direction of the normalized force/moment vector, namely,

$$\mathbf{p}_s = \begin{bmatrix} \cos \psi \\ \sin \psi \end{bmatrix} = \begin{bmatrix} \frac{f_i}{\mu f_n} \\ \frac{m_n}{m_{max}} \end{bmatrix}$$

The ratio of linear and rotational sliding velocities is

$$\frac{\|d\mathbf{r}_i/d\tau\|}{d\theta_{n,i}/d\tau} = \frac{v_{slip,i}}{\omega_{slip,i}} = \lambda_i \cot \psi_i = \frac{\lambda_i \cos \psi_i}{\sin \psi_i} \quad (6.33)$$

for each finger. From equation (6.4), geometric compatibility requires that

$$\begin{bmatrix} -l_1 \omega \\ 0 \\ \omega \end{bmatrix} = \begin{bmatrix} v_1 \\ 0 \\ 0 \end{bmatrix} + c_1 \begin{bmatrix} \lambda_1 \cos \psi_1 \\ 0 \\ \sin \psi_1 \end{bmatrix} \quad (6.34)$$

$$\begin{bmatrix} l_2 \omega \\ 0 \\ \omega \end{bmatrix} = \begin{bmatrix} -v_2 \\ 0 \\ 0 \end{bmatrix} + c_2 \begin{bmatrix} -\lambda_2 \cos \psi_2 \\ 0 \\ \sin \psi_2 \end{bmatrix} \quad (6.35)$$

where λ_i are the parameters for the individual limit surfaces, ω is the unknown angular velocity of the card, and c_i 's are constants corresponding to the unknown magnitudes of $\mathbf{v}_{slip,i}$. Eliminating c_1 and c_2 and solving for ω , we obtain:

$$\omega = -\frac{v_1 + v_2}{(2r + \lambda_1 \cot \psi_1 + \lambda_2 \cot \psi_2)}. \quad (6.36)$$

where the minus sign indicates that the card rotates clockwise. We can also find l_i and h .

$$l_1 = \frac{2r(v_1 + c_1 \lambda_1 \cos \psi_1)}{(v_1 + v_2 + c_1 \lambda_1 \cot \psi_1 + c_2 \lambda_2 \cot \psi_2)} \quad (6.37)$$

$$h = l_1 - r = \frac{r(v_1 - v_2 + \omega \lambda_1 \cot \psi_1 - \omega \lambda_2 \cot \psi_2)}{(v_1 + v_2 + \omega \lambda_1 \cot \psi_1 + \omega \lambda_2 \cot \psi_2)} \quad (6.38)$$

The horizontal velocity of the point at the midpoint of the contact centroids is found to be

$$v_x = -\omega h = \frac{rv_1 - rv_2 + v_1 \lambda_1 \cot \psi_1 - v_2 \lambda_2 \cot \psi_2}{(2r + \lambda_1 \cot \theta_1 + \lambda_2 \cot \theta_2)}. \quad (6.39)$$

Note that equations (6.36) and (6.39) yield same result as those in Example 6.3 when we have a symmetric grasp, i.e., when $v_1 = v_2$ and $\psi_1 = \psi_2$.

Solution by RB and NRB criteria:

The solution of the sliding motions can also be obtained directly by applying the minimization method in Proposition 6.1. In the following, equation (6.24) is employed to solve for the motion of the object directly.

First, since both fingers are sliding along the horizontal direction we can assume $\mathbf{v}_{slip,i} = c_i [\lambda_i \cos \psi_i \ 0 \ \sin \psi_i]^T$, obtained from the limit surfaces. Thus \mathbf{v}'_b can be solved by using equation (6.24).

$$\mathbf{v}'_b = \begin{bmatrix} \frac{(l_1 - l_2)(c_1 l_1^2 \sin \psi_1 + c_2 l_2^2 \sin \psi_2) + c_1(l_1^2 + l_1 l_2 + 2l_2^2)\lambda_1 \cos \psi_1 - c_2(2l_1^2 + l_1 l_2 + l_2^2)\lambda_2 \cos \psi_2}{(3l_1^2 + 2l_1 l_2 + 3l_2^2)} \\ 0 \\ \frac{2(c_1 l_1^2 \sin \psi_1 + c_2 l_2^2 \sin \psi_2) - (l_1 + l_2)(c_1 \lambda_1 \cos \psi_1 + c_2 \lambda_2 \cos \psi_2)}{(3l_1^2 + 2l_1 l_2 + 3l_2^2)} \end{bmatrix} \quad (6.40)$$

Employing equations (6.25), and (6.26), we can directly solve for ${}_{RB}\mathcal{V}$, ${}_{RB}\mathcal{V}_{slip}$ and the unknown parameters c_1 and c_2 . Unlike the previous approach, the solution of \mathbf{v}_b by this approach was derived without *a priori* knowledge of v_y being zero. The solutions for ${}_{RB}\mathcal{V}$, ${}_{RB}\mathbf{v}_{slip,i}$, c_i , l_i , and h are listed in Appendix D.4. The motion of the card with respect to the COR coordinates is

$$\mathbf{v}_b = \begin{bmatrix} 0 \\ 0 \\ \frac{-(v_1 + v_2)}{(l_1 + l_2 + \lambda_1 \cot \psi_1 + \lambda_2 \cot \psi_2)} \end{bmatrix} \quad (6.41)$$

which is exactly the same as the results obtained previously. The matrix \mathbf{v}_h is

$$\mathbf{v}_h = \begin{bmatrix} \frac{(l_1^2 + l_1 l_2 + 2l_2^2)v_1 - (2l_1^2 + l_1 l_2 + l_2^2)v_2}{(3l_1^2 + 2l_1 l_2 + 3l_2^2)} \\ 0 \\ \frac{-(l_1 + l_2)(v_1 + v_2)}{(3l_1^2 + 2l_1 l_2 + 3l_2^2)} \end{bmatrix} \quad (6.42)$$

6.5 Experimental results

In this section the experimental results of two soft fingers manipulating a planar object are presented. The experiments are essentially implementations of Examples 6.3 and 6.4. The planar manipulator described in Appendix A.8 is used with fingertips that hold circular rubber contact patches sliding on a card. The fingertips are designed with a low ($500N/m$) stiffness perpendicular to the plane of the card and a high stiffness in the plane of the card. By carefully adjusting the vertical deflection of the fingertips, we could control the normal force they applied. A three-axis force sensor was mounted between the fingertip and link 4 to measure the forces and moments in the plane.

A cartesian position controller was employed so that the fingertips followed desired trajectories and moved with constant velocity. The actual positions and orientations of the fingertips were recorded by the controller in real time so that we knew exactly when the fingers started to slide and what the sliding velocities were. The controller ran at $333Hz$. The forces and moments at the contacts were also recorded.

The position and orientation of the card was tracked by a computer vision system. The camera, which located two fiducials on the card, was mounted above the workspace and ran at 30 frames/sec for data acquisition. The coordinates of the bottom-most points of the two circular fiducials were obtained, from which the positions and orientations of the card could be derived by knowing the relative positions of the fiducials and the contacts. With this setup, the following parameters could be obtained:

1. The angular displacement of the card, $\Delta\Phi$, was obtained from the vision data.
2. The duration of sliding manipulation, Δt , was found from the data recorded by the controller.
3. The absolute velocities of the fingertips were obtained from the time history of the fingertip positions with a known sampling rate.

4. The relative linear and angular sliding velocities were computed from the orientation, $\Delta\Phi$, and the manipulator joint angles, using the forward kinematics.

With the above information, one can compare the theoretical predictions, using equations (6.41) and (6.42), with the experimental results.

Case I: The distance between contact centroids is small.

In this case, the distance between the contact centroids is $2r = 29\text{ mm}$. Finger 1 moves upward and finger 2 moves downward along the y direction. The fingertips move 8 mm and $\Delta\phi_1 = 0.036\text{ rad}$ for a duration of 1.7 sec . (ϕ_1 is the angle between the x axis and link 4 as shown in Figure A.3.) The two fiducials are 30 mm apart and the distance between the midpoints of the contacts and fiducials is 40 mm . The angular displacement of the card obtained from the vision data is 16° , or 0.28 rad clockwise. The vision data is plotted in Figure 6.7 which clearly shows that the two fiducials are following a circular trajectory.

The angular velocity from the experimental data is

$$\omega = \frac{-0.28}{1.7} = -0.165\text{ rad/sec}$$

The analytic solution can be obtained from equation (6.41) by knowing the absolute fingertip velocities, v_i , and the ratio of linear and angular sliding velocities, $\lambda_i \cot \psi_i$. From the data given above, we can obtain

$$v = v_1 = v_2 = \frac{8.0 \times 10^{-3}}{1.7} = 4.71 \times 10^{-3}\text{ m/sec.}$$

The magnitude of the relative linear sliding velocity is $v_{slip} = v - r\omega = 2.31 \times 10^{-3}\text{ m/sec}$ and the relative angular sliding velocity is $\omega_{slip} = \omega + \frac{\Delta\phi_1}{\Delta t} = 0.186\text{ rad/sec}$. Therefore,

$$\lambda_1 \cot \psi_1 = \lambda_2 \cot \psi_2 = \frac{v_{slip}}{\omega_{slip}} = 0.0125\text{ m}$$

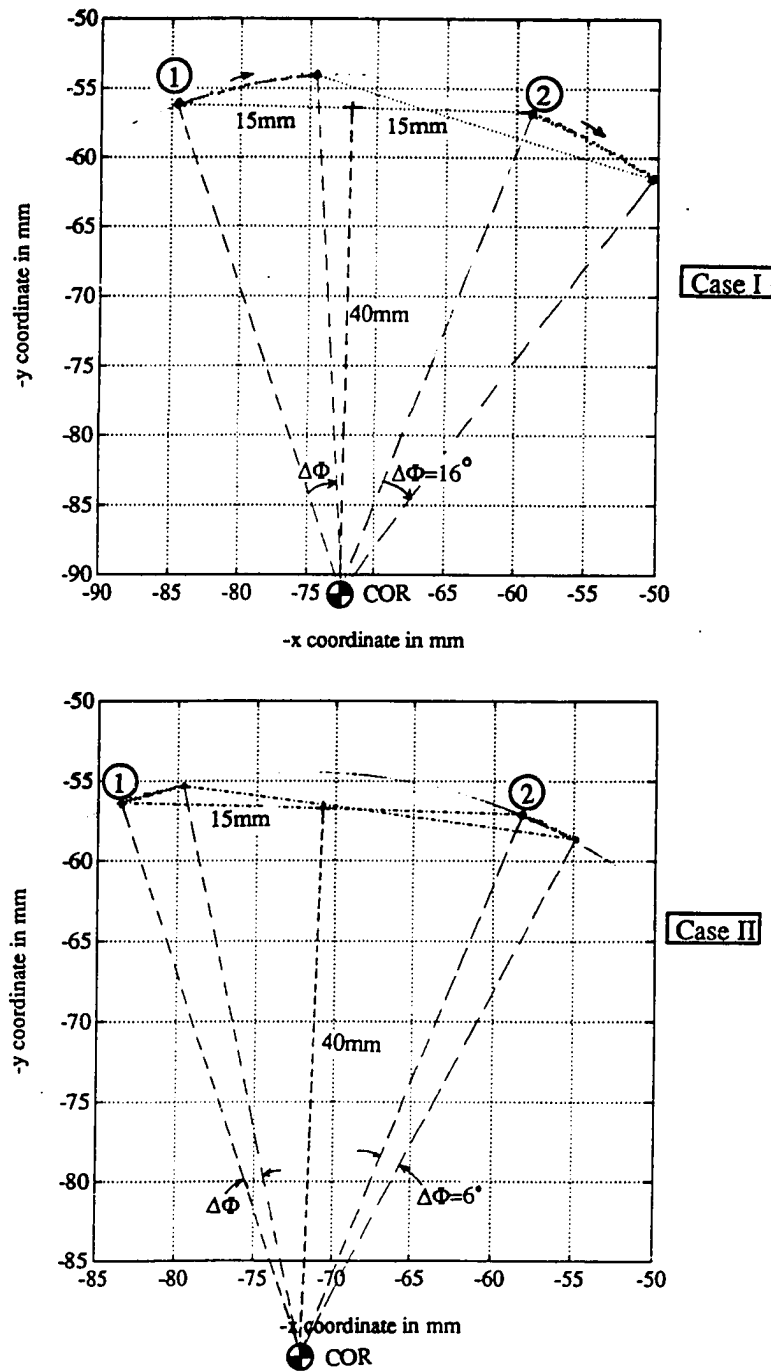


Figure 6.7: Locus of fiducials tracked by the vision camera for cases I and II

where λ can also be obtained by knowing the force and moment measurements for the contact patch. The angular velocity of the card is

$$\omega = \frac{-(v_1 + v_2)}{2r + \lambda_1 \cot \psi_1 + \lambda_2 \cot \psi_2} = -0.174 \text{ rad/sec} \quad (6.43)$$

Comparing equation (6.43) to the experimental result, the error is about 5%. Part of this error is from the large sliding displacement of the fingertips, such that the instantaneous analytical results need to be slightly modified for new positions. In other experiments that involve smaller linear and angular displacements the error was as small as 1%.

Case II: The distance between contact centroids is large.

In this case, the distance between the contact centroids is $2r = 143 \text{ mm}$. The fingers are commanded to move along the same direction. The fingertips move 8.2 mm and $\Delta\phi_1 = 0.037 \text{ rad}$ for a duration of 2.6 sec . The two fiducials are 30 mm apart and the distance between the midpoints of the contacts and fiducials is 40 mm . The angular displacement of the card obtained from the vision data is 6° , or 0.105 rad clockwise. The vision data are plotted in Figure 6.7.

The angular velocity from the experiment is

$$\omega = \frac{-0.105}{2.6} = -0.0403 \text{ rad/sec}$$

The velocity of the fingertips are $v = v_1 = v_2 = \frac{8.2 \times 10^{-3}}{2.6} = 3.15 \times 10^{-3} \text{ m/sec}$ and $\lambda_1 \cot \psi_1 = \lambda_2 \cot \psi_2 = v_{\text{slip}}/\omega_{\text{slip}} = (\frac{3.15 \times 10^{-3}}{2.6} - 0.0403 \times 71.5 \times 10^{-3})/(0.0403 + \frac{0.037}{2.6}) = 0.00535 \text{ m}$

The predicted angular velocity of the card is

$$\omega = -0.0409 \text{ rad/sec} \quad (6.44)$$

Comparing equation (6.44) to the experimental result, the error is about 1.5%.

Discussions:

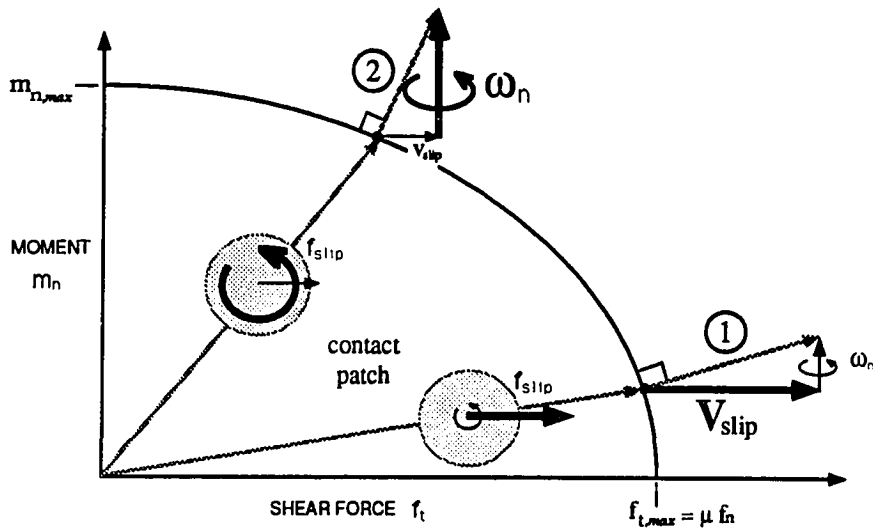


Figure 6.8: Comparison of the unit normals for the two cases in sliding manipulation

The ratios of linear and angular velocities, $\lambda \cot \psi$, for the two cases are compared and plotted in Figure 6.8. As expected, $\lambda \cot \psi$ is larger when the contact centroids are very close together which corresponds to case 1 in Figure 6.8. In the second case, the ratio is much smaller and the grasp approaches two point-contact fingers pivoting about their contact points, because the distance between contact centroids is large compared to the radius of the contact patch. This is shown as case 2 in Figure 6.8.

6.6 Summary

In this chapter, manipulation with multiple sliding and non-sliding fingers has been addressed. The solution can be obtained by formulating force equilibrium equations, constitutive equations and geometric (velocity) compatibility equations. An approach has been proposed which consists of decomposing the fingertip and sliding velocities into rigid-body (RB) and non-rigid-body (NRB) components which can be directly solved for by minimizing an objective function. The resulting solution provides NRB motions that are in the null space of the rigid body motion of the object and are orthogonal to the RB motions.

The approach is illustrated with some examples, including a revisit of the “twirling” problem discussed by Fearing [1986] and a manipulation problem with two sliding soft-contact fingers. Experimental results of sliding manipulation involving two soft fingers are also presented and found to agree closely with predicted results.

Chapter 7

Conclusions and Future Work

First, a systematic forward and reverse procedure for computing the stiffness of grasps has been presented. The procedure includes the structural compliance, contact constraints, and small changes in the grasp geometry. The approach can handle over- and under-constrained problems, as well as grasps that are over-constrained in some directions while under-constrained in others. It is also shown that as long as the servo stiffness, \mathbf{K}_θ , is positive definite, the resulting grasp stiffness matrix, \mathbf{K}_b , is positive definite. This is useful in indicating stability since \mathbf{K}_b changes considerably throughout the manipulation process, whereas \mathbf{K}_θ is often constant.

Some extensions of this infinitesimal motion analysis have been discussed and the results of experiments on a two-fingered planar manipulator have been presented. The experimental results match the predicted results completely, provided that uncertainties in joint friction are accounted for.

Next, friction models and friction limit surfaces have been examined. Models for soft contacts were explored and an elliptical approximation used to analyze the onset of slipping. The limit surface indicates whether a finger will slip and if it does slip, the instantaneous direction of sliding is.

Two measures for predicting sliding motions in general grasping have been proposed. The first measure singles out a “worst-case” finger that is most prone to slipping. The second measure, the “progression-toward-friction-limit” measure, predicts whether a given set of external forces and moments will cause individual fingers to become more or less likely to slip, and measures how fast each finger is progressing toward the friction limit. The results of the analysis suggest strategies for controlling the fingers of a hand to make it less vulnerable to slipping in the presence of task-induced forces. The concept of a “critical configuration” of a grasp was also defined, which can be useful in grasp planning.

Finally, the grasp stiffness, which correlates fingertip forces with displacements, and the limit surface, which yields the relationships between the contact force/moment and the direction of sliding, were combined to result in a first-order differential equation governing the motions of sliding fingers with respect to a grasped object. The equations of motion are expressed in terms of an independent geometric parameter since quasistatic motion is assumed. The solutions of the differential equations have a transient solution, due to initial grasp forces, and a steady-state solution.

Manipulation with multiple sliding and non-sliding fingers was also addressed. The solution can be obtained by formulating force equilibrium equations, constitutive equations and geometric (velocity) compatibility equations. An approach is proposed which consists of decomposing the fingertip and sliding velocities into rigid-body (RB) and non-rigid-body (NRB) components which can be obtained through minimizing an objective function. The resulting solution has orthogonal RB and NRB motions.

Looking ahead, numerous extensions of the ideas developed in this dissertation remain to be explored. The only fundamental limitation is that magnitudes of the forces must be independent of velocity. Therefore, viscous and viscoelastic effects cannot be considered. However, for many low-speed tasks with hard rubber or similar materials, these effects can be ignored. A second area of extension is to address realistic, three-dimensional grasps with larger numbers of fingers. The problem here is one of algebraic complexity and we will need to resort to numerical computation instead of

the analytic solutions presented in the examples.

Some implementation questions must also be answered before the analysis can actually be applied to manipulation with sliding. Is the computational burden for computing trajectories excessive for real-time use? Can variations in finger force be achieved rapidly enough to achieve control of sliding? An interesting point is that by a judicious choice of finger stiffnesses, the sensitivity of the sliding trajectory to variations in the finger force or the coefficient of friction may be reduced. This is significant since the coefficient of friction can easily vary by 30% with changes in surface texture or cleanliness.

Finally, it will be important to explore the role of tactile sensing in sliding. Clearly, when people manipulate objects they are not calculating transient and steady-state trajectories but are relying on the tactile information to help them determine where, and how, sliding is occurring and to keep track of the position and orientation of features on the grasped object. Of course, this argument does not invalidate an analytic approach for planning any more than similar arguments invalidate the use of Jacobians for robot kinematics, but it does suggest that tactile slip and force sensing are essential components of a practical approach to manipulation with sliding.

Appendix A

Forward and reverse procedures

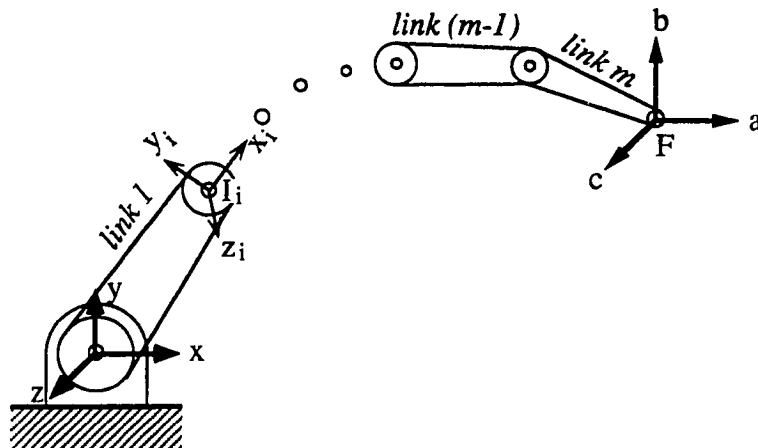
A.1 Structural compliance of fingers

The finger represented in Figure A.1 consists of m links as shown. Assume that we view each individual link as a cantilever beam and that there are no correlations among the structural compliances of the links. Referring to beam theory [Timoshenko 1962], we can find the compliance of a cantilever link in its local coordinates. We have

$$C_{l_i} = \begin{bmatrix} \frac{L}{EA} & 0 & 0 & 0 & 0 & 0 \\ 0 & \frac{L^3}{3EI} & 0 & 0 & 0 & \frac{L^2}{2EI} \\ 0 & 0 & \frac{L^3}{3EI} & 0 & -\frac{L^2}{2EI} & 0 \\ 0 & 0 & 0 & \frac{L}{GJ} & 0 & 0 \\ 0 & 0 & -\frac{L^2}{2EI} & 0 & \frac{L}{EI} & 0 \\ 0 & \frac{L^2}{2EI} & 0 & 0 & 0 & \frac{L}{EI} \end{bmatrix} \quad (A.1)$$

where E is the Young's modulus, G is the shear modulus $\frac{E}{2(1+\mu)}$, and L is the length of the link. Defining ${}^I\mathbf{J}_{l_i}$ as the transformation matrix of the local coordinates $I(xyz)$ with respect to the contact coordinate frame $F(abc)$, we can formulate the following equations:

$${}^I\mathbf{d}\mathbf{x}_i = {}^I\mathbf{J}_{l_i} {}^I\mathbf{d}\mathbf{x}_i \quad (A.2)$$

Figure A.1: A finger composed of m serial links

$${}^F\mathbf{C}_s = \sum_{i=1}^m {}_I^F\mathbf{J}_{l_i} {}^I\mathbf{C}_{l_i} {}_I^F\mathbf{J}_{l_i}^T \quad (\text{A.3})$$

where ${}^I\mathbf{d}\mathbf{x}_i$ is the deflection of the i -th link with respect to the local coordinates, ${}^F\mathbf{d}\mathbf{x}_i$ stands for the deflection of the i -th finger with respect to the contact coordinates, and ${}^F\mathbf{C}_s$ is the equivalent structural compliance of the finger in the contact coordinates.

A.2 Symbolic matrix inverse for point-contacts

If \mathbf{K}_f is block-diagonal, we can treat each fingertip separately. If we divide the fingertip stiffness matrix in equation (3.27) into 3×3 partitions

$$\mathbf{K}_{f_i} = \begin{bmatrix} \mathbf{K}_{11} & \mathbf{K}_{12} \\ \mathbf{K}_{21} & \mathbf{K}_{22} \end{bmatrix},$$

then, for point-contacts, the inverse of the matrix in equation (3.28) can be expressed as

$$\begin{bmatrix} \mathbf{K}_{f_i} & \mathbf{H}_i^T \\ \mathbf{H}_i & 0 \end{bmatrix}^{-1} = \begin{bmatrix} 0 & 0 & \mathbf{I}_3 \\ 0 & \mathbf{K}_{22}^{-1} & -\mathbf{K}_{22}^{-1} \mathbf{K}_{21} \\ \mathbf{I}_3 & -\mathbf{K}_{12} \mathbf{K}_{22}^{-1} & (\mathbf{K}_{12} \mathbf{K}_{22}^{-1} \mathbf{K}_{21} - \mathbf{K}_{11}) \end{bmatrix}$$

where the matrix \mathbf{H}_i is

$$\mathbf{H}_i = \begin{bmatrix} 1 & 0 & 0 & 0 & 0 & 0 \\ 0 & 1 & 0 & 0 & 0 & 0 \\ 0 & 0 & 1 & 0 & 0 & 0 \end{bmatrix}$$

for point contacts, and from equation (3.28), $\delta\mathbf{x}_{f_i}$ is simply

$$\delta\mathbf{x}_{f_i} = \begin{bmatrix} \mathbf{H}_i \delta\mathbf{x}_{p_i} \\ -\mathbf{K}_{22}^{-1} \mathbf{K}_{21} \mathbf{H}_i \delta\mathbf{x}_{p_i} \end{bmatrix}.$$

Similar symbolic expressions can be derived for soft contacts and very-soft contacts. Thus, the computation of $\delta\mathbf{x}_{f_i}$ need not be computationally expensive.

A.3 Differential Jacobian

In equation (3.30) we define a 6×6 transformation matrix between the initial $P(lmn)$ coordinate system and the new position and orientation after a small motion has taken place. If we denote a small linear and rotational motion with respect to the initial $P(lmn)$ coordinate system as $\delta\mathbf{x} = [dx, dy, dz, d\theta_x, d\theta_y, d\theta_z]^T$, we can express the cartesian transformation as:

$$\mathbf{D}^T = \begin{bmatrix} \Delta\mathbf{A} + \mathbf{I} & | & \mathbf{0} \\ \hline \mathbf{0} & + & \mathbf{0} \\ \Delta\mathbf{R}(\Delta\mathbf{A} + \mathbf{I}) & | & \Delta\mathbf{A} + \mathbf{I} \end{bmatrix} \quad (\text{A.4})$$

where $\Delta\mathbf{A}^T$ and $\Delta\mathbf{R}^T$ are small rotation and cross-product matrices, respectively. They can be generated from $\delta\mathbf{x}$ as

$$\Delta\mathbf{A}^T = \begin{bmatrix} 0 & -d\theta_z & d\theta_y \\ d\theta_z & 0 & -d\theta_x \\ -d\theta_y & d\theta_x & 0 \end{bmatrix} \quad \Delta\mathbf{R}^T = \begin{bmatrix} 0 & -dz & dy \\ dz & 0 & -dx \\ -dy & dx & 0 \end{bmatrix}$$

If the orientation and the point of application of the grasp force do not change, \mathbf{A} is simply an identity matrix and \mathbf{R} a null matrix.

If we neglect second order and smaller terms, we can express the differential Jacobian in equation (3.32) as

$${}^P_B \Delta \mathbf{J}^T = \begin{bmatrix} \Delta \mathbf{A} & | & \mathbf{0} \\ \hline \mathbf{0} & + & \mathbf{0} \\ \Delta \mathbf{R} & | & \Delta \mathbf{A} \end{bmatrix} \quad (\text{A.5})$$

A.4 Equations and expressions in examples

A.4.1 Example 3.1

We assume servo stiffnesses comparable to those achievable in the Stanford/JPL hand and add some coupling among the joints on different fingers to achieve a typical joint stiffness matrix:

$$\mathcal{K}_\theta = \mathcal{C}_\theta^{-1} = \begin{bmatrix} 10 & 0 & 0 & -1 & 0 & 0 \\ 0 & 5.65 & 0 & 0 & -1.5 & 0 \\ 0 & 0 & 3.66 & 0 & 0 & -1.1 \\ -1 & 0 & 0 & 10 & 0 & 0 \\ 0 & -1.5 & 0 & 0 & 5.65 & 0 \\ 0 & 0 & -1.1 & 0 & 0 & 3.66 \end{bmatrix}.$$

where units are in Nm, for rotational stiffness. The joint Jacobian and the structural compliance matrix for the first finger are:

$$\mathbf{J}_{\theta_1} = \begin{bmatrix} 0 & -0.0728 & -0.022 \\ -0.1329 & 0 & 0 \\ 0 & 0.0127 & 0.0127 \\ -0.866 & 0 & 0 \\ 0 & 1 & 1 \\ -0.5 & 0 & 0 \end{bmatrix} \quad \mathbf{C}_{s_1} = \begin{bmatrix} 1.02 & 0 & -0.14 & 0 & -11.1 & 0 \\ 0 & 1.71 & 0 & 9.21 & 0 & 5.32 \\ -0.14 & 0 & 0.184 & 0 & 2.64 & 0 \\ 0 & 9.21 & 0 & 856 & 0 & 34.6 \\ -11.1 & 0 & 2.64 & 0 & 1008 & 0 \\ 0 & 5.32 & 0 & 34.6 & 0 & 520 \end{bmatrix} \times 10^{-4}$$

The matrices for the second finger follow from symmetry. The structural compliance matrix was obtained by choosing values for the links comparable to those of the Stanford/JPL hand, which is about 8% of the compliance due to the servoing at the fingertip. A fingertip compliance matrix for a “very-soft” finger was then added,

with large rotational compliances in the l and m directions, corresponding to a small contact area and approaching the limiting case of a soft-finger contact. For very-soft fingertips, the contact matrix, \mathcal{H} , is a 12×12 identity matrix. The \mathbf{K}_b matrix is:

$$\mathbf{K}_b = \begin{bmatrix} 2490 & 0 & 0 & 0 & 258 & 0 \\ 0 & 28900 & 0 & 191 & 0 & 0 \\ 0 & 0 & 61610 & 0 & 0 & 0 \\ 0 & 191 & 0 & 22 & 0 & 0 \\ 258 & 0 & 0 & 0 & 37 & 0 \\ 0 & 0 & 0 & 0 & 0 & 35 \end{bmatrix}$$

where the units are in N/m and Nm for linear and rotational stiffness, respectively. The scaling matrix, \mathbf{S} , for a characteristic length of $0.1m$ is:

$$\mathbf{S} = \begin{bmatrix} 1 & 0 & 0 & 0 & 0 & 0 \\ 0 & 1 & 0 & 0 & 0 & 0 \\ 0 & 0 & 1 & 0 & 0 & 0 \\ 0 & 0 & 0 & 10 & 0 & 0 \\ 0 & 0 & 0 & 0 & 10 & 0 \\ 0 & 0 & 0 & 0 & 0 & 10 \end{bmatrix}$$

A.4.2 Example 3.2

We assume a diagonal joint stiffness matrix, with identical stiffnesses for both fingers:

$$\mathcal{K}_\theta = \begin{bmatrix} k_a & 0 & 0 & 0 & 0 & 0 \\ 0 & k_b & 0 & 0 & 0 & 0 \\ 0 & 0 & k_c & 0 & 0 & 0 \\ 0 & 0 & 0 & k_a & 0 & 0 \\ 0 & 0 & 0 & 0 & k_b & 0 \\ 0 & 0 & 0 & 0 & 0 & k_c \end{bmatrix}.$$

The joint Jacobian and coordinate transformation matrix for the left finger are

$$\mathbf{J}_{\theta_1} = \begin{bmatrix} 0 & -1 & -1 \\ 1 & 0 & 0 \\ 0 & 1 & 0 \\ 0 & 0 & 0 \\ 0 & 1 & 1 \\ -1 & 0 & 0 \end{bmatrix}; \quad {}^P_B \mathbf{J}_1 = \begin{bmatrix} 0 & -1 & 1 & 0 & 0 & r \\ 0 & 0 & 1 & 0 & r & 0 \\ -1 & 0 & 0 & 0 & 0 & 0 \\ 0 & 0 & 0 & 0 & -1 & 1 \\ 0 & 0 & 0 & 0 & 0 & 1 \\ 0 & 0 & 0 & -1 & 0 & 0 \end{bmatrix}.$$

The right finger follows from symmetry. The stiffness matrices \mathbf{K}_b and \mathbf{K}_j for each individual finger ($i = 1, 2$) are

$$\mathbf{K}_b = \begin{bmatrix} k_{b_i} + k_{c_i} & (-1)^{i+1}k_{c_i} & 0 & 0 & 0 & -rk_{c_i} \\ (-1)^{i+1}k_{c_i} & k_{c_i} & 0 & 0 & 0 & (-1)^i rk_{c_i} \\ 0 & 0 & k_{a_i} & 0 & (-1)^{i+1}rk_{a_i} & 0 \\ 0 & 0 & 0 & 0 & 0 & 0 \\ 0 & 0 & (-1)^{i+1}rk_{a_i} & 0 & r^2k_{a_i} & 0 \\ -rk_{c_i} & (-1)^i rk_{c_i} & 0 & 0 & 0 & r^2k_{c_i} \end{bmatrix}$$

$$\mathbf{K}_j = \begin{bmatrix} 0 & 0 & 0 & 0 & 0 & 0 \\ 0 & -f_n & 0 & 0 & 0 & (-1)^{i+1}f_n \\ 0 & 0 & 0 & 0 & 0 & 0 \\ 0 & 0 & 0 & 0 & 0 & 0 \\ 0 & 0 & (-1)^i f_n & 0 & -r f_n & 0 \\ 0 & (-1)^{i+1}(f_n + r f_n) & 0 & 0 & 0 & -rf_n - r^2 f_n \end{bmatrix}$$

A.4.3 Example 3.3

In Example 3, the general servo stiffness matrix is

$$\mathcal{K}_\theta = \mathcal{C}_\theta^{-1} = \begin{bmatrix} K_{\theta_{11}} & K_{\theta_{12}} & K_{\theta_{13}} & K_{\theta_{14}} \\ K_{\theta_{12}} & K_{\theta_{22}} & K_{\theta_{23}} & K_{\theta_{24}} \\ K_{\theta_{13}} & K_{\theta_{23}} & K_{\theta_{33}} & K_{\theta_{34}} \\ K_{\theta_{14}} & K_{\theta_{24}} & K_{\theta_{34}} & K_{\theta_{44}} \end{bmatrix}$$

where the elements of \mathcal{K}_θ correspond to individual joint stiffnesses or coupling terms

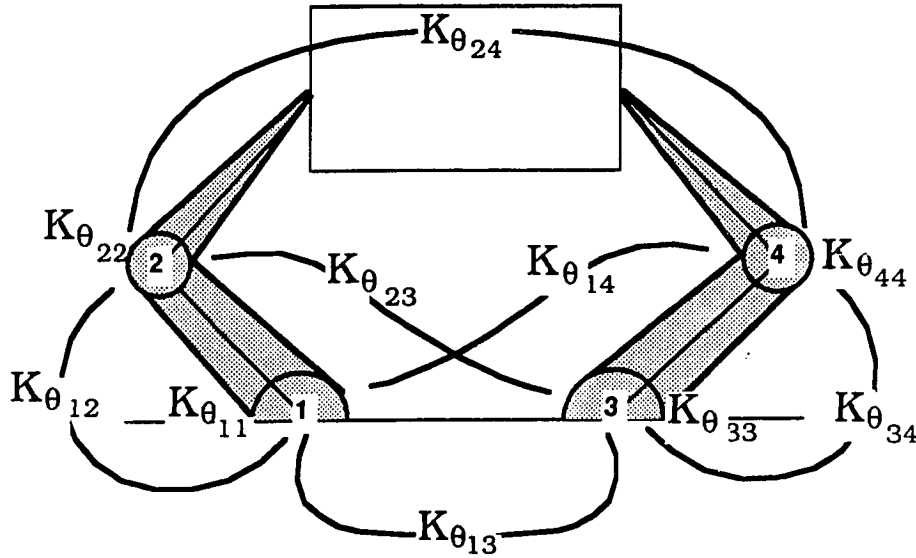


Figure A.2: Correlation between elements of \mathcal{K}_θ and coupled joint control

between different joints, as shown below in Figure A.2. We also assume symmetry in this example so that $K_{\theta_{23}} = K_{\theta_{14}}$, $K_{\theta_{33}} = K_{\theta_{11}}$, $K_{\theta_{44}} = K_{\theta_{22}}$, and $K_{\theta_{34}} = K_{\theta_{12}}$. The structural compliance matrix is assumed to be diagonal (fingertip compliance only) so that

$$\mathcal{H}\mathcal{C}_s = \begin{bmatrix} C_s & 0 & 0 & 0 \\ 0 & C_s & 0 & 0 \\ 0 & 0 & C_s & 0 \\ 0 & 0 & 0 & C_s \end{bmatrix}.$$

A.4.4 Example 3.4

The matrix Ω in this example has two bases which span the null space. They are $q_1 = [0 \ 3.76 \ 0 \ -1 \ 0 \ 0 \ 0 \ 0]$ and $q_2 = [0 \ 0 \ 0 \ 0 \ 0 \ 0 \ 3.76 \ 1]$ (translation in the a, b, c frame and rotation about c for each contact) which correspond to a single coupled motion in the object space, in which translation along the x axis is unavoidably coupled with rotation about y .

If we take a \mathbf{K}_p matrix that satisfies the constraints and apply the forward procedure,

we obtain a \mathbf{K}_b^\dagger matrix that almost matches the desired \mathbf{K}_b^\dagger matrix. The only significant difference is due to the unavoidable coupling between x axis translation and y axis rotation. The scaled \mathbf{K}_b^\dagger , using the same scaling matrix \mathbf{S} in Example 3.1, is

$$\mathbf{K}_b^\dagger = \begin{bmatrix} 35.3 & 0 & 0 & 0 & 14.2 & 0 \\ 0 & 104 & 0 & 0 & 0 & 0 \\ 0 & 0 & 490 & 0 & 0 & 0 \\ 0 & 0 & 0 & 0.1 & 0 & 0 \\ 14.2 & 0 & 0 & 0 & 14 & 0 \\ 0 & 0 & 0 & 0 & 0 & 27 \end{bmatrix} \times 10^2$$

A.5 Positive definiteness of the forward procedure

We want to prove that a positive definite \mathcal{K}_θ or \mathcal{C}_θ will result in a positive semi-definite \mathbf{K}_b . We begin by recalling the “Law of Inertia” for a congruence transformation:

Law of Inertia: If the transformation matrix \mathbf{T} in the congruence transformation, $\mathbf{T}^\top \mathbf{Q} \mathbf{T}$, is nonsingular, the signs of the eigenvalues are preserved [Strang 1988].

Therefore, we have the following two theorems:

Theorem 1: If \mathbf{Q} is positive definite, its congruence transformation is positive semidefinite, i.e.,

$$\forall \mathbf{Q} > 0 \Rightarrow \mathbf{T}^\top \mathbf{Q} \mathbf{T} \geq 0 \quad \text{for any matrix } \mathbf{T}$$

also,

$$\mathbf{Q} > 0 \Rightarrow \mathbf{T}^\top \mathbf{Q} \mathbf{T} > 0 \quad \text{when } \mathcal{N}(\mathbf{T}) = \{\}.$$

where $\mathcal{N}(\mathbf{T})$ is the null space of matrix \mathbf{T} .

Proof: To prove the positive definiteness of $\mathbf{T}^\top \mathbf{Q} \mathbf{T}$, we pre- and post-multiply by a vector \mathbf{x}^\top and \mathbf{x} . Therefore,

$$\mathbf{x}^\top (\mathbf{T}^\top \mathbf{Q} \mathbf{T}) \mathbf{x} = \mathbf{y}^\top \mathbf{Q} \mathbf{y}$$

where $\mathbf{y} = \mathbf{T}\mathbf{x}$ is a vector. Clearly, from definition of positive definiteness, $\mathbf{y}^T \mathbf{Q} \mathbf{y} > 0$ if $\mathbf{y} = \mathbf{T}\mathbf{x}$ is non-trivial. That is, if $\mathbf{y} \notin \mathcal{N}(\mathbf{T})$ then $\mathbf{T}^T \mathbf{Q} \mathbf{T} > 0$; otherwise, $\mathbf{T}^T \mathbf{Q} \mathbf{T} \geq 0$.

■

Theorem 2: If \mathcal{C}_θ or \mathcal{K}_θ is positive definite, then \mathcal{K}_b obtained in the forward procedure will be positive semi-definite. If the grasp is force-closure, then \mathcal{K}_b is positive definite.

Proof: If we begin with a positive definite \mathcal{C}_θ , then \mathcal{C}_j in equation (3.18) is positive semi-definite according theorem 1. Since \mathcal{C}_s is always positive definite, \mathcal{C}_f in equation (3.20) is positive definite. Therefore, $\mathcal{H}\mathcal{C}_f\mathcal{H}^T$ is positive definite from theorem 1, as is its inverse. \mathcal{K}_p and \mathbf{K}_b in equation (3.22) are therefore positive semi-definite. The stiffness matrix \mathbf{K}_b is thus positive semi-definite. If the grasp is force-closure then \mathbf{K}_b is nonsingular and therefore positive definite. ■

A.6 Obtaining joint stiffness in the reverse procedure

In this appendix, we find the expression for the joint stiffness matrix, \mathbf{K}_θ in terms of the structural compliance and the desired \mathbf{K}_p matrix. Note that all matrices discussed here can be the concatenated matrices for generalization. First, we use equations (3.18) and (3.20) to expand the product $(\mathbf{H}\mathbf{C}_f\mathbf{H}^T)^{-1}$:

$$(\mathbf{H}\mathbf{C}_f\mathbf{H}^T)^{-1} = (\mathbf{H}\mathbf{C}_s\mathbf{H}^T + \mathbf{H}\mathbf{J}_\theta\mathbf{C}_\theta\mathbf{J}_\theta^T\mathbf{H}^T)^{-1}.$$

Then, we use the standard matrix inverse formula [Kailath 1980],

$$(\mathbf{A} + \mathbf{B}\mathbf{C}\mathbf{D})^{-1} = \mathbf{A}^{-1} - \mathbf{A}^{-1}\mathbf{B}(\mathbf{D}\mathbf{A}^{-1}\mathbf{B} + \mathbf{C}^{-1})^{-1}\mathbf{D}\mathbf{A}^{-1},$$

(where \mathbf{A} and \mathbf{C} are nonsingular square matrices) to expand equation (3.21) as:

$$\mathbf{K}_p = \mathbf{H}^T \mathbf{C}_s'^{-1} \mathbf{H} - \mathbf{H}^T \mathbf{C}_s'^{-1} \mathbf{B} (\mathbf{B}^T \mathbf{C}_s'^{-1} \mathbf{B} + \mathbf{C}_\theta^{-1})^{-1} \mathbf{B} \mathbf{C}_s'^{-1} \mathbf{H} \quad (A.6)$$

where $\mathbf{C}'_s = \mathbf{H}\mathbf{C}_s\mathbf{H}^T$ represents structural compliance seen by the object through contact, and $\mathbf{B} = \mathbf{H}\mathbf{J}_\theta$, such that $\delta\mathbf{x}_{tr} = \mathbf{B}\delta\theta$.

We wish to invert the relationship in equation (A.6) to obtain \mathbf{C}_θ^{-1} in terms of \mathbf{K}_p and \mathbf{C}'_s . As a first step,

$$\mathbf{K}_p - \mathbf{H}^T \mathbf{C}'_s^{-1} \mathbf{H} = -\mathbf{H}^T \mathbf{C}'_s^{-1} \mathbf{B} (\mathbf{B}^T \mathbf{C}'_s^{-1} \mathbf{B} + \mathbf{C}_\theta^{-1})^{-1} \mathbf{B}^T \mathbf{C}'_s^{-1} \mathbf{H}.$$

All the matrix products in the above equation have the same form, with rows and columns of zeros determined by the contact matrix \mathbf{H} . Therefore, it makes no difference if we only consider only the non-trivial submatrices, that is, if we pre- and post-multiply by \mathbf{H} , and \mathbf{H}^T . Then since $\mathbf{H}\mathbf{H}^T = \mathbf{I}$, an $n \times n$ identity matrix,

$$(\mathbf{C}'_s - \mathbf{C}'_s \mathbf{H} \mathbf{K}_p \mathbf{H}^T \mathbf{C}'_s) = \mathbf{B} (\mathbf{B}^T \mathbf{C}'_s^{-1} \mathbf{B} + \mathbf{C}_\theta^{-1})^{-1} \mathbf{B}^T \quad (A.7)$$

Now, since $\mathbf{B} = \mathbf{H}\mathbf{J}_\theta$ is usually not square, there are two possibilities:

(I) If $m \leq n$, then $\mathbf{B}^T \mathbf{B} = \mathbf{I}_m$ and

$$\mathbf{C}_\theta^{-1} = \mathbf{K}_\theta = [\mathbf{B}^* (\mathbf{C}'_s - \mathbf{C}'_s \mathbf{H} \mathbf{K}_p \mathbf{H}^T \mathbf{C}'_s) \mathbf{B}^{T*}]^{-1} - (\mathbf{B}^T \mathbf{C}'_s^{-1} \mathbf{B}) \quad (A.8)$$

where the superscript * stands for generalized inverse and \mathbf{I}_m is an $m \times m$ identity matrix.

(II) If $m > n$, the finger has redundant joints and the optimal solution can be obtained from generalized inverse of \mathbf{B} by minimizing the norm of \mathbf{C}_θ in which case equation (A.8) for \mathbf{C}_θ still holds.

Ω in the reverse procedure: In the reverse procedure, we require that the desired matrix \mathbf{K}_p be chosen such that product $\Omega = (\mathbf{C}'_s - \mathbf{C}'_s \mathbf{H} \mathbf{K}_p \mathbf{H}^T \mathbf{C}'_s)$ has the same null space as \mathbf{B} . Ω represents the coupled directions, as seen through the contacts, of the motions of the fingers.

Theorem: The null space of matrix Ω is the same as that of \mathbf{B} , which is independent of the structural compliance, \mathbf{C}_s , and of \mathbf{C}_θ , as long as \mathbf{C}_θ is positive definite.

Proof: Substituting \mathbf{K}_p from equation (3.21) into Ω and expanding, we obtain

$$\begin{aligned}\Omega &= \mathbf{C}'_s - \mathbf{C}'_s \mathbf{H} \mathbf{H}^T (\mathbf{B} \mathbf{C}_\theta \mathbf{B}^T + \mathbf{C}'_s)^{-1} \mathbf{H} \mathbf{H}^T \mathbf{C}'_s \\ &= \mathbf{C}'_s - \mathbf{C}'_s [\mathbf{C}'_s^{-1} - \mathbf{C}'_s^{-1} \mathbf{B} (\mathbf{B}^T \mathbf{C}'_s^{-1} \mathbf{B} + \mathbf{C}_\theta^{-1})^{-1} \mathbf{B}^T \mathbf{C}'_s^{-1}] \mathbf{C}'_s\end{aligned}$$

or

$$\Omega = \mathbf{B} (\mathbf{B}^T \mathbf{C}'_s^{-1} \mathbf{B} + \mathbf{C}_\theta^{-1})^{-1} \mathbf{B}^T. \quad (\text{A.9})$$

Since \mathbf{C}_s is always positive definite, if we choose a positive definite \mathbf{C}_θ matrix then the matrix sum $(\mathbf{B}^T \mathbf{C}'_s^{-1} \mathbf{B} + \mathbf{C}_\theta^{-1})$ will be positive definite along with its inverse. From the above theorems and proofs, we conclude that Ω has the same null space as \mathbf{B}^T or the same left null space as \mathbf{B} , which is independent of the values of \mathbf{C}_s and \mathbf{C}_θ . ■

A.7 Derivation of changes in stiffness, $\Delta \mathbf{K}$

If the matrix $\mathbf{B} = \mathbf{H} \mathbf{J}_\theta$ is invertible or is of rank n , the number of degrees of freedom subject to the contact constraints, we can write

$$\mathbf{K}_p = \mathbf{H}^T \mathbf{B}^{-T} \mathbf{C}_\theta^{-1} \mathbf{B}^{-1} \mathbf{H} \quad (\text{A.10})$$

For small changes in \mathbf{J}_θ , the new states are

$$\begin{aligned}\mathbf{J}'_\theta &= \mathbf{J}_\theta + \Delta \mathbf{J}_\theta \\ \mathbf{B}' &= \mathbf{B} + \Delta \mathbf{B} = \mathbf{H} \mathbf{J} + \mathbf{H} \Delta \mathbf{J}_\theta\end{aligned}$$

The new value of \mathbf{K}_p , \mathbf{K}'_p can be obtained, by neglecting second-order and smaller terms,

$$\begin{aligned}\mathbf{K}'_p &= \mathbf{K}_p + \Delta \mathbf{K}_p \\ &= \mathbf{H}^T (\mathbf{B} + \Delta \mathbf{B})^{-T} \mathbf{C}_\theta^{-1} (\mathbf{B} + \Delta \mathbf{B})^{-1} \mathbf{H} \\ &\cong \mathbf{H}^T \mathbf{B}^{-T} (\mathbf{I} - \Delta \mathbf{B}^T \mathbf{B}^{-T}) \mathbf{C}_\theta^{-1} (\mathbf{I} - \mathbf{B}^{-1} \Delta \mathbf{B}) \mathbf{B}^{-1} \mathbf{H} \\ &= \underbrace{\mathbf{H}^T \mathbf{B}^{-T} \mathbf{C}_\theta^{-1} \mathbf{B}^{-1} \mathbf{H}}_{\mathbf{K}_p} + \mathbf{H}^T (-2 \mathbf{B}^{-T} \mathbf{C}_\theta^{-1} \mathbf{B}^{-1} \Delta \mathbf{B} \mathbf{B}^{-1} + \mathbf{B}^{-T} \Delta \mathbf{B}^{-T} \mathbf{B}^{-T} \mathbf{C}_\theta^{-1} \mathbf{B}^{-1} \Delta \mathbf{B} \mathbf{B}^{-1}) \mathbf{H} \quad (\text{A.11})\end{aligned}$$

By comparing equations (A.10) and (A.11), it is apparent that

$$\Delta \mathbf{K}_p = \mathbf{H}^T (-2\mathbf{B}^{-T}\mathbf{C}_\theta^{-1}\mathbf{B}^{-1}\Delta\mathbf{B}\mathbf{B}^{-1} + \mathbf{B}^{-T}\Delta\mathbf{B}^{-T}\mathbf{B}^{-T}\mathbf{C}_\theta^{-1}\mathbf{B}^{-1}\Delta\mathbf{B}\mathbf{B}^{-1})\mathbf{H} \quad (\text{A.12})$$

The grasp stiffness \mathbf{K}_b , resulting from the changes in forces, can be derived from equation (A.12) and $\mathbf{K}_b = \sum_{i=1}^{nf} {}_B^P\mathbf{J}_i^T \mathbf{K}_{p_i} {}_B^P\mathbf{J}_i$. Notice that the cartesian transformation matrix, ${}_B^P\mathbf{J}$, is constant relative to the grasped object unless the fingers slide or roll on the object; therefore, neglecting second-order and smaller terms, we have

$$\begin{aligned} \mathbf{K}'_b &= \mathbf{K}_b + \Delta\mathbf{K}_b \\ &= \sum_{i=1}^{nf} {}_B^P\mathbf{J}_i^T (\mathbf{K}_{p_i} + \Delta\mathbf{K}_{p_i}) {}_B^P\mathbf{J}_i \\ &\cong \underbrace{\sum_{i=1}^{nf} {}_B^P\mathbf{J}_i^T \mathbf{K}_{p_i} {}_B^P\mathbf{J}_i}_{\mathbf{K}_b} + \sum_{i=1}^{nf} {}_B^P\mathbf{J}_i^T \Delta\mathbf{K}_{p_i} {}_B^P\mathbf{J}_i. \end{aligned} \quad (\text{A.13})$$

Hence, the changes in the 6×6 stiffness matrix \mathbf{K}_b are

$$\Delta\mathbf{K}_b = \sum_{i=1}^{nf} {}_B^P\mathbf{J}_i^T \Delta\mathbf{K}_{p_i} {}_B^P\mathbf{J}_i. \quad (\text{A.14})$$

A.8 A two-fingered five-bar planar manipulator

Most of the experiments are conducted on a two-fingered five-bar planar manipulator (PM). The kinematic analysis of such direct-drive arms can be found in Asada [Asada 1984]. Each finger of the planar manipulator is driven by two DC motors located at the base link with L_0 distance apart, as shown in Figure A.3. There is an optical encoder connected to each motor to detect the angular position of the joints. The length of the links is listed in Table A.1. Links 0 to 4 forms a close loop chain. L_5 is the length of the coupler link, from the intersection of link 1 and 4 to the fingertip, i.e., $L_5 = L_4 + L_{offset}$ where L_{offset} is the distance from joint 4 to the fingertip.

The Jacobian matrix of each finger is a function of the joint angles $\theta_1, \theta_2, \phi_1$ and ϕ_2

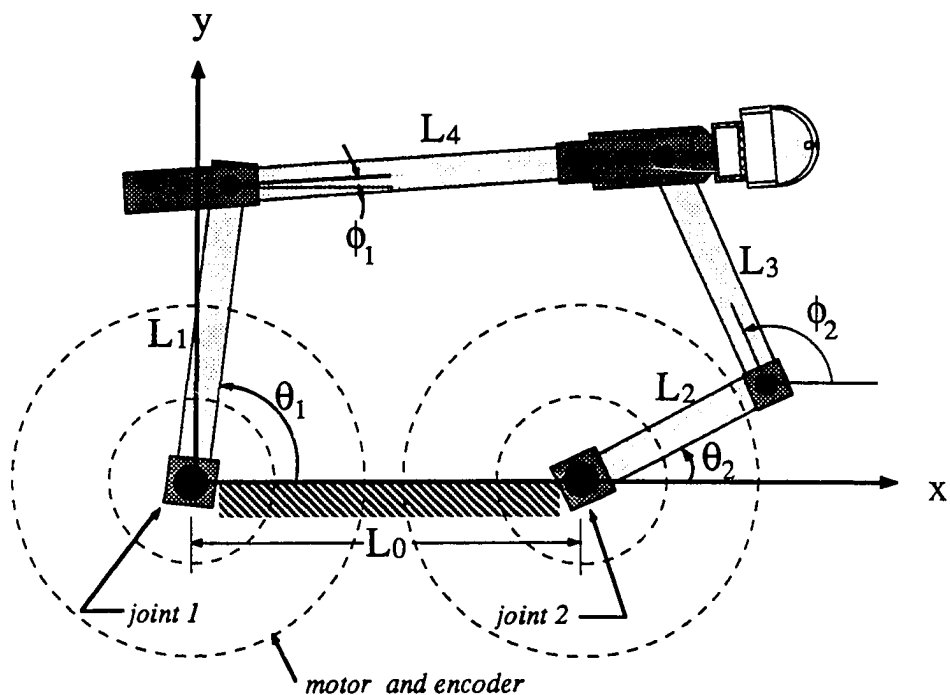


Figure A.3: Sketch of a five-bar direct-drive finger

<i>Link Length</i>	L_0	L_1	L_2	L_3	L_4	L_5
length in cm	11.94	9.53	6.35	8.0	13.33	21.5

Table A.1: Link length of the five-bar planar manipulator

as shown in Figure A.3.

$$\mathbf{J}_\theta = \begin{bmatrix} -L_1 \sin \theta_1 - \frac{L_1 L_5 \sin \phi_1}{L_4 \sin(\phi_2 - \phi_1)} \sin(\theta_1 - \phi_2) & L_1 \cos \theta_1 + \frac{L_1 L_5 \cos \phi_1}{L_4 \sin(\phi_2 - \phi_1)} \sin(\theta_1 - \phi_2) \\ \frac{-L_2 L_5 \sin \phi_1}{L_4 \sin(\phi_2 - \phi_1)} \sin(\phi_2 - \theta_2) & \frac{L_2 L_5 \cos \phi_1}{L_4 \sin(\phi_2 - \phi_1)} \sin(\phi_2 - \theta_2) \end{bmatrix} \quad (\text{A.15})$$

where angles ϕ_1 and ϕ_2 are functions of θ_1 and θ_2 . The relationships between these angles are listed in the following equations for elbow-out configuration and for the workspace that we are concerned with ($\theta_1 = [35^\circ, 125^\circ]$, $\theta_2 = [-20^\circ, 125^\circ]$).

$$\phi_1 = -\cos^{-1}\left(\frac{L_3^2 - L_4^2 - \|\mathbf{z}\|^2}{2L_4\|\mathbf{z}\|}\right) + \nu \quad (\text{A.16})$$

$$\phi_2 = -\cos^{-1}\left(\frac{L_3^2 - L_4^2 + \|\mathbf{z}\|^2}{2L_3\|\mathbf{z}\|}\right) + \nu \quad (\text{A.17})$$

where the vector $\mathbf{z} = [(L_1 \cos \theta_1 - L_2 \cos \theta_2 - L_0) \quad (L_1 \sin \theta_1 - L_2 \sin \theta_2)]^T$, and the angle $\nu = \text{atan2}\left(\frac{L_1 \sin \theta_1 - L_2 \sin \theta_2}{\|\mathbf{z}\|^2}, \frac{L_1 \cos \theta_1 - L_2 \cos \theta_2 - L_0}{\|\mathbf{z}\|^2}\right)$.

The position of the fingertip as a function of the joint angles is:

$$x = L_1 \cos \theta_1 + L_5 \cos \phi_1 \quad (\text{A.18})$$

$$y = L_1 \sin \theta_1 + L_5 \sin \phi_1 \quad (\text{A.19})$$

For example, if $\theta_1 = 90^\circ$, $\theta_2 = 45^\circ$, one can find that

$$\begin{aligned} \phi_1 &= 9.7^\circ & \phi_2 &= 114.3^\circ \\ x &= 0.212\text{cm} & y &= 0.132\text{cm} \\ \mathbf{J}_\theta &= \begin{bmatrix} -0.0842 & -0.0167 \\ -0.0644 & 0.0976 \end{bmatrix} \end{aligned}$$

Appendix B

Grasp measures for sliding

B.1 Results of the spherical grasp example

As in equation (1.4), the cartesian transformation matrices of the grasp in Example 4.1 can be determined by the matrices \mathbf{A}_i and \mathbf{R}_i . The rotation matrices, \mathbf{A}_i are:

$$\mathbf{A}_1^T = \begin{bmatrix} 0 & 1 & 0 \\ 0 & 0 & 1 \\ 1 & 0 & 0 \end{bmatrix} \text{ and } \mathbf{A}_j^T = \begin{bmatrix} 0 & 1 & 0 \\ \frac{(-1)^j \sqrt{3}}{2} & 0 & -\frac{1}{2} \\ -\frac{1}{2} & 0 & \frac{(-1)^{(j-1)} \sqrt{3}}{2} \end{bmatrix} \text{ for } j = 2, 3$$

The matrices \mathbf{R}_i can be obtained from the position vectors of each contact point.

The effective stiffness matrix of the grasp, \mathbf{K}_e , can be obtained by neglecting the \mathbf{K}_i matrix, if the initial grasp force is not large. Therefore,

$$\mathbf{K}_e = \sum_{i=1}^3 {}_B^P \mathbf{J}_i^T \mathbf{K}_{p_i} {}_B^P \mathbf{J}_i$$

Substituting \mathbf{J}_i and \mathbf{K}_{pi} into the previous equation, we have

$$\mathbf{K}_e = \begin{bmatrix} \frac{3}{2}(k_{22} + k_{33}) & 0 & 0 & \frac{3}{2}k_{12}R & 0 & \frac{3}{2}k_{13}R \\ 0 & 3k_{11} & 0 & 0 & -3k_{12}R & 0 \\ 0 & 0 & \frac{3}{2}(k_{22} + k_{33}) & -\frac{3}{2}k_{13}R & 0 & \frac{3}{2}k_{12}R \\ \frac{3}{2}k_{12}R & 0 & -\frac{3}{2}k_{13}R & \frac{3}{2}k_{11}R^2 & 0 & 0 \\ 0 & -3k_{12}R & 0 & 0 & 3k_{22}R^2 & 0 \\ \frac{3}{2}k_{13}R & 0 & \frac{3}{2}k_{12}R & 0 & 0 & \frac{3}{2}k_{11}R^2 \end{bmatrix}$$

Then, $\delta\mathbf{x}_b = \mathbf{K}_e^{-1}\delta\mathbf{f}$,

$$\delta\mathbf{x}_b = \begin{bmatrix} \frac{-2k_{11}df}{3(k_{11}k_{22}+k_{11}k_{33}-k_{12}^2-k_{13}^2)} \\ \frac{-k_{22}df}{3(k_{11}k_{22}-k_{12}^2)} \\ 0 \\ \frac{2k_{12}df}{3R(k_{11}k_{22}+k_{11}k_{33}-k_{12}^2-k_{13}^2)} \\ \frac{-k_{21}df}{3R(k_{11}k_{22}-k_{12}^2)} \\ \frac{2k_{13}df}{3R(k_{11}k_{22}+k_{11}k_{33}-k_{12}^2-k_{13}^2)} \end{bmatrix}. \quad (\text{B.1})$$

From equation (4.5), we can find the changes in the contact forces by substituting $\delta\mathbf{x}_b$ from equation (B.1). If we further assume that $k_{ij} = 0, \forall i \neq j$, (decoupled fingertip stiffness matrices) the grasp forces at each contact, after $\delta\mathbf{f}$ is applied, are

$$\mathbf{f}_1 = \begin{bmatrix} -\frac{1}{3}df \\ 0 \\ f - \frac{2k_{33}}{3(k_{22}+k_{33})}df \\ 0 \\ 0 \\ 0 \end{bmatrix} \quad \mathbf{f}_2 = \begin{bmatrix} -\frac{1}{3}df \\ \frac{-k_{22}}{\sqrt{3(k_{22}+k_{33})}}df \\ f + \frac{k_{33}}{3(k_{22}+k_{33})}df \\ 0 \\ 0 \\ 0 \end{bmatrix} \quad \mathbf{f}_3 = \begin{bmatrix} -\frac{1}{3}df \\ \frac{k_{22}}{\sqrt{3(k_{22}+k_{33})}}df \\ f + \frac{k_{33}}{3(k_{22}+k_{33})}df \\ 0 \\ 0 \\ 0 \end{bmatrix}$$

The “worst-case-finger” measure, α_i , can be obtained using equation (4.9).

B.2 “Progression-toward-friction-limit” measure - the first order approximation

The “Progression-toward-friction-limit” measure is defined in Sections 4.4.3 and 4.4.4. A first order approximation can be obtained as follows.

B.2.1 First order approximation

From equation (4.13) in Section 4.4.3, the potential function is defined as:

$$V = (f_l^2 + f_m^2)^{1/2} - \mu |f_n|$$

where f_l , f_m , and f_n are the initial grasp forces in the l , m , and n directions. The sensitivity of the function V with respect to the force, $\mathbf{f} = [f_l \ f_m \ f_n]^T$, is

$$\frac{\partial V}{\partial \mathbf{f}} = [f_l(f_l^2 + f_m^2)^{-1/2} \ f_m(f_l^2 + f_m^2)^{-1/2} \ -\mu \operatorname{sgn}(f_n)] \quad (\text{B.2})$$

where $\operatorname{sgn}(f_n)$ is the signum function¹ of f_n . Ignoring second and higher order terms, we can write

$$\delta V \cong \frac{\partial V}{\partial \mathbf{f}} \delta \mathbf{f}$$

where $\delta \mathbf{f} = [\delta f_l \ \delta f_m \ \delta f_n]^T$. Therefore, we have

$$\delta V = \left(\frac{f_m \delta f_m + f_l \delta f_l}{\sqrt{f_m^2 + f_l^2}} - \mu \operatorname{sgn}(f_n) \delta f_n \right). \quad (\text{B.3})$$

B.2.2 Error analysis of the approximation

In addition to the first order approximation, we also derived the second order approximation by forming $\partial^2 V / \partial^2 \mathbf{f}$. However, the results of the error analysis show

¹The signum function is defined as: $\operatorname{sgn}(f) = \begin{cases} 1 & \text{if } f > 0 \\ -1 & \text{if } f < 0 \end{cases}$

that the first order approximation is close enough to the exact values and the second order approximation does not significantly improve accuracy; therefore, the first order approximation is adopted for convenience.

The results of equation (B.3) were compared to the exact values from equation (4.14) in numerical simulation and they showed that (B.3) is a close approximation, especially when $\delta f_m/f_m$ is close to $\delta f_l/f_l$. Generally, the error is less than 1% if $\delta f_m/f_m$ is equal to $\delta f_l/f_l$, and within 2% for many cases of infinitesimal motions.

B.3 Results of the 2D grasp examples

In Example 4.2, a diagonal joint stiffness is given for the current configuration, as shown in Figure 4.7, for both fingers to make it a symmetric grasp.

$$\mathbf{K}_\theta = \begin{bmatrix} k_{\theta_1} & 0 \\ 0 & k_{\theta_2} \end{bmatrix}$$

The joint Jacobian matrices can be easily found with respect to the coordinates (n_i, l_i, θ_m) assuming each link is of length $\sqrt{2}$ units. We have

$$\mathbf{J}_{\theta_1} = \begin{bmatrix} 2 & 1 \\ 0 & -1 \\ 1 & 1 \end{bmatrix} \text{ and } \mathbf{J}_{\theta_2} = \begin{bmatrix} -2 & -1 \\ 0 & -1 \\ 1 & 1 \end{bmatrix}$$

The cartesian transformation matrices are:

$${}^P_B \mathbf{J}_1 = \begin{bmatrix} -1 & 0 & 0 \\ 0 & -1 & 1 \\ 0 & 0 & 1 \end{bmatrix} \text{ and } {}^P_B \mathbf{J}_2 = \begin{bmatrix} 1 & 0 & 0 \\ 0 & 1 & 1 \\ 0 & 0 & 1 \end{bmatrix}$$

Therefore, the stiffness of the grasp is:

$$\mathbf{K}_b = \sum_{i=1}^2 {}^P_B \mathbf{J}_i^T \mathbf{K}_\theta {}^P_B \mathbf{J}_i = \begin{bmatrix} \frac{k_{\theta_1}}{2} & 0 & \frac{-k_{\theta_1}}{2} \\ 0 & \frac{k_{\theta_1}+4k_{\theta_2}}{2} & 0 \\ \frac{-k_{\theta_1}}{2} & 0 & \frac{k_{\theta_1}+4k_{\theta_2}}{2} \end{bmatrix} \quad (B.4)$$

where the stiffness in the y direction is clearly decoupled due to symmetry.

For a given $\delta\mathbf{f} = [df_x \ df_y \ dm]^T$,

$$\delta\mathbf{x}_b = \begin{bmatrix} \frac{4df_x k_{\theta_2} + (dm + df_x)k_{\theta_1}}{2k_{\theta_1}k_{\theta_2}} \\ \frac{2df_y}{k_{\theta_1} + 4k_{\theta_2}} \\ \frac{dm + df_x}{2k_{\theta_2}} \end{bmatrix} \quad (\text{B.5})$$

The changes in grasp forces can be obtained by substituting equation (B.5) into $\delta\mathbf{f}_{p_i} = \mathbf{K}_{p_i B}^P \mathbf{J}_i \delta\mathbf{x}_b$.

$$\delta\mathbf{f}_{p_1} = \begin{bmatrix} -\frac{(df_x + df_y)k_{\theta_1} + 4df_x k_{\theta_2}}{2k_{\theta_1} + 8k_{\theta_2}} \\ \frac{dm - df_y}{2} \\ 0 \end{bmatrix} \quad \delta\mathbf{f}_{p_2} = \begin{bmatrix} \frac{(df_x - df_y)k_{\theta_1} + 4df_x k_{\theta_2}}{2k_{\theta_1} + 8k_{\theta_2}} \\ \frac{dm + df_y}{2} \\ 0 \end{bmatrix} \quad (\text{B.6})$$

Appendix C

Quasistatic sliding manipulation

C.1 Analytical solution of the trajectories of the frame and disk for an applied force profile

Applying equation (5.21), the trajectory of the disk is found to be:

$$\mathbf{r}(\tau) = \begin{cases} [0, 0]^T & \text{if } 0 \leq \tau \leq \pi/4 \\ c_1[\sin \tau - \frac{1}{\sqrt{2}}, -\cos \tau + \frac{1}{\sqrt{2}}]^T & \text{if } \pi/4 \leq \tau < \pi/2 \\ c_1[\frac{\sqrt{2}-1}{\sqrt{2}}, \frac{1}{\sqrt{2}}]^T & \text{if } \pi/2 < \tau \leq 3\pi/4 \\ [c_2 \sin \tau + \frac{(\sqrt{2}-1)c_1-c_2}{\sqrt{2}}, -c_2 \cos \tau + \frac{c_1-c_2}{\sqrt{2}}]^T & \text{if } 3\pi/4 \leq \tau \leq \pi . \end{cases}$$

The trajectory of the frame is then found to be:

$$\mathbf{r}_e(\tau) = \begin{cases} \zeta[\frac{2\sqrt{2}}{\pi}\tau, \frac{2\sqrt{2}}{\pi}\tau]^T & \text{if } 0 \leq \tau \leq \pi/4 \\ c_1[\sin \tau - \frac{1}{\sqrt{2}}, -\cos \tau + \frac{1}{\sqrt{2}}]^T + \zeta[\cos \tau, \sin \tau]^T & \text{if } \pi/4 \leq \tau < \pi/2 \\ [\frac{\sqrt{2}-1}{\sqrt{2}}c_1 - \frac{4\zeta}{\sqrt{2}\pi}(\tau - \frac{\pi}{2}), \frac{1}{\sqrt{2}}c_1 + \frac{1}{\sqrt{2}}\zeta]^T & \text{if } \pi/2 < \tau \leq 3\pi/4 \\ [c_2 \sin \tau + \frac{(\sqrt{2}-1)c_1-c_2}{\sqrt{2}}, -c_2 \cos \tau + \frac{c_1-c_2}{\sqrt{2}}]^T + \zeta[\cos \tau, \sin \tau]^T & \text{if } 3\pi/4 \leq \tau \leq \pi \end{cases}$$

where $\zeta = \mu f_n/k$. The plot shown in Figure 5.11 is for $c_1 = c_2 = 1$ and $\zeta = 0.5$. The constants c_1 and c_2 depend on $d\tau/ds$ of the curve, which is determined by the rate of change of force.

C.2 The cartesian stiffness matrices for Example 5.5

In the first case, the stiffness matrix with respect to the l, m, n and θ_n coordinates is:

$$\mathbf{HK}_p \mathbf{H}^T = \begin{bmatrix} 1650 & 440 & 310 & | & 14 \\ 440 & 1580 & 190 & | & 14 \\ 310 & 190 & 1060 & | & 0.9 \\ --- & --- & --- & + & - \\ 14 & 14 & 0.9 & | & 0.9 \end{bmatrix} \quad (\text{C.1})$$

where the units are N/m and Nm for linear and rotational stiffness terms, respectively. In this case we assume that the Jacobians and contact locations are continually updated using known kinematics of the finger so that \mathbf{K}_p is constant. In the second case, we assume that the fingertip stiffness is kept constant in the world $O(XYZ)$ frame through cartesian stiffness control so that the actual \mathbf{K}_p matrix varies as the finger moves along the sphere and the orientation of the $P(lmn)$ frame changes with respect to the $O(XYZ)$ frame. The world stiffness is chosen so that \mathbf{K}_p for this case matches the first case when the finger is mid-way along the curve. At the start and end of the curve, the stiffness matrices are:

$$\mathbf{HK}_{p,0^\circ} \mathbf{H}^T = \begin{bmatrix} 1175 & 35 & 85 & 0 \\ 35 & 2055 & 350 & 20 \\ 85 & 350 & 1060 & 0.9 \\ 0 & 20 & 0.9 & 0.9 \end{bmatrix} \quad \mathbf{HK}_{p,90^\circ} \mathbf{H}^T = \begin{bmatrix} 2055 & -35 & 350 & 20 \\ -35 & 1175 & -85 & 0 \\ 350 & -85 & 1060 & 0.9 \\ 20 & 0 & 0.9 & 0.9 \end{bmatrix}$$

For points in between, the \mathbf{K}_p matrix varies smoothly between these extremes.

Appendix D

Motions of sliding manipulation

D.1 Weighting matrix of function “g”

The concatenated weighting matrix \mathcal{W} , subject to the contact constraints, is defined as:

$$\mathcal{W} = \mathcal{H}^T \begin{bmatrix} \mathbf{W}_1 & 0 \\ 0 & \mathbf{W}_2 & \ddots \end{bmatrix} \mathcal{H} \quad (\text{D.1})$$

where \mathbf{W}_i is a positive-definite and symmetric scaling matrix for each finger that can be constructed according to the position vector $\mathbf{r} = [r_x \ r_y \ r_z]^T$ from the origin of the body coordinates to the i 'th contact:

$$\mathbf{W}_i = \begin{bmatrix} \mathbf{I}_3 & 0 \\ 0 & -\mathbf{R}^2 \end{bmatrix} \quad (\text{D.2})$$

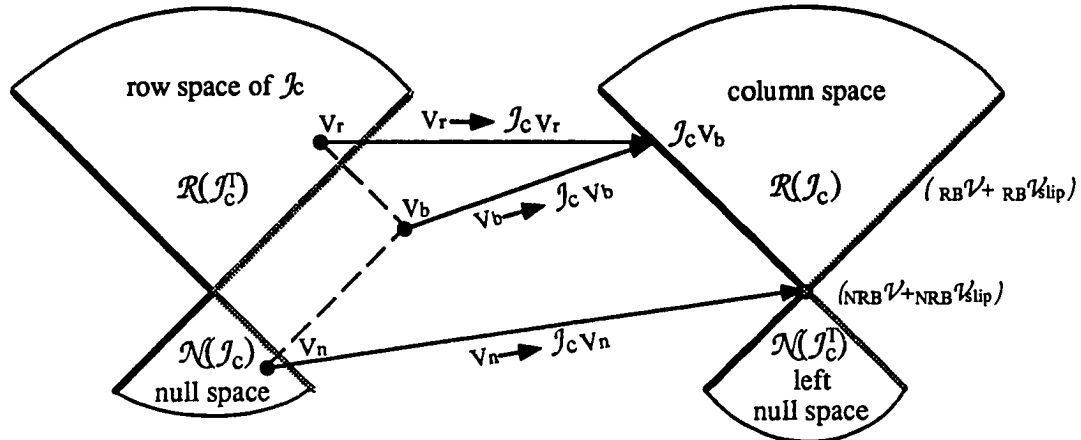


Figure D.1: Geometric visualization of the row space and null space

or formed by the characteristic length of the grasp, r_c :

$$\mathbf{W}_i = \begin{bmatrix} 1 & 0 & 0 & 0 & 0 & 0 \\ 0 & 1 & 0 & 0 & 0 & 0 \\ 0 & 0 & 1 & 0 & 0 & 0 \\ 0 & 0 & 0 & r_c^2 & 0 & 0 \\ 0 & 0 & 0 & 0 & r_c^2 & 0 \\ 0 & 0 & 0 & 0 & 0 & r_c^2 \end{bmatrix} \quad (\text{D.3})$$

D.2 The optimal solution with minimum norm

The solution of \mathbf{v}_b is obtained from equation (6.7). Since the row space of J_c , $R(J_c^T)$, is orthogonal to its null space, $N(J_c)$, the solution of \mathbf{v}_b can always be broken into two components, namely

$$\mathbf{v}_b = \mathbf{v}_r + \mathbf{v}_n \quad (\text{D.4})$$

where $\mathbf{v}_r \in R(J_c^T)$ and $\mathbf{v}_n \in N(J_c)$. This can be visualized geometrically as shown in Figure D.1, where the NRB space corresponds to null the space of the motion of the grasped object.

The solution of equation (D.4) obeys the Pythagoras' law since the two components are orthogonal:

$$\|\mathbf{v}_r + \mathbf{v}_n\|^2 = \|\mathbf{v}_r\|^2 + \|\mathbf{v}_n\|^2$$

The solution that has the minimum norm is apparently \mathbf{v}_r . That is, we should choose the null space component to be zero, leaving a solution that is entirely in the row space of \mathcal{J}_c . By Definition 6.1, the NRB components have no net rigid-body component and therefore correspond to \mathbf{v}_n . Consequently, the choice is $\mathcal{J}_c \mathbf{v}_n = \mathcal{H}_{NRB} \mathcal{V} +_{NRB} \mathcal{V}_{slip} = 0$.

D.3 Proof that $v_y = 0$ in the business card example

To show that the grasped object can not move in the y direction, proof by contradiction is employed. First, from the equation of equilibrium, $\sum \mathbf{F} = 0$, so $f_{y1} + f_{y2} = 0$. Assume that $f_{y1} = f_y \geq 0$ and $f_{y2} = -f_y$. We can then write the velocity compatibility equations with respect to coordinates at the COR as:

$$\begin{bmatrix} -l_1 \omega \\ v_y \\ \omega \end{bmatrix} = \begin{bmatrix} v_1 \\ 0 \\ 0 \end{bmatrix} + c_1 \begin{bmatrix} \lambda_1 \cos \psi_1 \cos \alpha_1 \\ \lambda_1 \cos \psi_1 \sin \alpha_1 \\ \sin \psi_1 \end{bmatrix} \quad (D.5)$$

$$\begin{bmatrix} l_2 \omega \\ v_y \\ \omega \end{bmatrix} = \begin{bmatrix} -v_2 \\ 0 \\ 0 \end{bmatrix} + c_2 \begin{bmatrix} -\lambda_2 \cos \psi_2 \cos \alpha_2 \\ -\lambda_2 \cos \psi_2 \sin \alpha_2 \\ \sin \psi_2 \sin \alpha_2 \end{bmatrix} \quad (D.6)$$

where α_i is the angle between f_{xi} and f_{yi} , and ψ_i is the angle of the unit normal to limit surface, as in Example 6.3. Both angles ψ and α are limited between 0 and $\frac{\pi}{2}$, i.e., $0 \leq \psi_i \leq \frac{\pi}{2}$ and $-\frac{\pi}{2} \leq \alpha_i \leq \frac{\pi}{2}$. From equations (D.5) and (D.6), we know that $\omega = c_1 \sin \psi_1 = c_2 \sin \psi_2$ and

$$v_y = c_1 \lambda_1 \cos \psi_1 \sin \alpha_1 = -c_2 \lambda_2 \cos \psi_2 \sin \alpha_2 \quad (D.7)$$

Since $f_{y1} = -f_{y2} = f_y \geq 0$, we know $0 \leq \alpha_i \leq \frac{\pi}{2}$; therefore, $\sin \alpha_1$ and $\sin \alpha_2$ are both positive. Moreover, equation (D.7) can be reduced to $(\lambda_1 \cot \psi_1 \sin \alpha_1 = -\lambda_2 \cot \psi_2 \sin \alpha_2)$ and since $\sin \alpha_1$ and $\sin \alpha_2$ carry the same sign, it is obvious that

$\cot \psi_1 \cot \psi_2 \leq 0$. However, this is a contradiction to the fact that $0 \leq \psi_1, \psi_2 \leq \frac{\pi}{2}$. Therefore, $\alpha_1 = \alpha_2 = 0$ and $v_y = 0$. That is, the card will not move in the vertical direction. The same proof can be shown for $f_{y2} = -f_{y1} = f_y \geq 0$. As a result, $v_y = 0$.

In addition, $f_{y1} = f_{y2} = 0$ must hold, otherwise the elliptical cross section of the limit surface would have f_y components and result in non-zero v_{yi} , which contradicts what we have just shown.

D.4 Results of unsymmetric grasp example

With direct computation by equations of RB and NRB motions, we obtain the following parameters as a function of the grasp.

The vector \mathbf{v}'_b obtained from the minimization theorem is

$$\mathbf{v}'_b = \begin{bmatrix} \frac{\sum_{i=1}^2 (-1)^i c_i [-l_i^3 \sin \psi_i + l_1 l_2 l_i \sin \psi_i - (2l_1^2 + l_1 l_2 + 2l_2^2 - l_i^2) \lambda_i \cos \psi_i]}{(3l_1^2 + 2l_1 l_2 + 3l_2^2)} \\ 0 \\ \frac{\sum_{i=1}^2 2c_i (l_i^2 \sin \psi_i - r \lambda_i \cos \psi_i)}{(3l_1^2 + 2l_1 l_2 + 3l_2^2)} \end{bmatrix}$$

We substitute the solution of \mathbf{v}'_b into equations (6.25) and (6.26) to solve for ${}_{RB}\mathbf{v}$ and ${}_{RB}\mathbf{v}_{slip}$. The magnitude of $\mathbf{v}_{slip,1}$ and $\mathbf{v}_{slip,2}$, c_1 and c_2 , are obtained by applying equation (6.11) for the two fingers and equate the expressions for \mathbf{v}_b :

$$c_i = \frac{-(v_1 + v_2)}{(l_1 + l_2 + \lambda_1 \cot \psi_1 + \lambda_2 \cot \psi_2) \sin \psi_i}$$

We can then substitute the values of c_1 and c_2 back to equation (6.11) to solve for \mathbf{v}_b . Because the motion is with respect to the COR, we can set the v_x term of \mathbf{v}_b to zero to obtain an equation of l_1 and l_2 . Since we know $l_1 + l_2 = 2r$, we can solve for

$$\begin{aligned} l_1 &= \frac{v_1(2r + \lambda_2 \cot \psi_2) - v_2 \lambda_1 \cot \psi_1}{v_1 + v_2} \\ l_2 &= \frac{v_2(2r + \lambda_1 \cot \psi_1) - v_1 \lambda_2 \cot \psi_2}{v_1 + v_2} \end{aligned}$$

and

$$h = l_1 - l_2 = \frac{2(r + \lambda_2 \cot \psi_2)v_1 - 2(r + \lambda_1 \cot \psi_1)v_2}{v_1 + v_2}$$

The velocity of the point at the middle of the line connecting the two contact centroids is

$$\mathbf{v} = \begin{bmatrix} \frac{rv_1 - rv_2 + v_1\lambda_2 \cot \psi_2 - v_2\lambda_1 \cot \psi_1}{(l_1 + l_2 + \lambda_1 \cot \psi_1 + \lambda_2 \cot \psi_2)} \\ 0 \\ \frac{-(v_1 + v_2)}{(l_1 + l_2 + \lambda_1 \cot \psi_1 + \lambda_2 \cot \psi_2)} \end{bmatrix}$$

Bibliography

- [1] H. Asada. *Studies on Prehension and Handling by Robot Hands With Elastic Fingers*. PhD thesis, Kyoto University, April 1979.
- [2] H. Asada and I. H. Ro. A linkage design for direct-drive robot arms. Paper no. 84-det-143, ASME, 1984.
- [3] D. L. Brock. Enhancing the dexterity of a robot hand using controlled slip. Technical report, MIT, May 1987.
- [4] D. L. Brock. Enhancing the dexterity of a robot hand using controlled slip. In *Proceedings of 1988 IEEE International Conference on Robotics and Automation*, pages 249–251, Philadelphia, Pennsylvania, April 24-29 1988.
- [5] R. C. Brost. Automatic grasp planning in the presence of uncertainty. *The International Journal of Robotics Research*, 7(1):1–17, February 1988.
- [6] J. W. Burdick. *Kinematic Analysis and Design of Redundant Robot Manipulators*. PhD thesis, Stanford University, March 1988.
- [7] C. Cai and B. Roth. On the spatial motion of a rigid body with line contact. In *The Proceedings of IEEE Internatioanl Conference on Robitics and Automation*, pages 1036–1041, Philadelphia, Pennsylvania, April 24-29 1988.
- [8] J. J. Craig. *Introduction to Robotics*. Addison-Wesley, 2nd edition, 1989.
- [9] M. R. Cutkosky. *Robotic Grasping and Fine Manipulation*. Kluwer Academic Publishers, Boston, Mass, 1985.

- [10] M. R. Cutkosky, P. Akella, R. Howe, and I. Kao. Grasping as a contact sport. In R. Bolles and B. Roth, editors, *Robotics Research: the Fourth International Symposium*, pages 199–206, Cambridge, MA, 1988. MIT Press.
- [11] M. R. Cutkosky and I. Kao. Computing and controlling the compliance of a robotic hand. *IEEE Transaction of Robotics and Automation*, 5(2):151–165, April 1989.
- [12] M. R. Cutkosky and P. Wright. Friction, stability and the design of robotic fingers. *International Journal of Robotics Research*, 5(4):20–37, 1986.
- [13] M.R. Cutkosky and P.K. Wright. Active control of a compliant wrist in manufacturing tasks. *ASME Journal of Engineering for Industry*, 108(1):36–43, 1985.
- [14] M. P. do Carmo. *Differential Geometry of Curves and Surfaces*. Englewood Cliffs, N.J., Prentice-Hall, 1976.
- [15] R. Fearing. Implementing a force strategy for object reorientation. In *Proceedings of 1986 IEEE International Conference on Robotics and Automation*, pages 96–102, 1986.
- [16] Charles F. Van Loan Gene H. Golub. *Matrix computations*. Johns Hopkins University Press, 2nd edition, 1989.
- [17] S. Gopalswamy and R. S. Fearing. Grasping polyhedral objects with slip. In *Proceedings of 1989 IEEE International Conference on Robotics and Automation*, pages 296–301, Scottsdale, Arizona, May 1989.
- [18] C. Gosselin. Stiffness mapping for parallel manipulators. *IEEE Transactions on Robotics and Automation*, 6(3):377–382, June 1990.
- [19] S. Goyal, A. Ruina, and J. Papadopoulos. Limit surface and moment function description of planar sliding. In *Proceedings of 1989 IEEE International Conference on Robotics and Automation*, pages 794–799, Scottsdale, Arizona, May 1989.

- [20] R. Hill. *The Mathematical Theory of Plasticity*. Oxford University Press, 1950.
- [21] N. Hogan. Impedance control: An approach to manipulation: Part i, ii, and iii. *Journal of Dynamic Systems, Measurement, and Control, Transactions of the ASME*, 107:1–24, March 1985.
- [22] R. Howe, I. Kao, and M. Cutkosky. Sliding of robot fingers under combined torsion and shear loading. In *Proceedings of 1988 IEEE International Conference on Robotics and Automation*, volume 1, pages 103–105, Philadelphia, Pennsylvania, April 24-29 1988.
- [23] R. D. Howe, N. Popp, P. Akella, I. Kao, and M. R. Cutkosky. Grasping, manipulation, and control with tactile sensing. In *Proceedings of the 1990 IEEE International Conference on Robotics and Automation*, Cincinnati, Ohio, May 13–18 1990. IEEE society of Robotics and Automation, IEEE.
- [24] J. Jameson and L. Leifer. Quasi-static analysis: A method for predicting grasp stability. In *Proceedings of 1986 IEEE International Conference on Robotics and Automation*, pages 876–883, April 1986.
- [25] J. W. Jameson. *Analytic Techniques for Automated Grasp*. PhD thesis, Stanford University, June 1985.
- [26] Z. Ji. *Dexterous Hand: Optimizing Grasp by Design and Planning*. PhD thesis. Stanford University, 1987.
- [27] T. Kailath. *Linear Systems*. Prentice-Hall, Inc., Englewood Cliffs, N.J. 07632 : Prentice-Hall, 1 edition, 1980.
- [28] I. Kao. Effective stiffness and compliance, and their application to sliding analysis. Technical report, SIMA, Stanford University, March 1987.
- [29] I. Kao and M. R. Cutkosky. Dexterous manipulation with compliance and sliding. In *The 5th International Symposium on Robotics Research*, Tokyo, Japan, Aug 28 – 31 1989. MIT Press.

- [30] I. Kao and M. R. Cutkosky. Quasistatic sliding manipulation – on the transient response of quasistatic manipulation. In *Proceedings of the 4th IEEE International Symposium on Intelligent Control*, pages 438–443, Albany, New York, 25-27, September 1989.
- [31] J. Kerr. *Analysis of Multifingered Hands*. PhD thesis, Stanford University, 1986.
- [32] H. Kobayashi. Control and geometrical considerations for an articulated robot hand. *The International Journal of Robotics Research*, 4(1):3–12, 1985.
- [33] S.-H. Lee and M. R. Cutkosky. Fixture planning with friction. *ASME Journal of Engineering for Industry*, in press, 1990.
- [34] Z. Li, P. Hsu, and S. Sastry. Grasping and coordinated manipulation by a multi-fingered robot hand. *The International Journal of Robotics Research*, 8(4):33–50, August 1989.
- [35] M. T. Mason. On the scope of quasi-static pushing. In *The Proceedings of Third International Symposium on Robotics Research*, October 1985.
- [36] M. T. Mason and J. K. Salisbury. *Robot Hands and the Mechanics of Manipulation*. The MIT Press, 1985.
- [37] B. Mishra and N. Silver. Some discussion of static gripping and its stability. *IEEE Transaction on Man, and Cybernetics*, 19(4):783–796, July/August 1989.
- [38] David J. Montana. The kinematics of contact and grasp. *The International Journal of Robotics Research*, 7(3):17–32, June 1988.
- [39] R. M. Murray and S. S. Sastry. Control experiments in planar manipulator and grasping. In *Proceedings of IEEE International Conference on Robotics and Automation*, pages 624–629, Scottsdale, Arizona, May 1989.
- [40] Y. Nakamura. Contact stability measure and optimal finger force control of multi-fingered robot hands. In *Crossing Bridges: Advances in Flexible Automation and Robotics*, pages 523–528. ASME, The Proceedings of the USA-Japan Symposium on Flexible Automation, July 1988.

- [41] V. Nguyen. Constructing stable grasps. *The International Journal of Robotics Research*, 8(1):26–37, Feburary 1989.
- [42] Van-Duc Nguyen. Constructing force-closure grasps. *The International Journal of Robotics Research*, 7(3):3–16, June 1988.
- [43] M. Ohwovoriole. *An extension to screw theory and its applications to the automation of industrial assemblies*. PhD thesis, Stanford University, April 1980.
- [44] T. Okada. Object-handling system for manual industry. *IEEE Transactions on Systems, Man and Cybernetics*, SMC-9(2):79–89, Feburary 1979.
- [45] T. Okada. Computer control of multijointed finger system for precise handling. *IEEE Transactions on Systems, Man and Cybernetics*, SMC-12(3):289–299, June 1982.
- [46] Y. C. Park and G. P. Starr. Optimal grasping using a multifingered robot hand. In *Proceedings of the 1990 IEEE International Conference on Robotics and Automation*, pages 689–694, Cincinnati, Ohio, May 13–18 1990. IEEE.
- [47] R. P. Paul. *Robot Manipulators: Mathematics, Programming, and Control. The Computer Control of Robot Manipulators*. MIT Press, 1981.
- [48] M. A. Peshkin. *Planning Robotic Manipulation Strategies for Sliding Objects*. PhD thesis, Carnegie Mellon University, 1986.
- [49] M. A. Peshkin and A. C. Sanderson. Minimization of energy in quasistatic manipulation. In *Proceedings of 1988 IEEE Conference on Robotics and Automation*, pages 421–428, Philadelphia, Pennsylvania, April 1988.
- [50] M. H. Raibert and B. K. P. Horn. Manipulator control using the configuration space method. *The Industrial Robot (UK)*, 5(2):69–73, June 1978.
- [51] J. K. Salisbury. Active stiffness control of a manipulator in cartesian coordinates. In *Proceedings 19th IEEE Conference on Decision and Control*, pages 87–97, Albuquerque, NM, December 1980.

- [52] G. Strang. *Linear Algebra and Its Applications*. Harcourt, Brace, Jovanovich, 3rd edition, 1988. Call No. QA184.S8 1988 General treatment of Linear Algebra.
- [53] S. P. Timoshenko and J. N. Goodier. *Theory of Elasticity*. McGraw-Hill Book Company, third edition, 1970.
- [54] S. P. Timoshenko and D. H. Young. *Elements of Strength of Materials*. D. Van Nostrand Company, Inc., 4th edition, 1962.
- [55] D. E. Whitney. Part mating theory for compliant parts. First report, The Charles Stark Draper Laboratory Inc., August 1980. NSF Grant No. DAR79-10341.